A novel dosimetric protocol for high energy photon radiotherapy beams in Norway using radiochromic film

Thesis for the degree Master of Science,
Institute of Physics, University in Oslo

Statens strålevern
Norwegian Radiation Protection Authority

Abstract:

In 2008, a master's thesis project was carried out at the NRPA, concentrating on the implementation and use of radiochromic film for dosimetric purposes in photon radiotherapy. A method for the use of radiochromic film in a clinical setting was developed and tested at 7 of Norway's 10 radiotherapy hospitals. This report contains the finished thesis in its entirety.

Resymé:

I 2008 ble det gjennomført et prosjekt i form av en masteroppgave ved Statens Strålevern, som omhandlet bruk av radiokromisk film til dosimetriformål innen stråleterapi. En metode for bruk av radiokromisk film i klinisk sammenheng ble utviklet og uttestet ved 7 av landets 10 stråleterapisentra. Rapporten inneholder den ferdige masteroppgaven i sin helhet.

Veiledere:

Hilde M. Olerud (Strålevernet, UiO), Hans Bjerke (SSDL, Strålevernet),
Ståle Ølberg (Oslo Universitetssykehus - Ullevål), Eli Olaug Hole (UiO)

A novel dosimetric protocol for high energy photon radiotherapy beams in Norway using radiochromic film

Thesis for the degree Master of Science, Institute of Physics, University in Oslo

Alexander Mauring

NRPA's introduction

Since 2000 the Norwegian Radiation Protection Authority (NRPA) has established and developed a national quality assurance programme in radiotherapy, KVIST (Norwegian acronym). The programme aims to stimulate collaboration by focussing on clinical, technical and administrative problems that can be solved through a national plan. An important objective is to establish a positive attitude towards quality assurance and better communication between centres and the various professions involved in radiotherapy. A Working Group is dealing with dosimetric problems in close collaboration with the NRPA's secondary standard dosimetry laboratory (SSDL). The group did early recognise a need for dosimetry revision methodology. In connection with a national introduction of a new dosimetric protocol from the IAEA (TRS 398), theoretical and practical training was provided in concurrence with a national dosimetric intercomparison. All therapy centres have been visited and standard protocols have been utilised since 2003. The implementation is described in StrålevernRapport 2003:11. The continual development of new improvements in high energy beam radiotherapy requires the use of sharply defined radiation fields. KVIST recognized the need to develop new routines for quality assurance and 2D dosimetry, especially for modalities like IMRT and use of asymmetric fields. A Master student was recruited from the Department of Physics at University of Oslo (UiO) to study this issue. The supervisors for the project have been:

Hans Bjerke, senior adviser
NRPA secondary standard laboratory (SSDL)

Ståle Ølberg, medical physicist
Oslo University Hospital, Ullevål

Hilde M. Olerud, head of section
NRPA and UiO/Institute of Physics

Eli Olaug Hole, Professor
UiO, Department of Physics/Research group for Biophysics and Medical Physics

Alexander Mauring presented his Master Thesis 19. December 2008 at the Institute of Physics, University in Oslo. He is liable for the methodology, results and analyses. The thesis is published as a NRPA Report as feedback to all radiotherapy centres in Norway contributing to the task. We would like to thank all local physicists for welcoming Alexander, helping him with advice and valuable discussions during the experimental tests and carrying out the dosimetry revisions. We also have an impression the proposed model has been acknowledged in the community.

The Master Thesis can be downloaded from NRPA website www.nrpa.no (click publications), where you also will find reports in Norwegian about additional results from the work.

Yours sincerely,

Gunnar Saxebøl

Head of Deptartment for Radiation Protection and Nuclear Safety, NRPA

A novel dosimetric protocol for high energy photon radiotherapy beams in Norway using radiochromic film

by Alexander Mauring

Department of Physics
University of Oslo

Thesis submitted for the degree Master of Science
November 2008

Abstract

The continual development of new improvements in high energy beam radiotherapy in Norway urges for a revision in dosimetric quality controls. It is favorable to use sharply defined fields, but existing routines for quality assurance are lacking, especially in for modalities such as asymmetric fields and IMRT.

The thesis suggests a new procedure for implementing radiochromic film as a tool for quality assurance in radiotherapy, in cooperation with the Norwegian Radiation Protection Authority (NRPA). GafChromic® EBT type film has been used for the experiments. The procedure is based on the general method first suggested by Devic et al [1], with several modifications. Films have been calibrated using the Co-60 gammatron at the NRPA Secondary Standard Dosimetry Laboratory, and measurements have been performed on 14 treatment units at 7 different hospitals in Norway. In addition to film irradiation, reference dosimetry according to TRS-398 protocol [2] using an ionization chamber in a water phantom was performed at 13 of 14 linacs.

Measurements show that measured dose for a 10x10 cm^2 field at reference conditions with an ionization chamber in a water phantom was within 2 % limit for all linear accelerators, for both 6 MV and 15 MV photon energies.

Radiochromic film measurements were inaccurate for absolute dosimetry due to difficulties in the absolute calibration of the film. However, relative measurements using radiochromic film show that values for field size, penumbra, flatness and symmetry are close to expected clinical values.

Different asymmetric field setups are also investigated using radiochromic film. In the case where two asymmetric half-collimated fields are spliced together, high over- and underdosages of more than 20 % are detected in the border between the fields, both with and without collimator rotation. These discrepancies are not corrected for in dose planning software. Studies of fields with overtravel in both x- and y-directions show that field sizes vary within 7 % of the desired values, and measured doses do not fully agree with the calculated doses in treatment planning software.

Radiochromic film shows promise as a tool in radiotherapy quality assurance, but the existing method is not accurate enough to satisfy needs for clinical use. A modified method is suggested that will potentially improve the detected uncertainties.

Acknowledgments

"If we knew what it was we were doing, it would not be called
research, would it?"

- Albert Einstein

This work would never have been finished if it hadn't been for the support of some great people!

First, I would like to thank my supervisors: Hilde Olerud, for being my main supervisor during the course of the thesis and giving me countless important pieces of advice on my writing. Hans Bjerke, for helping me with the practical aspects and providing me with insight in aspects of dosimetry that would otherwise have puzzled and confused me. Ståle Ølberg, for teaching me about the practical aspects of the linear accelerator and dose planning software at Ullevål University Hospital. Eli Olaug Hole, for your help with practical issues through the course of my master's degree.

Jomar Frengen and Sigrun Saur for taking the time to teach me about using and analyzing radiochromic film. Per Otto Hetland, for assistance during measurements and advice on measurement technique. Ellen Wasbø for letting me use her IDL application in my thesis. Physicists at all hospitals that took the time and resources to accomodate me. All the nice people at the NRPA that welcomed me as one of their own and made me feel at home. And everyone affiliated with the biophysics group at the University of Oslo, who I have had a great time with during my studies.

Ones interest in physics has to begin somewhere, and mine began during my junior year in high school. I would therefore like to thank Michal Ortiz, Anna Lettinga and Rick Wilson, who inspired me to pursue a degree in the physical sciences.

Finally I thank my parents, friends and girlfriend for all the patience and support I could ever ask for. You have pushed me further than I could ever imagine I was capable of. Thank you!

Alexander Mauring, November 2008

Contents

Glossary of terms and acronyms

BIPM — Bureau International des Poids et Mesures

Co-60 — Cobalt 60

DICOM — Digital Imaging and Communications in Medicine

EBT — External Beam Therapy

FWHM — Full Width at Half Maximum

KERMA — Kinetic Energy Released per unit MAss

KVIST — Quality assurance in radiation therapy (Kvalitetssikring i Stråleterapi)

IAEA — International Atomic Energy Agency

IDL — Interactive data language

IMRT — Intensity Modulated Radiation Therapy

Linac — Linear accelerator

MLC — Multi-leaf collimator

MU — Monitor unit

netOD — Net Optical Density (see eq. 30)

NRPA — Norwegian Radiation Protection Authority

QA — Quality Assurance

ROI — Region Of Interest

RTQA — Radiotherapy Quality Assurance

SAD — Source Axis Distance

SSD — Source Surface Distance

SSDL — Secondary Standard Dosimetry Laboratory

TIFF — Tagged Image File Format

TPR — Tissue-Phantom Ratio

UUS — Ullevål University Hospital (Ullevål UniversitetsSykehus)

1   Introduction

Radiation therapy (or radiotherapy) refers to the treatment of cancer tumors by using high-energy radiation to kill the cancer cells. The linear accelerator (Linac) is currently the most commonly used device for the application of high-energy x-rays to cancer tumors, so-called external beam therapy. In this type of therapy, the patient is placed on a couch and the tumor is subjected to radiation from an external source.

The radiotherapy planning process is very comprehensive. Usually the tumor is first mapped out using imaging techniques such as computed tomography (CT) or magnetic resonance (MRI). Once the tumor has been defined, this data is imported into dose planning software where different radiation fields can be visualized as 3-dimensional dose distributions in the tissue. When planning these treatments it is essential to calculate these x-ray dose distributions accurately. The main goal is to deliver enough radiation dose to the tumor to destroy it, while still limiting the dose to the surrounding normal tissue. [3]
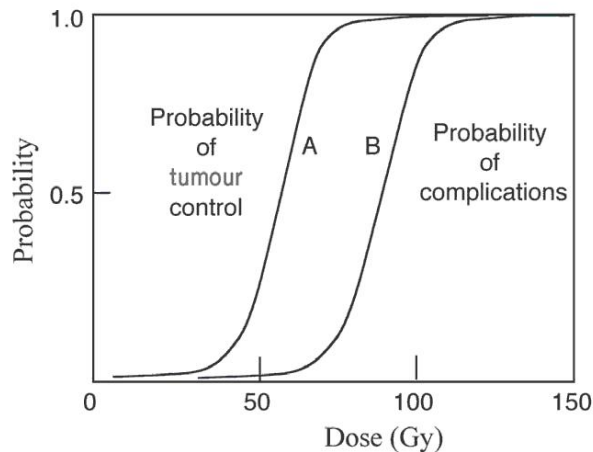
Figure 1: Response curves for a cancer tumor (curve A) and normal tissue (curve B) as a function of dose. The curves show the probability of tumor control and normal tissue complications, respectively. Figure taken from "Basic Radiobiology" by Suntharalingam et al (2005) [4].

Figure 1 shows response curves for tumor control probability (TCP, curve A) and normal tissue complication probability (NTCP, curve B) as a function of dose. Clinical radiotherapy treatments should be optimized so that the TCP is as high as possible while the NTCP is as low as possible, in order to avoid malevolent effects and later complications such as surrounding organ damage, radiation induced cancer or failure to destroy the tumor. The difference between the two curves is exaggerated in the figure, thus the margins between successful and unsuccessful treatment can be small. There is a need for rigorous dosimetry and quality controls in order to to ensure good treatment through precision and accuracy of dose estimation in treatment planning software.

In Norway today there are currently 10 hospitals that offer radiotherapy. Figure 2 shows the location of these hospitals. Table 1 shows quantitatively

Figure 2: A map of Norway with dots marking the locations of hospitals that offer external beam radiotherapy. Two hospitals are located in Oslo (blue dot)

how the number of treatment units and patients undergoing radiotherapy have increased over the last few years.

The Norwegian Radiation Protection Authority (NRPA) has national responsibility for the radiation-related units Gray, Sievert and Becquerel in Norway. Additionally, the NRPA's dosimetry laboratory (SSDL) covers the need for calibration of ionization chambers for high-energy radiotherapy across the country [5, 6]. The NRPA was given a mandate for quality assurance in radiotherapy, KVIST [7, 8], as a part of "Nasjonal Kreftplan" (National cancer plan) [9]. Proposed by KVIST, the NRPA reviewed the dosimetry at the different radiotherapy institutions, leading to the implementation of a new dosimetric protocol in 2002. This protocol is based on the TRS-398 protocol, and is based on point measurements with an ionization chamber in a water phantom [2, 10].

Table 1: Table showing the increasing activity of radiotherapy in Norway from 2001-2006. From left to right: Number of linear accelerators in use, equivalent number of effective linear accelerators (LAE), mean age of all linear accelerators in use, number of patients undergoing treatment, number of new patients, and the total amount of field exposures used for radiotherapy treatment. Data has been taken from the KVIST portal (http://kvist.nrpa.no/).

Year	No of linacs	LAE	Mean linac age	Patients	New patients	Field exp
2001	26	24.9	5,69 yrs	7212	6170	375585
2002	29	26.6	6,00 yrs	7714	6595	419838
2003	30	29.5	6,30 yrs	8443	7218	493608
2004	33	31.7	5,70 yrs	9316	7919	563236
2005	33	32.1	5,91 yrs	9829	8363	645660
2006	38	34.0	4,66 yrs	10012	8480	710738

At the present time, more advanced radiation treatment techniques call for more accurate geometric precision. With the implementation of conformal treatment techniques such as IMRT, the demands for quality assurance increases further. As a result of these requirements, there need for new dosimetric revisions that involve extending the dosimetry to two and three dimensions.

This thesis considers a simple dosimetric procedure using radiochromic film, which is a special type of film that changes color instantaneously upon exposure, and the application of this procedure on a number of radiotherapy institutions i Norway in cooperation with NRPA personnel. First, standard setups with ionization chambers and reference geometry will be studied to confirm the correlation between relative dosimetry and dose planning systems for high-energy photon radiation at the institutions. Then the dose planning systems will be tested with a number of asymmetric fields to see whether they are able to predict accurate doses in these special cases, for example in the case where half the field blocked by a secondary collimator. These fields will also be analyzed using radiochromic film in order to relate film and ionization chamber dosimetry, as well as check field uniformity in special cases such as field setups with asymmetric spliced fields, rotated fields and overtravel fields.

Each film is scanned and calibrated in order to tie the film dosimetry to absolute dosimetry using ionization chambers in a water phantom. This will test the film's characteristics with regard to accurate absolute film dosimetry. A method will be developed for the use of radiochromic film in clinical environments. Some of the main targets for the development of this method will be to:

- Select photon field configurations that will be reproducible at all hospitals for all treatment planning systems, as well as shed light on special techniques.

- Develop procedures for handling of the film before, during and after exposure.

- Calibrate the film and scanner.

- Write algorithms in Matlab to process, extract and analyze relevant parameters from the radiochromic film.

- Test the experimental methods at UUS and the NRPA before carrying out measurements at different hospitals.

Once the method has been developed and tested, measurements will be performed on linear accelerators at different radiotherapy institutions in Norway. An evaluation of the dosimetry of these linacs will be composed and presented.

The thesis takes the first steps in developing a functional method that will hopefully in the future be part of a clinical audit. The aim of this particular thesis was to test radiochromic film in several different clinical environments and see if the results are within reason. This in turn will determine whether the film is useful for clinical applications. The main hypothesis for this thesis is that the radiochromic film can be used to successfully compare dose distributions of linear accelerators across the country. It is assumed that the hospitals have sufficient quality controls so as to uphold accurate dosimetry for their radiotherapy treatments, so the results from different hospitals will be comparable.

2 Theoretical background

2.1 Basic concepts in dosimetry

In order to perform accurate dosimetry, it is necessary to define some basic but important concepts that will be used later on.

2.1.1 Particle fluence and energy fluence

Particle fluence, Φ, is defined as the number of particles dN traversing a sphere with cross-sectional area dA. This can be written as

$$\Phi = \frac{dN}{dA} \tag{1}$$

The unit for particle fluence is m^{-2}. Another important concept is the energy fluence, Ψ, which is defined as the total energy dE of the particles traversing a sphere with cross-sectional area dA.

$$\Psi = \frac{dE}{dA} \tag{2}$$

Energy fluence has units of J/m^2, and is a scalar quantity. It can also be written as

$$\Psi = \frac{dN}{dA}E = \Phi E \tag{3}$$

In eq. 3, E is the particle energy, and dN is the number of particles with energy E. [11, 12, 13]

2.1.2 Kerma, collision kerma and dose

A very central concept in dosimetry is, not surprisingly, the absorbed dose. Dose is closely related to another quantity called the Kinetic Energy Released per unit Mass (Kerma).

Photons can not directly impart energy as they have no charge. Instead, photons transfer energy to secondary charged particles (electrons), which then can transfer energy to the medium through ionizations and excitations. Hence, the energy imparted depends on the average amount of energy that is transferred from uncharged ionizing radiation (photons) to charged ionizing radiation (electrons). Kerma quantifies the energy transferred to charged particles, and can be defined as the energy transferred per unit mass

$$K = \frac{d\epsilon_{tr}}{dm} \tag{4}$$

Kerma can also be related to the energy fluence by the following formula:

$$K = \Psi \left(\frac{\mu_{tr}}{\rho} \right)_{E,Z} \tag{5}$$

$\left(\frac{\mu_{tr}}{\rho} \right)_{E,Z}$ is the mass-energy transfer coefficient. It depends on the photon energy E and the atomic number Z of the medium. It has a unit of m^2/kg and can be looked up in tables, such as the one found in Attix (1986). Kerma

can be subdivided into two parts, collision kerma K_c and radiative kerma K_r. K_c represents the quantity of the kerma that is spent creating ionizations and excitations in V, while K_r is the energy carried away from V. In other words, the total kerma can be written as $K = K_c + K_r$.

The collision kerma can now be defined as

$$K_c = \frac{d\epsilon_{en}}{dm} \tag{6}$$

Where ϵ_{en} is the net energy transferred to the volume excluding the energy that escapes due to radiative losses (K_r). Thus the only difference between kerma and collision kerma is that collision kerma takes into account and subtracts the radiative losses that leave the volume V. The collision kerma can also be related to the energy fluence of photons:

$$K_c = \Psi \left(\frac{\mu_{en}}{\rho} \right)_{E,Z} \tag{7}$$

Here $\left(\frac{\mu_{en}}{\rho} \right)_{E,Z}$ is called the mass-energy absorption coefficient. In addition to being dependent on the photon energy E and the atomic number Z, it is also dependent on the material it traverses. Values for $\left(\frac{\mu_{en}}{\rho} \right)_{E,Z}$ have a unit m^2/kg and are found in tables such as in Attix (1986).

The energy imparted ϵ to a volume V is equal to the net energy transferred *plus* the energy transferred from charged particles in the medium. The only difference between ϵ and ϵ_{tr} is that ϵ also takes charged particles into account.

Finally, the absorbed dose to the system is defined as the energy imparted $d\epsilon$ to a volume of mass dm:

$$D = \frac{d\epsilon}{dm} \tag{8}$$

Dose is measured in Gy (Gray), which is equivalent to basic SI units J/kg or m^2/s^2. [13, 14]

2.1.3 Linear attenuation and stopping power

When a photon beam enters a medium, the particle fluence (eq. 1) will decrease as a function of depth as more and more photons engage in particle interactions. This phenomenon is called linear attenuation. The particle fluence at depth x in a medium is given by

$$\Phi = \Phi_0 e^{-\mu x} \tag{9}$$

Φ_0 is the particle fluence at the medium surface, and μ is the *linear attenuation coefficient*. The linear attenuation coefficient has units m^{-1}. From eq. 9 it is clear that photons do not have a finite range as Φ never reaches zero, but the photon fluence does decrease exponentially as a function of depth.

For electrons, the concept of an attenuation coefficient does not apply. The stopping power refers to the total energy lost by electrons in a medium as a function of path length:

$$S_{tot} = \frac{dE}{dl} \tag{10}$$

In eq 10, dE is the total energy lost by the electron while traversing a length dl. The stopping power is measured in the units keVm^{-1}.

Going one step further, total mass stopping power is the stopping power normalized to the density ρ of the medium:

$$\left(\frac{S}{\rho}\right)_{tot} = \frac{dE}{\rho dl} \tag{11}$$

which has the units eVm^{2}g^{-1}. The total mass collision stopping power can be separated into two parts:

$$\left(\frac{S}{\rho}\right)_{tot} = \left(\frac{S}{\rho}\right)_{col} + \left(\frac{S}{\rho}\right)_{rad} \tag{12}$$

$\left(\frac{S}{\rho}\right)_{col}$ is the contribution from collisional losses due to ionization and excitation events, while $\left(\frac{S}{\rho}\right)_{rad}$ is the contribution from radiative losses (bremsstrahlung). Thus, only $\left(\frac{S}{\rho}\right)_{col}$ contributes to the locally absorbed dose to the medium. [12, 13]

2.2   Ionization chamber dosimetry

Ionization refers to the creation of an ion pair due to energy transferred from ionizing radiation. If the energy transferred to an atom is greater than the electron binding energy, an electron may be ejected from the atom resulting in a positively charged ion and a negatively charged electron. The defining property of ionizing radiation for ionization chamber dosimetry is its ability to ionize gas. This is essential for measuring doses with ionization chambers.

2.2.1   Basic ionization chamber setup

Ionization chambers are today the most common type of dosimeter used in external beam radiotherapy for determination of radiation dose [3]. The most simple ionization chamber consists of a gas-filled encapsulated space with two electrodes. A voltage is applied to these electrodes, resulting in a potential difference usually in the range of 200-400 V and most commonly 300 V. As the gas is exposed to ionizing radiation, radiation interactions ionize the gas. The electric field created by the electrodes cause the ionized particles to travel towards the electrode of opposite charge. This creates a current between the electrodes that is measurable by an electrometer.

The electrometer is connected to the ionization chamber, and provides the electronics necessary to measure the charge or current. It also provides the appropriate voltage to the electrodes. The voltage should be of such magnitude that the ions are collected before they have the chance to recombine with each other. The charge collected by the electrodes is displayed on the electrometer, usually in units of nC. This charge will need to be converted into dose using calibration coefficients, and this dose will need to be corrected in order to accurately determine the dose to a medium. This will be explained in section 2.2.4. [15]

2.2.2 Bragg-Gray cavity theory

In order to accurately determine the dose to a medium from the dose to the gas inside the ionization chamber, it is necessary to take special precautions. Usually the dosimeter is not the same material as the medium, and this is where cavity theory comes into play. Cavity theory relates the absorbed dose to the cavity (in this case the air-filled ionization chamber) to the absorbed dose to the medium of interest.

Bragg-Gray cavity theory has two conditions that have to be fulfilled in order for a cavity to be classified as a Bragg-Gray cavity. These are:

1. The presence of the cavity must not disturb the charged particle fluence in the medium that exists in the absence of the cavity.

2. The absorbed dose to the cavity is deposited exclusively by the charged particles crossing it.

The first condition implies that the size of the cavity needs to be smaller than the range of the electrons traversing the medium, so it does not perturb the electron paths. The second condition suggests that any contribution from photons to the dose needs to be negligible, which is only true for a photon beam. This also means that secondary electrons are neither created nor stop inside the cavity; all electrons depositing dose completely cross the cavity. A schematic of Bragg-Gray cavity theory can be seen in figure 3.
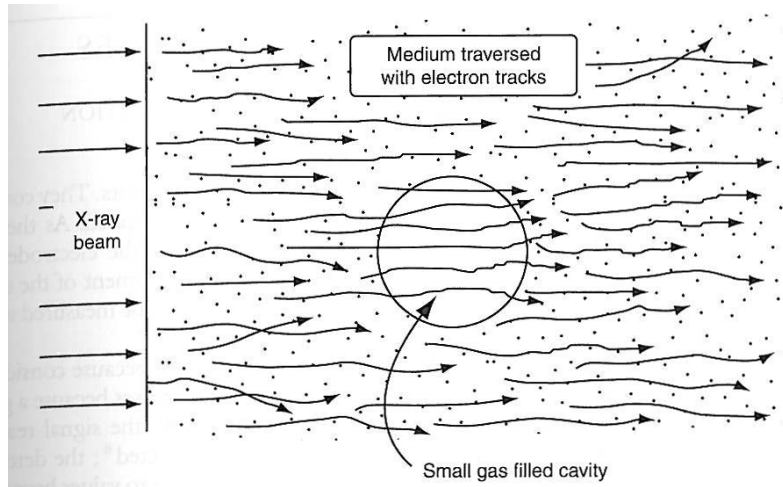
Figure 3: Bragg-Gray cavity theory. Figure from Johns et al (1983) [16]

The fulfillment of the two conditions depend on the cavity size, the composition of the medium as well as the electron energy, as electron range increases with increasing energy. It is clear that Bragg-Gray cavity theory applies most successfully to high-energy photon beams.

The absorbed dose to a medium can be calculated from the absorbed dose in the cavity using the following formula:

$$D_{med} = D_{cav} \left(\frac{\overline{S}}{\rho} \right)_{cav}^{med} \tag{13}$$

In this formula, D_{med} is the absorbed dose to the medium, D_{cav} is the absorbed dose to the cavity, and $\left(\overline{S}/\rho\right)_{cav}^{med}$ is the ratio of spectrum averaged electron mass collision stopping powers (see section 2.1.3) for the medium and cavity, respectively. $\left(\overline{S}/\rho\right)_{cav}^{med}$ can be calculated using advanced Monte Carlo techniques. In reality, there are several factors that complicate formula 13, but it holds true for a perfect Bragg-Gray cavity in a homogeneous medium. [11, 12, 13, 15, 17]

2.2.3 Cavity chambers

Cavity chambers have chamber walls surrounding an air volume. There are two main types of cavity chambers; cylindrical and plane-parallel [18]. For this thesis only a cylindrical chamber, also known as thimble chamber, was used. A schematic of a standard cylindrical chamber is shown in Figure 4.
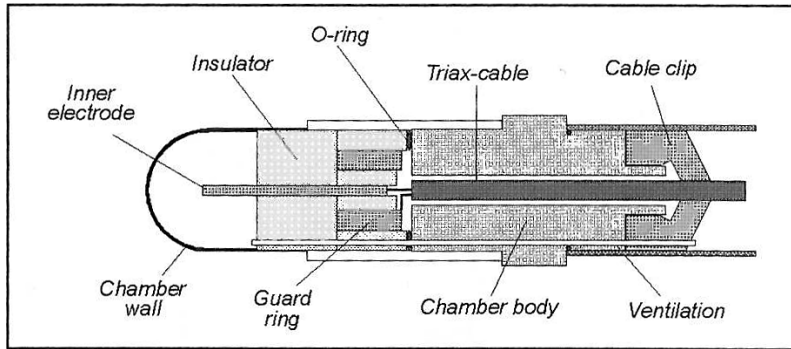
Figure 4: A standard thimble-type ionization chamber, similar to the ionization chamber used in experimental measurements in this thesis. Figure taken from Metcalfe et al (1997) [3].

This type of chamber is similar to the basic chamber introduced in section 2.2.1. The chamber wall acts as one of the electrodes, and the central rod, which is usually made from aluminum, acts as the other electrode. [15]

2.2.4 Calculating dose using an ionization chamber

The principle behind ionization chamber dose measurement lies in that the dose can be related to the number of ion pairs created within an air cavity. This is because of the fact that an electron that slows down in air produces a constant amount of charge per unit energy lost, independent of the electron's energy [17]. In other words, the energy deposited in an air cavity is directly proportional to the number of ion pairs created. This relationship is expressed with the following formula:

$$E_{air} = \left(\frac{\overline{W}_{air}}{e}\right) Q_{air} \qquad (14)$$

E_{air} is the energy lost by electrons in the air, Q_{air} is the charge released in the air, and $\left(\overline{W}_{air}/e\right)$ is the energy lost per charge produced. For air, $\left(\overline{W}_{air}/e\right)$

23

is equal to 33.9 eV. From the definition of absorbed dose (eq. 8), the relationship between the absorbed dose to the air, D_{air}, and Q_{air} becomes:

$$D_{air} = \left(\frac{\overline{W}_{air}}{e}\right)\frac{Q_{air}}{m_{air}} \qquad (15)$$

Applying Bragg-Gray cavity theory (eq. 13), a the dose for an air-filled ionization chamber in a water phantom, D_{med}, and Q_{air} becomes:

$$D_w = D_{air}\left(\frac{\overline{S}}{\rho}\right)_{air}^{w} = \left(\frac{\overline{W}_{air}}{e}\right)\frac{Q_{air}}{m_{air}}\left(\frac{\overline{S}}{\rho}\right)_{air}^{w} = constant \cdot Q_{air} \qquad (16)$$

For a given ionization chamber, the volume and hence the mass of the air in the cavity will be supplied through the calibration coefficient. This coefficient is retrieved either from the manufacturer or from a standards laboratory. The stopping power ratios can be found from a table such as in Attix (1986). It has already been established that $\left(\overline{W}_{air}/e\right)$ is constant. This means that for an ionization chamber in a water phantom, the only variable is the charge collected, Q_{air}, while the remaining terms are constant for identical conditions. In reality, there are several factors that complicate the calculations, including atmospheric conditions, ion recombination, beam quality, chamber perturbation etc. These are explained in greater detail in section 2.2.5. [2, 11, 15]

2.2.5 Ionization chamber dosimetry according to TRS-398

The International Atomic Energy Agency (IAEA) is an agency in the United Nations family concerned with the nuclear field. It strives to monitor nuclear technologies and promote nuclear safety. One of the duties of the IAEA is to issue recommendations in the field of dosimetry. One of these recommendations is the Technical Report Series #398 (TRS-398) that is concerned with dose determination based on absorbed dose to water [2].

According to IAEA TRS-398, the absorbed dose to water measured with an ionization chamber is

$$D_{w,Q_0} = M_{Q_0} N_{D,w,Q_0} \qquad (17)$$

In the above formula, M_{Q_0} is the reading of the dosimeter at a standards laboratory, and N_{D,w,Q_0} is the calibration coefficient obtained for the ionization chamber with respect to the dosimeter at a standard laboratory at reference beam quality Q_0. Q_0 is normalized to Co-60 for this thesis. The calibration factor is determined in units of µGy/nC. However, equation 17 is only true if conditions are identical to the conditions at the standards laboratory. This is generally not the case, which means that some corrections have to be done to compensate for the differences. The IAEA has a set of factors for the calibration of ionization chambers. These will be summed up in this section.

- **Beam quality factor k_{Q,Q_0}:** The beam quality factor k_{Q,Q_0} is a factor to correct for difference in the ionization chamber response to the beam quality factor of the user beam Q and reference beam Q_0. It is defined as

$$k_{Q,Q_0} = \frac{N_{D,w,Q}}{N_{D,w,Q_0}} = \frac{D_{w,Q}/M_Q}{D_{w,Q_0}/M_{Q_0}} \qquad (18)$$

For high energy photons with a beam quality Q, k_{Q,Q_0} is specified by the Tissue-Phantom Ratio $\mathrm{TPR}_{20,10}$,which can be found using equation 19.

$$TPR_{20,10} = \frac{D(20,S,E)}{D(10,S,E)} \qquad (19)$$

where the beam energy E and field size S are held constant. Using a 10cm x 10cm field size and a constant SAD of 100 cm, the absorbed dose is measured at a depth of 10 g/cm^2 and then at a depth of 20 g/cm^2. From this calculated value of the $\mathrm{TPR}_{20,10}$, a corresponding beam quality factor k_{Q,Q_0} can be looked up in a table. Typically the value for k_{Q,Q_0}ranges from 0.96 to 1.005. [2]

- **Atmospheric factor $k_{\mathbf{TP}}$:** The gas in the ionization chamber is subject to change with varying temperature and pressure. Therefore an atmospheric factor k_{TP}, given by eq. (20), has to be taken into account if atmospheric conditions are different from the conditions at the time of calibration

$$k_{TP} = \frac{(273.2 + T)}{(273.2 + T_0)} \frac{P_0}{P} \qquad (20)$$

where P and T are the pressure and temperature in the chamber at the time of measurement, while T_0 and P_0 are the reference conditions of the chamber. In Norway the reference conditions are T_0= 20°C and P_0= 101.3 kPa.

- **Ion recombination factor k_s:** Some of the ion pairs created recombine before they are registered by the electrodes. The ion recombination factor corrects for this:

$$k_s = a_o + a_1 \left(\frac{M_1}{M_2} \right) + a_2 \left(\frac{M_1}{M_2} \right)^2 \qquad (21)$$

Where M_1 and M_2 are the electrometer readouts at $V_1$and V_2, respectively. Constants a_0, a_1, a_2 depend on the value of $\frac{V_1}{V_2}$, and are retrieved from a table as calculated by Weinhous et al (1984). Typical values range from 1.002 - 1.008. [19]

- **Polarity factor k_{pol}:** This effect is mostly negligible for photon beams, but can be prominent for charged-particle beams. It is given by

$$k_{pol} = \frac{|M_+| + |M_-|}{2M} \qquad (22)$$

where M_+ and M_- are electrometer readings obtained at positive and negative polarity, respectively. M is the electrometer reading at the routinely used polarity. The polarity correction was not taken into account for the photon measurements in this thesis as its effect is assumed to be negligible in photon beams. [2]

- **Perturbation factors:** The ionization chamber perturbs the beam due to the cavity inside the chamber, the chamber wall and the waterproof sleeve. For high energy photon beams in a water phantom, all of these effects are assumed to be accounted for in the k_{Q,Q_0} factor. [2]

2.3 High energy photon beams - apparatus

2.3.1 A brief introduction to the linear accelerator and its components

The info in this section is only intended to give an idea of how the linear accelerator is built up, not to give a broad understanding of how the individual components work.

A schematic of a typical linear accelerator is shown in Figure 5.
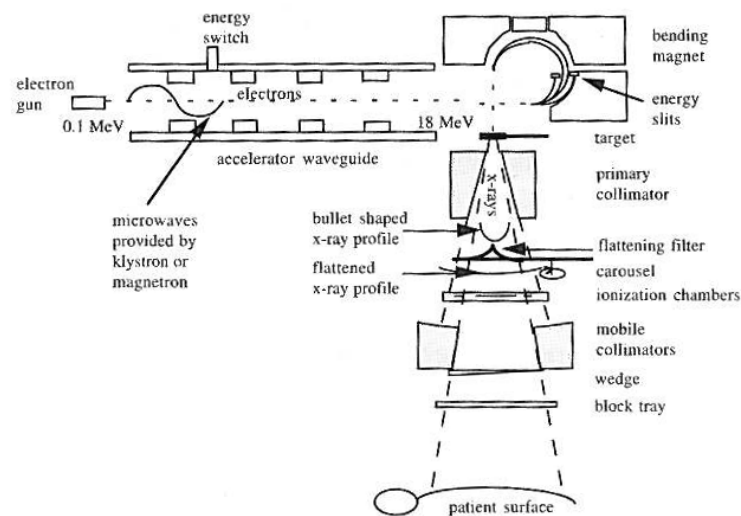
Figure 5: Schematic of the components of a typical linear accelerator showing an example of a 270° bending magnet. Figure taken from Metcalfe et al (1997) [3].

Electrons are shot out from the electron gun with an energy of about 0.1 MeV, and then enter the accelerator waveguide. Here the electrons experience very high-power microwaves produced by a klystron or magnetron, and they "surf" on these microwaves causing their energy to drastically increase. By the time the electrons exit the waveguide their energy has been amplified to the order of several MeV. In connection with the accelerating waveguide is an auxiliary system that controls the pressure, temperature and shields the surroundings from radiation. Although not directly responsible for accelerating electrons this system is important in other respects.

In order to focus the accelerated electron beam it is now bent with the use of a bending magnet. There are currently three different types of bending magnets; 90° bending, 112.5° slalom bending and 270° achromatic bending.

After bending, the electron beam enters the treatment head, which contains a number of beam-shaping elements as well as some quality control elements. First, there is a removable target that is used to produce high-energy x-ray photons for photon radiation. The resulting photon radiation will have a bullet-like profile, so a flattening filter is used to flatten the dose profile. If the target is removed, the electrons can be scattered using an electron scattering foil.

Exiting the flattening filter, the beam traverses two independent ionization

chambers (see section 2.2) that constantly monitor the beam output and shut down the linac if discrepancies are detected. The ionization chambers measure so-called monitor units (MU). These units are a relative measure of machine output. 100 MU usually corresponds to a dose of 1 Gy at 10 cm depth with 100 cm SSD and 10cm x 10cm field size, but this can vary. Once a predetermined number of MU is detected, the primary ionization chamber shuts down the linear accelerator. If the primary ionization chamber fails to shut down the linear accelerator, the secondary ionization chamber will shut it down as a safety measure, usually if the detected number of MU exceeds the predetermined number by a certain amount. Finally, the beam is shaped by a set of different collimators, as described in the next section. [20, 3, 21]

2.3.2 Beam shaping

a)   b)
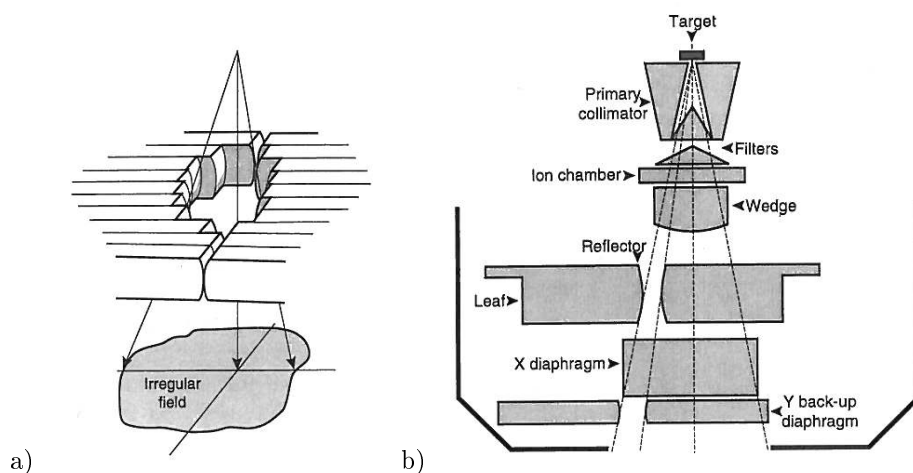
Figure 6: a) A simplified multi-leaf collimator (MLC), used to create irregular fields. b) Schematic diagram if a collimator head with an integrated MLC. Figures taken from Greene and Williams (1997) [20]

Collimators are usually made of tungsten or lead, and very efficiently block the radiation. The primary collimator has a shape that resembles a hollow cone with the top cut off. This collimator helps prevent scattered photons from exiting the treatment head. The resulting field has a circular shape and represents the maximum field size possible. The two sets of secondary collimators are shaped like jaws, which can be adjusted to produce different size rectangular fields. Optionally, the beam will then pass through a Multi-Leaf Collimator (MLC, see fig. 6). The MLC allows for a very specified beam, and tailors the dose profile to individual tumors [22]. An example of a collimator head with an integrated MLC can be seen in figure 6.

The gantry is the movable arm on the linear accelerator, shown in figure 7. It allows the beam to be rotated around the patient.

The collimator jaws will be labeled according to the standard defined by the IEC. The Y2 parameter is closest to the gantry, Y1 furthest away from the gantry, X1 at the patients right and X2 at the patients left. The beam axis is

defined as the line between the radiation source and the geometric field center. The collimator axis is the line from the source to the isocenter. [23, 24]

Figure 7: External view of linear accelerator. Figure taken from IEC 1217 [23]

2.3.3 Cobalt-60

Cobalt-60 (Co-60) is a radioactive isotope that was up until the 1980's the main source for radiation in radiotherapy. Artificial Co-60 is produced by bombarding Co-59 with slow neutrons. In the decay process, Co-60 emits one electron with an energy of up to 315 keV, and then two gamma rays with energies 1.173 MeV and 1.333 MeV in equal quantities. It has a relatively long half life of 5.27 years which, combined with the nearly monochromatic high-energy photon emission, makes it a favorite for calibration and laboratory work. A schematic of a typical Co-60 machine can be seen in figure 8.

Whereas the ionizing radiation in a linear accelerator is created mechanically inside the machine, the Co-60 machine contains a radioactive source and hence the radiation present all the time, unlike the linear accelerator where the radiation is created mechanically. This means that the Co-60 source has to be shielded from its environment when the machine is not operational, and exposed only when needed. The housing for the source is called the source head, and it consists of a steel shield filled with lead for protection, and some device that can bring the source to the front of an opening and back. [12, 25]

The Co-60 source at the NRPA SSDL was used to calibrate the film batches for this thesis, see section 3.3 for further details.

Figure 8: Co-60 Gammatron at the NRPA. Photo taken by Hans Bjerke.

2.3.4 Calibration and measurement conditions according to standard

The IAEA Technical Report Series no. 398 considers the determination of absorbed dose in external beam radiotherapy, as well as calibration of the necessary instruments to determine this dose.

A Co-60 (Cobalt) source is the most commonly used radiation quality for calibration and reference. In Norway calibration of ionization chambers have traditionally been performed at the secondary standard dosimetry laboratory (SSDL) at the NRPA. The standard ionization chambers at the SSDL have in turn been calibrated at a primary standard dosimetry laboratory (PSDL) [5, 6]. The IAEA TRS-398 and ICRU report 64 recommends measuring the absorbed dose in a water phantom. This water phantom should have dimensions that extends 5 cm from each side of the radiation field (R50), and the measurement should be made no less than 5g/cm² from the bottom of the tank. For reference measurements in a water phantom on linear accelerators, both 5 g/cm² and 10 g/cm² depths can be used, according to IAEA TRS-398. [2, 26] More on the practical aspects of ionization chamber calibration is explained in chapter 3.1.3.

2.4 High energy photon beams - characteristics

2.4.1 Depth dose and build-up

A typical depth dose curve for photons is shown in figure 9. It shows the relationship between photon fluence and depth in the medium. One important thing to note is that the maximum dose D_{max} is not at the surface, but at a some depth. This is because of the range of the secondary electrons. The electrons that are excited at the surface will, on average, travel a given distance before they deposit dose. This rapid increase in absorbed dose the first mm is called dose build-up. The point in which the deposited dose is highest is called the dose max (or d_{max}), and is measured from the surface of the medium. [3, 27]
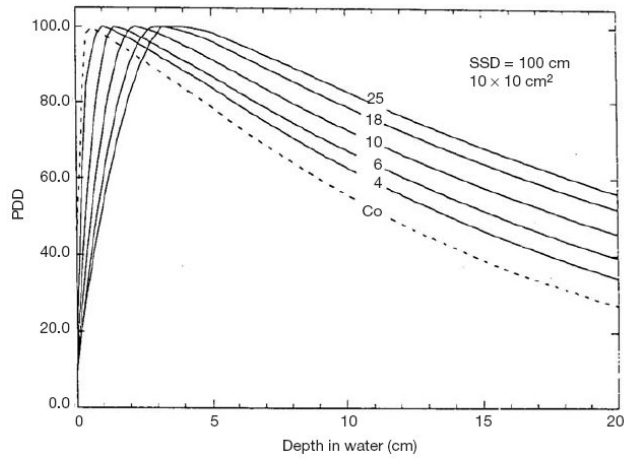
Figure 9: Photon depth dose distribution curve for a 10x10 field at 100 cm SSD for different beam qualities. Figure taken from Podgorsak (2005) [27].

2.4.2 SAD and SSD
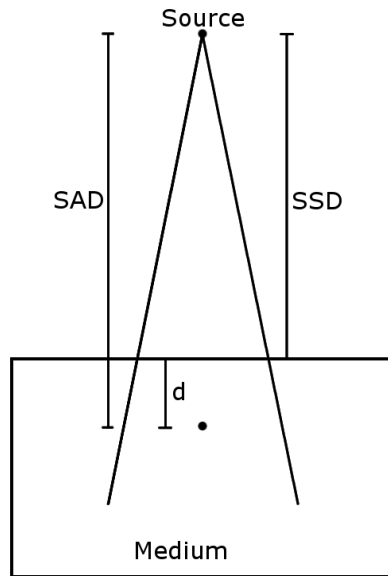
Figure 10: Relationship between SSD, SAD and d in a medium.

Dose is generally measured in a reference point d that lies in a medium of some sort (usually water). There are several terms that describe the distance to the source of radiation, but the two that will be used in this thesis are Source-Axis Distance and Source-Surface Distance. The Source-Axis Distance (SAD) is defined as the distance between the radiation source and the geometric center

of the radiation field(s). It is usually set to 100 cm. The Source-Surface Distance (SSD) is the distance from the radiation source to the surface of the medium. The SSD and SAD are closely related with the formula:

$$SAD = SSD + d \qquad (23)$$

This relationship is also shown in figure 10. The SSD is an important part of determining how dose varies with depth. This variation can be approximated using the following relationship:

$$D_d = D_{max} \frac{(SSD + d_{max})^2}{(SSD + d)^2} f(d, A) \qquad (24)$$

where D_d is the dose at depth d, D_{max} is the dose at depth d_{max}, and $f(d, A)$ is an exponential function dependent on the depth d and field A. [28, 29]

2.4.3 Lateral dose distribution
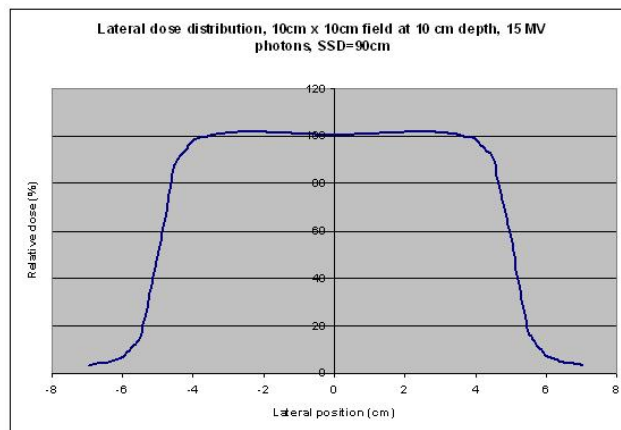
Figure 11: 15 MV photon lateral dose distribution. Taken from Eclipse dose planning software.

The lateral dose distribution shows how the dose is distributed at a given depth. Figure 11 shows the lateral distribution of a 10x10 cm^2 15 MV photon field at 10 cm depth with 90 cm SSD. In radiotherapy, it is beneficial to have a sharply defined field in order to minimize the dose to surrounding normal tissue. However, it is clear from the lateral dose distribution that the radiation field edges have a slope. This is because some radiation will always pass through the edges of the collimator blocks. The edge of the field usually coincides with the point that receives 50 % of the max dose.

The penumbra of a radiation field is defined as the distance between the point with 80 % max dose and the point with 20 % of the max dose. This can be seen in figure 11. Penumbra is used as a measure of field sharpness, and it is generally desirable to have penumbra values that are as low as possible. [3, 12]
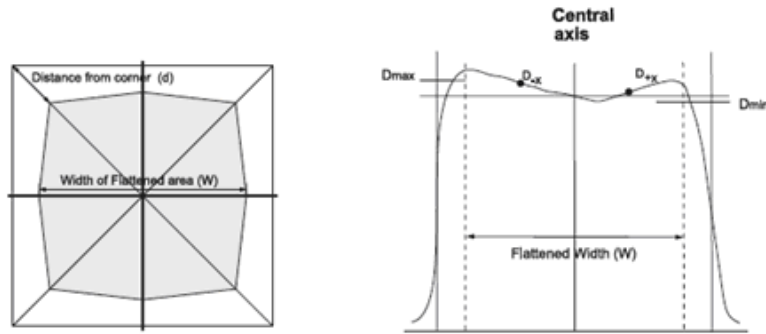
Figure 12: Field flatness and symmetry, showing the flattened area

2.4.4 Flatness and symmetry

An ideal beam has a uniform profile. However, it is clear from figure 11 and 12 that this is not the case as the dose peaks on each side of the central axis. The uniformity of a megavoltage x-ray beam is measured on dose profiles taken through the center of the x-axis and y-axis. It is usually measured through two quantified parameters, field flatness and symmetry. These are determined within a flattened area of the beam profile, which is defined at 80 % of the field size for 10x10cm^2 -30x30 cm^2 fields(see figure 12). For fields smaller than 10x10 cm^2, the flattened width W is 2 cm less than the field size. Flatness and symmetry are then defined according to the flattened beam profile. [3, 24]

- Flatness is defined as the ratio between D_{max} and D_{min} within W.

$$F = \frac{D_{max}}{D_{min}} \cdot 100\% \qquad (25)$$

  Ideally this value should be close to 1, indicating a completely flat beam profile.

- Symmetry is given by the maximum value of the ratio between D_{-x} and D_{+x} within the flattened area.

$$S = \left(\frac{D_{-x}}{D_{+x}} \right)_{max} \cdot 100\% \qquad (26)$$

  Ideally this value should be close to 1, indicating a completely symmetrical beam.

2.4.5 Relevant special techniques for beam shaping

Modern linear accelerators are equipped with secondary collimators that can be moved individually of each other and rotated. In addition, many linacs are equipped with multi-leaf collimators. This means that a lot of irregular fields are used in clinical treatments.

Asymmetric fields are basically fields that are not symmetrical over the collimator axis. A half-collimated field refers to a field where one of the secondary collimators is placed up to the collimator axis. This is equivalent to one of the

collimator parameters (X1, X2, Y1 or Y2) being set equal to zero. This means
that the beam axis is different from the collimator axis. An example of a half-
collimated beam can be seen in figure 13. Overtravel refers to the case where
one or more of the collimators are forced beyond the collimator axis, and thus
the field does not include the isocenter. Spliced fields refers to the case where
two fields border each other, but do not intentionally overlap. The formalism of
dose calculations to such fields is to broad to be discussed here, but for manual
dose calculations in asymmetric and irregular fields, see Khan (2003) [12].
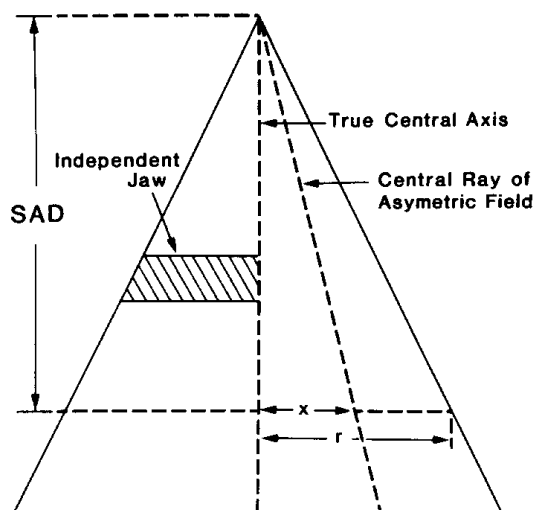
Figure 13: Half-collimated field, a type of asymmetric field. Notice that the
new beam axis is vastly different from the true central axis, or collimator axis.
Taken from Khan et al (1986) [30]

Experimental procedures in this thesis include exposing radiochromic film
to different asymmetric fields, with and without collimator rotation. More info
about the technical details of the experimental field setups can be found in
section 3.4. The main purpose was to test how the dose planning systems
predicted dose distributions of non-standard fields.

3   Experimental methods and equipment

A substantial part of this thesis has been to develop a method for dosimetry using the radiochromic film in relation to the absorbed dose to an ionization chamber in a water phantom in order to perform absolute dosimetry using film. It is important to relate the new film dosimetry to existing procedures. With new modalities such as Intensity Modulated RadioTherapy (IMRT) becoming more common, methods limiting the absolute dosimetry to measuring the dose in one point in a 10x10 cm^2 field are becoming insufficient. Much care was taken to develop a functional setup that would be easily reproducible at all radiotherapy institutions in Norway, and sufficient for obtaining relevant parameters.

3.1   Absolute dosimetry in reference conditions

3.1.1   Ionization chamber

Figure 14: The ionization chamber type used in all measurements pictured along with its protective sleeve. The picture is taken from the product brochure. [31]

The chamber used for the experimental measurements was a Wellhöfer FC65-G thimble chamber (Scanditronix Wellhöfer, Schwarzenbruck, Germany) with serial no 446. A photo of the chamber type can be seen in figure 14.

This type of ionization chamber has an active volume of 0.65 cm^3. The outer electrode is made from graphite and the inner electrode is made from aluminum. [31]

3.1.2   The water phantom

The "Bjerke Phantom" [32] is a water phantom built to the standards suggested in the IAEA TRS-398, as described in section 2.3.4 . Its lateral dimensions are 27cm x 26cm, and the depth is 18 cm. It can therefore accommodate a maximum field size of 15cm x 15cm and a measuring depth of 10cm while staying within the recommendations presented in IAEA TRS-398 [2]. The Bjerke phantom is shown in figure 15.

The Bjerke phantom is compatible with both cylindrical (thimble) and plane-parallel chambers. For the experiments, only a cylindrical chamber was used. [10, 32]
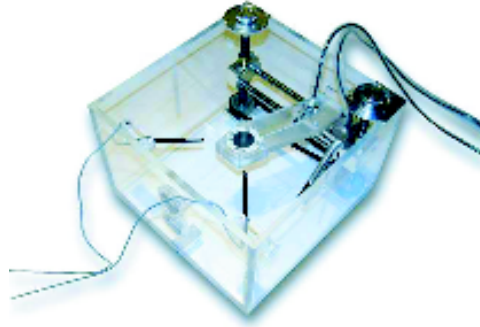
Figure 15: Photo of the Bjerke phantom, the water phantom used for ionization chamber measurements. Picture taken from poster presentation of the phantom. [32]

3.1.3 Calibrating the ionization chamber

The ionization chamber was calibrated on the Co-60 source at the NRPA SSDL prior to use, and used for all absolute measurements at the hospitals. The calibration procedure was carried out as recommended by the NRPA [33]:

1. A 30x30x30 cm^3 water phantom was set up with the center of the ionization chambers at 5g/cm^2 depth, and the ionization chambers were exposed to a 10x10cm ^{2} beam for 2 minutes.

2. The electrode current was measured using a Capintec PR-06G ionization chamber (Capintec Inc., Ramsey, NJ, USA) calibrated at BIPM, and the dose rate in water was calculated using the equation

$$D_w = I_{c,std} \times k_{TP} \times N_{D,w,std} \tag{27}$$

   where $I_{c,std}$ is the average value of 50 electrometer current readings taken at 1 per second, k_{TP} is the atmospheric correction factor as mentioned in section 2.2.5, and $N_{D,w,std}$ is the calibration coefficient calculated at the SSDL.

3. The setup was repeated for the user chamber, and the user chamber calibration coefficient was defined to be

$$N_{D,w} = \frac{D_w}{I_c \times k_{TP}} \tag{28}$$

   In this equation, D_w is the dose rate to water calculated from equation 27, I_c is the average electrometer current reading and k_{TP} is again the atmospheric correction.

The uncertainty for this procedure is reported to be 0.72 %, equivalent to 2 standard deviations [34].

3.1.4 Ionization chamber setup
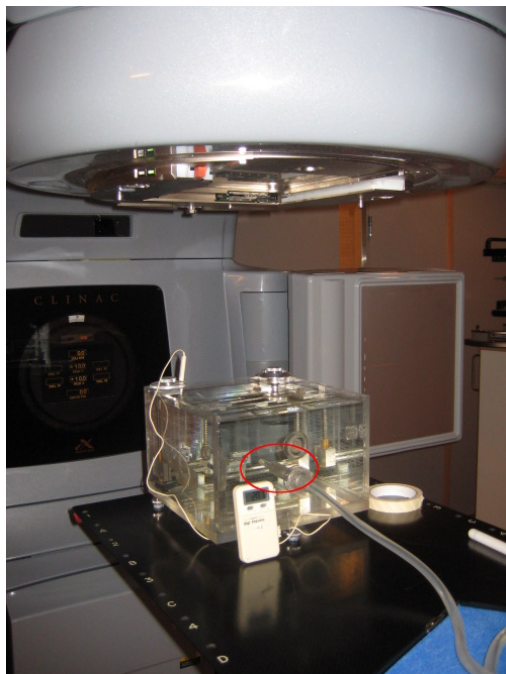
Figure 16: Ionization chamber setup for absolute dosimetry verification. The location of the ionization chamber is marked with a red circle. Picture taken at UUS.

In order to link the film to absolute dosimetry locally at the hospital, measurements were done at reference conditions recommended by the IAEA [2]. An ionization chamber was set up in a water phantom (see section 3.1.2) at 10 g/cm^2 depth and 90 cm SSD. It was placed in the isocenter of a 10x10cm^2 field and exposed to a number of monitor units (MU) corresponding to 2 Gy at the measuring point. For most linear accelerators, this was equivalent to 200 MU, but for some it was equivalent to 260 MU. Collected charge was measured with a Keithley 35040 Therapy Dosimeter (Keithley Instruments Inc., Cleveland, OH, USA) . Measurements were done at 15 MV and 6 MV energies for most linear accelerators, and at both 300 V and 100 V to measure electron recombination (see section 2.2.5).

3.1.5 Ionization chamber dose calculation

The ionization chamber was subjected to both 6 MV and 15 MV photons on most linear accelerators, with a potential difference on the chamber of both 300 V and 100 V, to be able to account for recombination. Measurements were not performed for 6 MV photons on linear accelerators where the calibration depth differed from 10 g/cm^2. The average of three measurements was used for the value of the collected charge for each energy and chamber voltage, a total of 12 readings per linear accelerator. For each setup, the temperature and air

pressure was recorded to account for atmospheric effects on the chamber. The uncertainty in this procedure is within 2 %.

To easily and efficiently calculate the dose to the chamber, a standardized Excel spreadsheet made by the IAEA was used [35]. The spreadsheet was slightly modified for this thesis to suit the experimental methods better.

3.2   Radiochromic film

Radiochromic film responds to ionizing radiation by changing optical density when exposed. In short, this means that there is a detectable color change in the film when it is irradiated. The GafChromic® (International Specialty Products, Wayne, NJ, USA) type of film has an active layer of crystalline diacetylene monomers that when radiated combine to form diacetylene polymers, releasing a special dye that causes the film to change color [36]. Because the color change happens near instantaneously, it is time-saving in comparison to conventional films that need to be developed in a darkroom.

It is also cost-effective because each film can be cut into smaller pieces and they can also be scanned on a commercial flatbed scanner. The reduced costs of not depending on a darkroom or an expensive medical scanner has led to a much more wide-spread use of film for dosimetry purposes in hospitals.

Two film types were used in this thesis: GafChromic® EBT (External Beam Therapy) and GafChromic® RTQA (RadioTherapy Quality Assurance). GafChromic® EBT type film was used for nearly all the experiments.

GafChromic® RTQA film was only used in the starting phases of the experiments, to check the correlation between the light field and the radiation field. For the remainder of the thesis "radiochromic film" refers to GafChromic® EBT, unless otherwise specified.

3.2.1   Optical density and dose

It is assumed that the absorbed dose to the film is reflected by a change in its optical density (OD). This assumption is crucial for film dosimetry. The general expression for OD can be written as:

$$OD = \log\left[\frac{I_0}{I}\right] \tag{29}$$

Equation 29 shows the simple way of looking at optical density. I and I_0 correspond to the pixel intensities of exposed and unexposed films, respectively.

In order to connect the optical density to the dose a sensiometric calibration curve is required (see section 3.3.2 and figure 21). The sensiometric curve relates the dose to optical density change through a curve approximation, which will be explained in greater detail in section 3.3. [37]

3.2.2   GAFCHROMIC® EBT

GafChromic® EBT film is manufactured by International Specialty Products (Wayne, NJ, USA), and is intended for use in external beam radiotherapy (EBT). It can be used for quantitative as well as qualitative dosimetry. This type of film has a layer structure that can be seen in figure 17. The film has

double active layers that increase its precision. A 6 µm surface layer is sandwiched between the two 17 µm active layers, which are both covered by a 97 µm clear polyester layer. The clear polyester layers allow for easy handling of the film and minimizes effects of UV radiation.
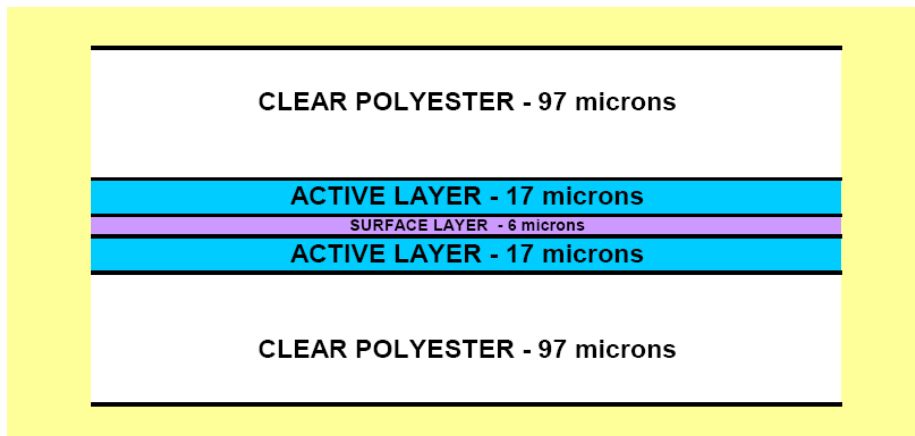
Figure 17: Layer structure of GafChromic® EBT film. Figure taken from product presentation [38].

Having a double active layer attributes to a high sensitivity. This makes the film ideal for IMRT verification and other advanced treatments. The absorption spectrum of the film is shown in figure 18. The film is most sensitive at wavelengths around 635 nm, which corresponds to the color red. This means that the best signal can be obtained from isolating the red color channel after scanning the film.

The film has a transparent light blue color when unexposed, which changes to dark blue as the film is exposed to ionizing radiation. The atomic composition of the GafChromic® EBT film is H (39.7 %), C (42.3 %), O (16.2 %), N (1.1 %), Li (0.3 %) and Cl (0.3 %). This composition gives the film an effective atomic number, Z_{eff}, of 6.98 which is very close to Z_{eff} for water which is 7.4 [1, 38]. A typical exposed film is shown in figure 19. The film has been exposed to two 200 MU 20x10 cm^2 fields as well as two 200 MU 5x8 cm^2 fields. This means that the film was exposed to 400 MU where the fields overlap. The correlation between the dose given and change in optical density is evident.

According to the manufacturer, the film is not sensitive to room light, but can be sensitive to direct sunlight. In addition, the film can be sensitive to extreme temperatures. Therefore it is recommended to keep the films in a dark dry environment at normal room temperature (20-25°C). GafChromic® films can be submersed in water up to an hour, allowing for the film to be irradiated while in a water phantom. [38]

The optical density change in the films is reported to be very weakly dependent on the energy of the radiation. The manufacturer claims that the film is energy independent from kV to MV energies. Recent studies show that there is at most a marginal difference in optical density change from radiation in the megavoltage (MV) range as compared with radiation in the kilovoltage (kV) range. In the MV range the variation has been found to be within the uncer-
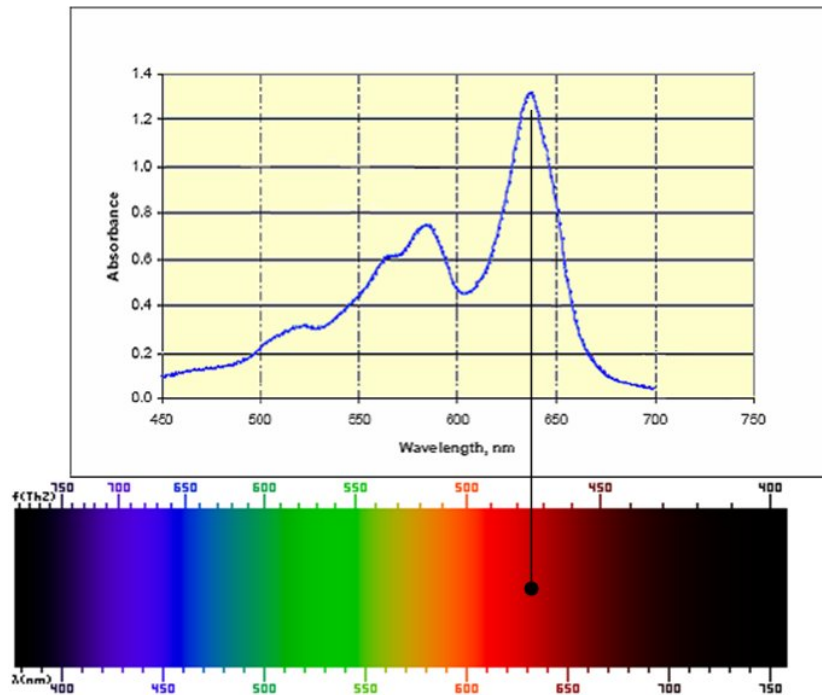
Figure 18: Absorption spectrum of GafChromic® EBT film. The absorption peak is at approx 635 nm, corresponding to red color. Spectrum taken from EBT product brochure [36].

tainty of the film [39, 40]. This means that films exposed to a certain photon energy can be calibrated to a curve that has been obtained at a different photon energy (see sections 3.3 and 3.3.2). Studies show that noticeable optical density changes occur within the first 6 hours after exposure [41]. This is important to take into account when scanning the films, see section 3.5.1 for more detail.

GafChromic® EBT films come in batches with individual lot numbers, and it is reported that films from the same batch have identical response to ionizing radiation [38]. However, the response may vary from batch to batch. When calibrating films for absolute dosimetry, a calibration curve has to be created for each film batch. This is explained in detail in section 3.3.

3.2.3   GAFCHROMIC® RTQA

GafChromic® RTQA (RadioTherapy Quality Assurance) film is produced by International Specialty Products, and is intended for use in Quality Assurance only. The film has a single active layer, and changes color from orange to brown when radiated. GafChromic® RTQA has a three-layer laminate configuration; a top substrate of clear orange polyester, an active layer as discussed earlier, and a base substrate of opaque white polyester. Hence it is reflective, not transparent like other types of radiochromic film. [42]. The film's structure is shown in Figure 20.

Figure 19: Typical example of an exposed GafChromic® EBT film. The film has been exposed to two 200 MU 10x20 cm^2 fields as well as two 200 MU 5x8 cm^2 fields.
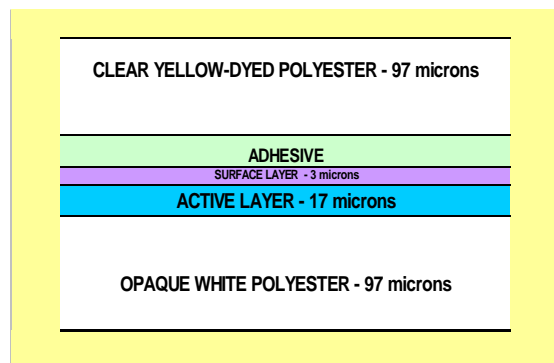
Figure 20: Layer structure of GAFCHROMIC® RTQA film. Exact thickness of the layers can vary slightly [36]

GafChromic® RTQA film is ideal for testing the correlation between light fields and radiation fields, as well as simple field homogeneity tests. This type of film can not be used for obtaining quantitative results, but was utilized for some light field alignment and geometrical calibration procedures.

3.3 Film calibration

Recent literature has reported that GafChromic® EBT film can be used for absolute dosimetry with a relative error of about 1.3 % [43]. In order to perform absolute dosimetry, the films have to be calibrated to a sensiometric curve. An example of a sensiometric curve can be seen in figure 21.
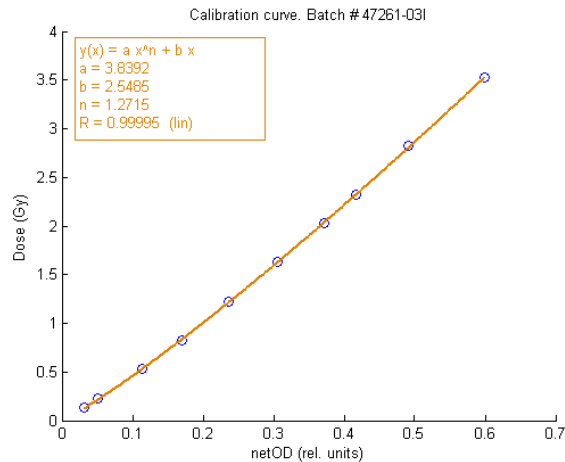
Figure 21: An example of a sensiometric calibration curve. The figure has been created using SensiometriCal (see section 3.6).

3.3.1 Calibration setup

For the calibration procedure, a piece of film was cut into strips of approx 12.5cm x 3cm. These strips were held in place using a self-made clamp-like apparatus at the top and bottom of the strip and submerged in water at 5 g/cm^2 depth with a SSD of 95 cm. This setup can be seen in figure 22. As studies have shown that the optical density, and thus the dose, is not energy dependent [38], films were calibrated using the Co-60 source at the NRPA SSDL. For each batch 11 film strips were exposed to different doses. The doses used were approximately 0.1, 0.2, 0.5, 0.8, 1.2, 1.6, 2, 2.3, 2.8 and 3.5 Gy. The exact given doses were measured before each calibration procedure using an ionization chamber placed at 5 g/cm^2 depth. A 10 x 10 cm^2 field was used, with the film piece placed at the center of the field, meaning that most of the film was well within the beam edges. This was done to give the main part of the film piece a homogeneous dose.

After exposure the films were scanned according to the procedure described in section 3.5.1. The averaged scans were imported into Matlab, where a 5x5 pixel Wiener filter was applied to the image. The netOD was calculated for each pixel using equation 30.

A region of interest (ROI) of approximately 20x20 pixels was defined in the center of each calibration film, and the median netOD value of this ROI was used as the pixel intensity. This median value was plotted against the dose for each calibration film, producing a sensiometric curve.

3.3.2 Absolute dosimetry using GAFCHROMIC® EBT film

In literature several different polynomial approximations are used for a curve fit of the measured data points. Devic et al (2005) recommends a curve fit of the form $D(OD) = a(OD)^n + b(OD)$ where a, b and n are parameters to be decided [1, 44]. However, Paelinck et al (2007) found that a third-order polynomial curve fit produced satisfactory results [45].
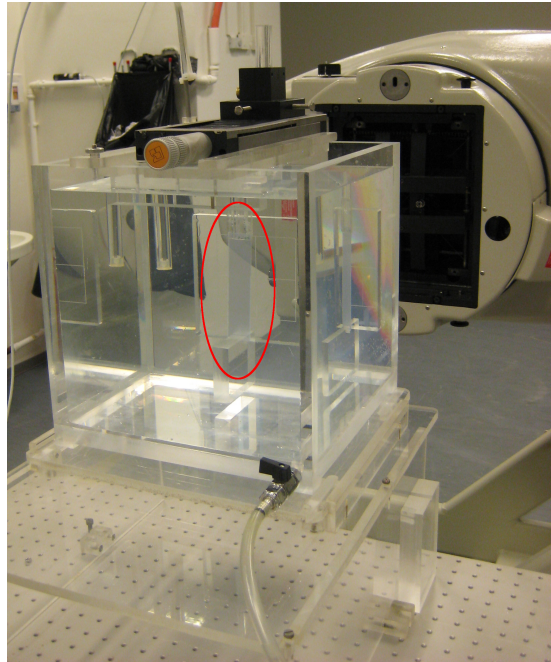
Figure 22: Film calibration setup. The film (marked with a red circle) is held in place at the top and bottom by clamps in order to hold the film in place at 5 g/cm^2 depth. Photo taken at the NRPA.

For the measurements in this thesis, calibration values were plotted as described in section 3.3. The points were fitted with a curve on the form $D(OD) = a(OD)^n + b(OD)$ for each batch of films, but a a third-order polynomial approximation was also calculated to see whether this curve had a better fit, which it did not have for any of the batches used. For each film used in the experiments, the dose was determined applying the calibration curve formula on each pixel in processed image.

3.4 Film setups

For the film experiments three radiochromic films were used for each photon energy. Each film was cut into two pieces, and each piece was placed under a 20x20x10 cm^3 PMMA water tank at 90 cm SSD. The tank was filled with water to a level equivalent to the film piece being at 10g/cm^2 depth. This setup can be seen in figure 23.

The films were cut using a sharp rolling-blade paper cutter. When handling films, gloves were used to avoid fingerprints and smudges. The film was kept in light-proof envelopes before and after exposure, to minimize light exposure. Two films were used for each photon energy, each cut into two pieces. One film was cut into a 20x15 cm^2 piece and a 20x10 cm^2 piece, and the other film was cut into equal parts of 20x12.5cm^{2}pieces. The fields were given in a single fraction of 200 MU normalized to equal an absorbed dose of 2 Gy at 10 g/cm^2 depth, or equivalent. The collimator parameters are defined according to IEC
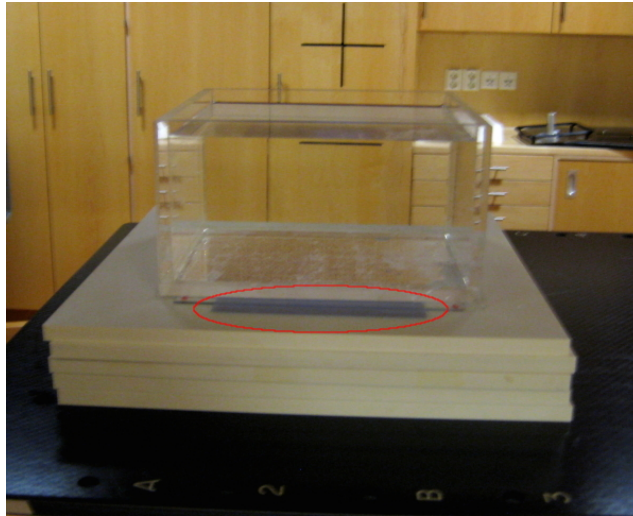
Figure 23: Film irradiation setup. Films are inserted into a slit at 10 g/cm^2 depth under a water phantom. This slit is shown in the red circle. For backscatter, approx five 1 cm solid water plates were used. Photo taken at UUS.

international standard 1217 [23].

The fields were chosen based on the following criteria:

- The fields must be reproducible at all hospitals and for all linear accelerator manufacturers. This was proved to not always hold true for setup #2 as not all linear accelerators have overtravel capability in both secondary collimator directions.

- The fields must be of a character that allows for easy extraction of relevant parameters in Matlab or other image processing software

- The selected fields must shed light on areas where ordinary quality controls are lacking, e.g. collimator rotation, spliced fields, overtravel fields.

3.4.1 Treatment planning

All fields that were used for film exposures were planned out in dose planning software. For Varian treatment units, the fields were planned in Eclipse™ Treatment Planning System by Varian Medical Systems (Palo Alto, CA, USA). For Siemens and Elekta units, the fields were planned in Oncentra MasterPlan (Nucletron B.V. ,Veenendaal, The Netherlands). Dose matrices were for the most part calculated at 10 cm depth with a resolution of 1.25 mm or better using a collapsed cone convolution algorithm to approximate the dose. In some cases a pencil beam convolution algorithm was used.

The dose matrices were exported as DICOM (Digital Imaging and Communications in Medicine) files, a standard format for transmitting information in medical imaging [46]. These files could then be analyzed with VerA (see section 3.6) in order to compare the calculated distribution from dose planning software to the measured distribution from the film. Treatment plan reports from Eclipse are attached in appendix A.8.

3.4.2 10x10 setup

A 15x20 cm^2 piece of film was exposed to a 10x10 cm^2 field, the same field as for the ionization chamber setup. This gives a secondary measure of the absolute dosimetry, as the dose at the isocenter obtained from the film should equal the dose measured at the isocenter using the standard setup with ionization chamber.

3.4.3 Setup #1
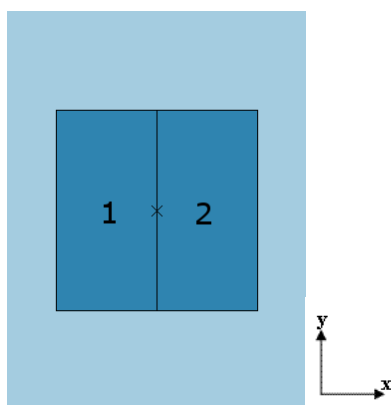
Figure 24: Beams-eye view of experimental setup #1 consists of two 5x10 cm^2 adjoining fields on a 20x15 cm^{2}film piece. The field isocenter is denoted by ×, and the positive y-direction points towards the gantry.

For the first setup, the 20x15 cm^2 film piece was exposed to two 5x10 cm^2 fields, which can be seen in figure 24. This setup will serve as a test of the precision of the secondary collimator jaws without rotation, in a spliced fields technique. The two 5x10 cm^2 fields have parameters:

1. X1 = 5 cm, X2 = 0 cm, Y1 = 5 cm, Y2 = -5 cm. Collimator angle 0°

2. X1 = 0 cm, X2 = 5 cm, Y1 = 5 cm, Y2 = -5 cm. Collimator angle 0°

3.4.4 Setup #2

For the second setup, the 20x10 cm^2 piece left over from setup #1 was exposed to two 3x5 cm^2 overtravel fields (see section 2.4.5). This setup was used to see how linear accelerators handle overtravel geometry, and if dose planning systems are accurate in predicting dose distributions for such fields.

3. X1 = 5 cm, X2 = -2 cm, Y1 = -2 cm, Y2 = -7 cm. Collimator angle 0°

4. X1 = -2 cm, X2 = 5 cm, Y1 = -2 cm, Y2 = -7 cm. Collimator angle 0°

3.4.5 Setup #3

The last two setups were used as a test of the x- and y-collimators when rotating the collimators 180°. First the y-collimator jaws were tested by running the Y1-collimator up to the central axis of the beam and rotating the collimators by

45
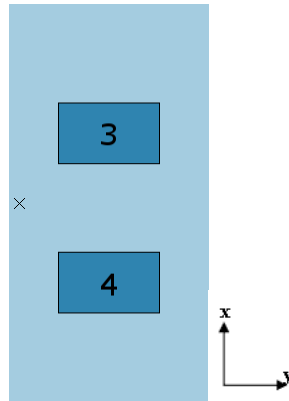
Figure 25: Beams-eye view of experimental setup #2 - two 3x5 cm^2 overtravel fields on a 20x10 cm^2 film piece. The field isocenter is denoted by ×, and the positive y-direction points towards the gantry.

180°. For Varian treatment units, the collimator angle cannot be set at 180°. Therefore the angles were set at 90° and 270°, respectively. The phantom was rotated accordingly to make up for this angular shift on certain machines.
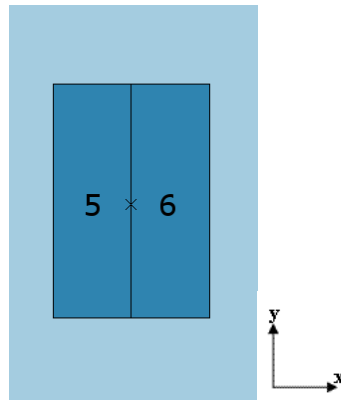
Figure 26: Beams-eye view of experimental setup #3. The field isocenter is denoted by ×, and the positive y-direction points towards the gantry.

5. X1 = 6 cm, X2 = -6 cm, Y1 = 0 cm, Y2 = -4 cm. Collimator angle 0°/ 90° for Varian

6. X1 = 6 cm, X2 = -6 cm, Y1 = 0 cm, Y2 = -4 cm. Collimator angle 180°/ 270°for Varian

3.4.6   Setup #4

The last setup repeats setup #3 for the x-collimator pair:

7. X1 = 0 cm, X2 = -4 cm, Y1 = 6 cm, Y2 = -6 cm. Collimator angle 0°/ 90° for Varian
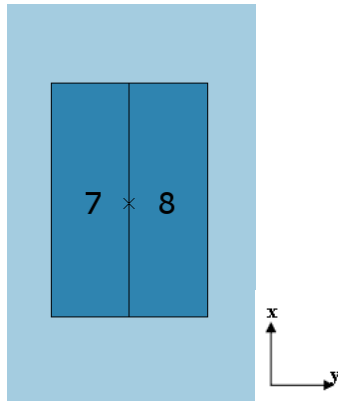
Figure 27: Beams-eye view of experimental setup #4. The field isocenter is denoted by ×, and the positive y-direction points towards the gantry.

8. X1 = 0 cm, X2 = -4 cm, Y1 = 6 cm, Y2 = -6 cm. Collimator angle 180°/ 270°for Varian

3.5 Film processing and analysis

3.5.1 Scanner procedure

The scanner used to scan the films was an Epson V750 model scanner and Epson Scan software running in Professional mode. As specified in the "Scanner User's Protocol", all films were scanned in the same direction, as "Film (Film with area guide)" document type. All films were scanned in the landscape format [47]. The films were scanned as "Positive Film", using 48 bit color and a resolution of 72 dpi. All image adjustments were turned off in Epson Scan software [48]. Cheung et al reported a 9-11 % post-irradiation increase in optical density within the first six hours following irradiation of GafChromic® EBT films in the dose range 1-5 Gy [41]. The films used for analysis were scanned at least 12 hours after irradiation.

A preview was taken before each film was scanned. Five consecutive scans were taken of each exposed film. In addition, five scans were taken of an unexposed film. Films were saved as 16-bit .tiff (tagged image file format) files. Paelinck et al found that the optical density of the first scan was about 1 % higher than for subsequent scans due to the heating of the scanner lamp [45]. Therefore, only the last three scans were averaged and used for analysis.

3.5.2 Processing

The film and background scans were imported into a self-written algorithm using the Student edition of Matlab® 7.4 with Image Processing Toolbox™ 5.4. Some algorithms can be seen in appendix A.3.

First, the averages of the film and background scans were imported, and the red data channel extracted as its own image matrix. The image was then subjected to a noise-reduction algorithm. Two types of noise filters were used:

47

a)   b)

Figure 28: a) The Epson V750 scanner with the film area guide in place taken from the Epson Scan user's manual [49].b) Screen shot of the Epson Scan software with relevant settings.

median filtering and wiener filtering [50, 51]. More info about these techniques is included in appendix A.1.

A region was defined for each exposed film, and the same region was defined for the unexposed film from the same batch. The netOD was calculated using formulas derived by Devic et al (2004). For the ith film packet at dose point D_j, the net optical density is given by eq. 30.

$$netOD^i(D_j) = OD^i_{exp}(D_j) - OD^i_{unexp}(D_j) = \log_{10} \frac{I^i_{unexp}(D_j)}{I^i_{exp}(D_j)} \qquad (30)$$

I^i_{unexp} and I^i_{exp} are the mean pixel values for the unexposed and exposed film, respectively. The background scan included in Devic et al (2005) has been omitted. Instead, the entire scan field was scanned to check prior to each scanning procedure to check for dead pixels or other abnormalities. The netOD represents the change in optical density as the film is exposed to ionizing radiation. [1, 44]

3.5.3   Scanner flatness correction

It has been reported in recent literature that the response of the scanner is not homogeneous over the entire scan field. Figure 29 shows a typical scanner response for an Epson scanner similar to the scanner used for this thesis.

A scanner flatness correction similar to the one suggested by Lewis, in which small pieces of film are exposed to different doses and then scanned in different places on the scan field [47] was first considered. However, the method used in this thesis does not require a scanner correction. A correction factor would

CCD Scanner Schematic - Light scattering film

Light source - fluorescent lamp or cold-cathode lamp

Scattering medium - e.g. GAFCHROMIC EBT film (exposed or unexposed) or exposed silver film

Focusing element

Linear CCD array

CCD Scanner Response: The Effect of Light Scattering in a Film of Uniform Density

Greyscale Value

Position Across the Film

Figure A1-4
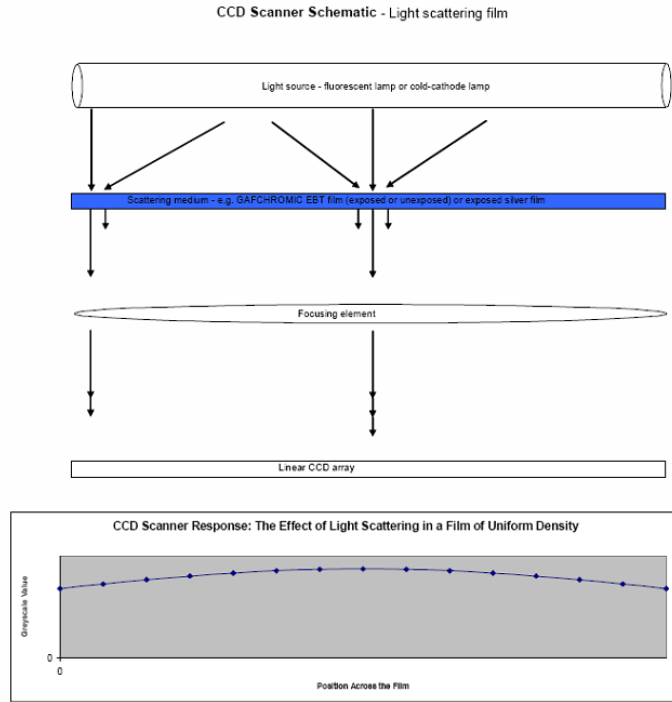
Figure 29: Scanner response for Epson scanner, taken from Lewis (2007) [47]

be of the form $I_{corr} = k_{corr}(x) \times I$, where x is the position on the scan field perpendicular to the scanning direction. However, this correction factor would be equal for the exposed and unexposed images in the pixel-by-pixel division shown in equation 30. In other words

$$
\begin{aligned}
netOD^i(D_j)_{corr} &= \log_{10} \frac{I_{unexp}^{corr}(D_j)}{I_{exp}^{corr}(D_j)} = \log_{10} \frac{k_{corr}(x) \times I_{unexp}(D_j)}{k_{corr}(x) \times I_{exp}(D_j)} \quad (31) \\
&= \log_{10} \frac{I_{unexp}^i(D_j)}{I_{exp}^i(D_j)} \quad (32)
\end{aligned}
$$

The method of subtracting the scan of an unexposed film is based on the method suggested by Devic et al (2004).

3.5.4 Full Width at Half Maximum (FWHM)
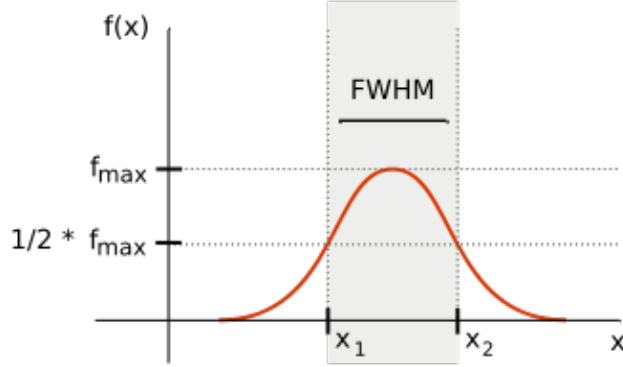
Figure 30: Schematic showing the concept of FWHM. Figure created by Arne Nordmann. [52]

For the film setups that used spliced fields, it was necessary to calculate the width of peaks or valleys in the dose distribution as a part of the analysis. In these cases a Full Width at Half Maximum (FWHM) technique is useful. Figure 30 shows a schematic outlining the basics of FWHM.

FWHM is defined as the distance between points on the curve at which the dependent function reaches half its maximum value [53]. In this thesis, the peak f_{max} was defined as the absolute difference between d_{ref} for setup 1 and the 10x10 field, unless otherwise specified. $f_{max}/2$ is thus the average dose value of the two d_{ref} values.

3.5.5 Gamma index

The gamma evaluation is a method for comparing dose distributions, first suggested by Low et al (1998). It is a quantitative way of comparing calculated and measured dose distributions, which means it is useful in the comparison between dose planning software (calculated) and film (measured). The gamma evaluation method is based on a simple pass-fail method. It is a combination of two criteria: distance-to-agreement (DTA) is used as a criteria in areas with a high dose gradient and dose difference is used in areas with a low dose gradient.

DTA is a measure of the distance between a reference point in the calculated dose distribution and the closest point in the measured distribution exhibiting the same dose. Points are accepted or rejected based on the magnitude of this distance. For dose difference, points are accepted or rejected based on the magnitude of dissimilarity between the dose of the reference point and the dose of the measured point. [54, 55]

A schematic representation of the gamma evaluation method can be seen in figure 31. The ellipsoid in the figure marks the boundary between acceptance and rejection. The ellipsoid is described by the formula

$$\sqrt{\frac{\Delta r^2}{\Delta d_M^2} + \frac{\Delta D^2}{\Delta D_M^2}} = 1 \tag{33}$$
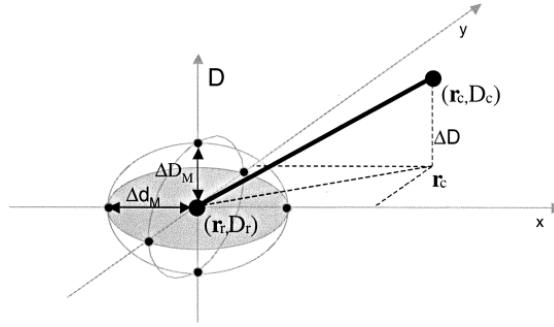
Figure 31: Schematic representation of the Gamma method of comparing dose distributions. Points within the ellipsoid are accepted, and points outside are rejected based on preset criteria.

The gamma function equal to

$$\Gamma_r\left(\vec{r_c}, D_c\right) \equiv \sqrt{\frac{\Delta r^2}{\Delta d_M^2} + \frac{\Delta D^2}{\Delta D_M^2}} \tag{34}$$

for a given dose point. In the above formulas the following notation is used:

- $\Delta r = |\vec{r_c} - \vec{r_r}|$ is the shortest distance between the reference point and a point with the same dose level in the compared distribution.

- $\Delta D = D_c(\vec{r_c}) - D_r(\vec{r_r})$ is the dose difference at position r_c in the compared distribution relative to point r_r in the reference distribution.

- Δd_M and ΔD_M are the maximum values for distance and dose difference, respectively. Reasonable values for clinical use are boundary values of $\Delta d_M = 3$mm and $\Delta D_M = 3\%$. [56]

The gamma index is then defined to be the minimum of $\Gamma_r\left(r_c, D_c\right)$:

$$\gamma\left(\vec{r_r}\right) = \min\left\{\Gamma\left(\vec{r_c}, \vec{r_r}\right)\right\} \forall \left\{\vec{r_c}\right\} \tag{35}$$

Depuydt et al (2002) modified the gamma factor to a discrete pass/fail criterion rather than a continuous function.

The criterion is such that

$\gamma\left(\vec{r_r}\right) \leq 1$ \qquad dose point passes the criterion

$\gamma\left(\vec{r_r}\right) < 1$ \qquad dose point fails the criterion
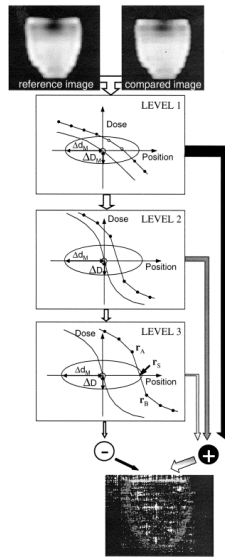
Figure 32: The points are accepted on three different levels, as explained below. Figure taken from Depuydt et al (2002) [57].

Three levels of acceptance are used for a given point. These levels can be seen schematically for the 1-dimensional case in figure 32:

1. The first acceptance level is derived from the standard gamma criterion as outlined above, but concentrates on calculating $\Gamma_r\left(r_c, D_c\right)$ in the pixel's local neighborhood rather than for all pixel values. Once a pixel has been found for which $\Gamma_r\left(r_c, D_c\right)$ is less than 1, the calculation stops and the point is accepted.

2. Points pass the second level if the dose distribution intersects, but has no data points within, the ellipsoid of acceptance. This case is possible due to the discrete nature of the dose distribution.

3. Points are accepted on the third level if the dose distribution intersects the ellipsoid, but has one point within and one point beyond Δd_M.

If the point does not achieve acceptance on the third level, it is finally classified as not accepted. [57]

The gamma evaluation was used to compare the calculated fields from dose planning software to the fields measured using the film. The VerA software developed by Sigrun Saur has support for calculating the gamma index. An example of a continuous and a discrete gamma distribution can be seen in figure 33.
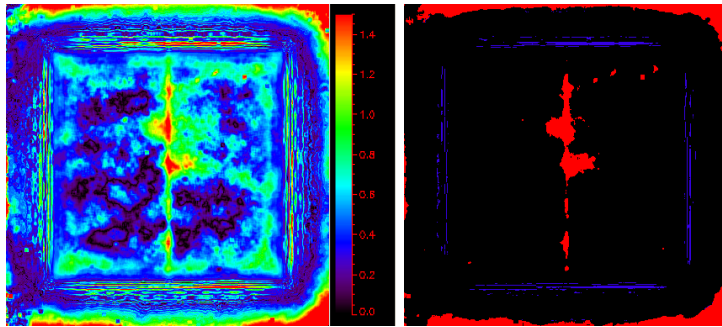
Figure 33: Examples of the gamma distribution. To the right, a continuous gamma distribution. To the left, a discrete version of the same distribution. In this image the black pixels represent acceptance on level 1, blue pixels represent acceptance on level 2 and red pixels fail all three levels of acceptance. All gamma images have been created using VerA.

3.6 Matlab and IDL routines

For image processing and analysis, Matlab was mostly used due to the authors previous experience with it. However, some tasks were performed using IDL (Interactive Data Language). Both are commonly used data analysis software packages. The versions used were Matlab® Student Edition 7.4 with Image Processing Toolbox™ 5.4, and IDL 7.0.

3.6.1 SensiometriCal
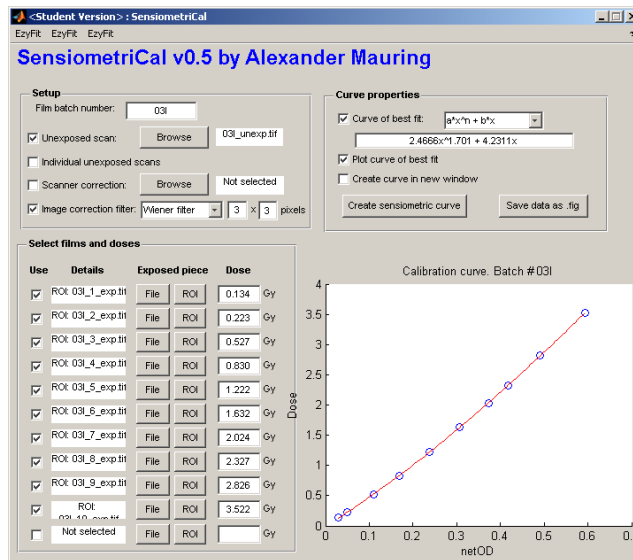
Figure 34: Screen shot of SensiometriCal 0.5, an application developed for this thesis in Matlab and used for calculating calibration curves.

SensiometriCal is a Matlab GUI program written by Alexander Mauring

53

designed specifically for this thesis. Its main function is to obtain calibration data in order to create a calibration curve for each film batch as described in section 3.3.

SensiometriCal allows the calibration to be done using one or several pieces of film. The calibration data can either be loaded as an image file or by selecting a suitable ROI from any .Tiff image file. The latter makes use of the "Image: Select ROI" Matlab GUI applet written by Andriy Nych[1]. SensiometriCal gives the option of median or wiener filtering to minimize random noise in the image, for example dust on the film (see appendix A.1). For calibration purposes, a 3x3 pixel median filter was used as standard.

After importing the desired image files/ROIs, the corresponding doses are entered and a plot of dose vs optical density (OD) is created. This plot is approximated by a curve on the form $D(OD) = a(OD)^n + b(OD)$, using free Matlab toolbox Ezyfit [58]. The data is saved in Matlab ".fig" format which allows for easy access to the data from Matlab later on.

3.6.2 ProcessEBT

ProcessEBT was also created in Matlab GUI by Alexander Mauring. It can perform simple image processing tasks such as wiener and median filtering, image normalization etc. It can also analyze images, retrieve line profiles in both x- and y-directions, plane profiles and contour lines.
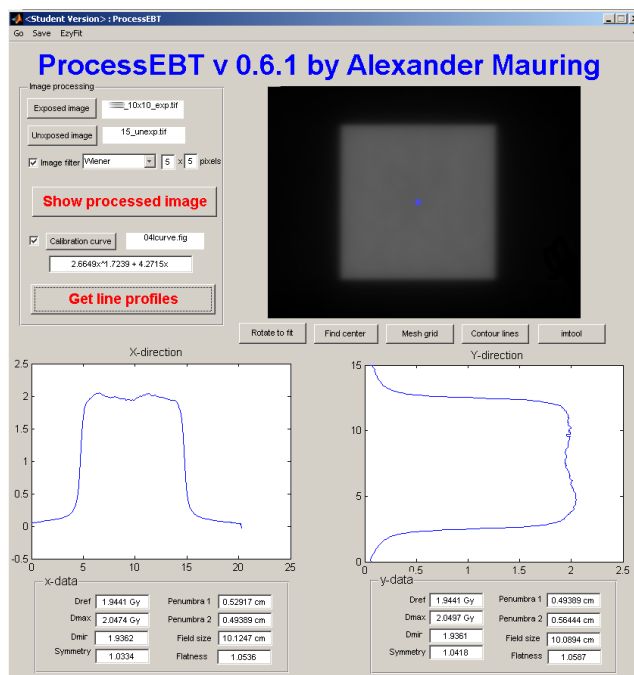
Figure 35: Screen shot of ProcessEBT 0.6.1, a Matlab application created for this thesis. It's main purpose is to process scanned images of radiochromic film and calculate different parameters.

---

[1] http://www.mathworks.com/matlabcentral/fileexchange/loadFile.do?objectId=15717&objectType=FILE

Exposed and unexposed image files are imported into the program. The red channel is extracted from both and the image files are subtracted to obtain a normalized image. The image noise can then be filtered using either a wiener filter or a median filter. A calibration curve can then be imported from a Matlab ".fig" file created by SensiometriCal, and absolute dose values are calculated automatically by ProcessEBT. All analysis can be performed with or without absolute calibration. For the work done in this thesis, a 5x5 wiener filter and calibration was used as standard.

Later versions of ProcessEBT allows for rotation of the image with respect to the radiation field and automatic location of the field center. Also, algorithms were added to automatically calculate the following parameters for line profiles in both directions:

- Dose values: D_{ref}, the reference dose at the field center, D_{max}, the maximum measured dose inside the flattened width W, and D_{min}, the minimum measured dose inside the flattened width W.

- Field size and penumbra values.

- Field symmetry and flatness, as defined in section 2.4.4.

A special menu option saves these parameters into a ".mat" file, which is a Matlab file type used for saving basic ASCII data in an array.

3.6.3 VerA

VerA is an IDL-based application designed by Ellen Wasbø at St Olavs Hospital and later at Haukeland University Hospital. It was used for much of the film analysis, especially statistics and the gamma function. It supports the DICOM image format (section 3.4.1).
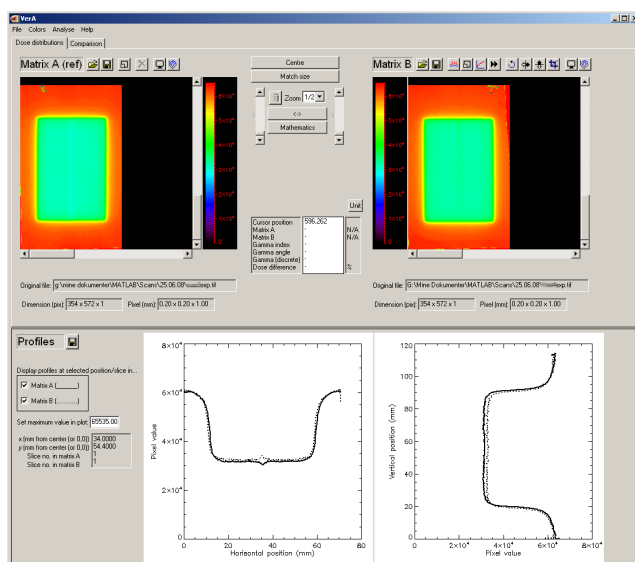
Figure 36: Screen shot of VerA 3.0, an IDL application created by Ellen Wasbø for processing and analysis of radiochromic films.

All gamma index calculations (section 3.5.5) were done using VerA version 3.1. VerA was used with Wasbø's approval.

3.7   Data extracted from films

Some Matlab codes used for the processing and analysis can be found in Appendix A.3, thus no codes will be included in this chapter. The analysis done on each film setup includes:

- 10x10 cm^2 reference field setup:

  - The median dose over a 11x11 pixel region in the isocenter of the radiation field was extracted from the film, and compared to the absolute dose from the ionization chamber measurements. This was done to approximate the same point dose measured with an ionization chamber.
  - Penumbra size, field size, field homogeneity (flatness) and field symmetry was calculated from the measured distribution.
  - Measured distribution compared to calculated distribution from dose planning software

- Film setup #1:

  - Difference in dose was measured between the field centers of the two half-collimated fields and the border area, to calculate an eventual under- or overdosage.
  - Fields were compared for similarity: penumbra, field size.
  - Measured distribution compared to calculated distribution from dose planning software

- Film setup #2:

  - The two fields were compared to each other.
  - Measured distribution compared to calculated distribution from dose planning software

- Film setups #3 and #4:

  - Difference in dose was measured between the field centers of the two half-collimated fields and the border area, to calculate an eventual under- or overdosage.
  - Setups #3 and #4 were compared to each other to see the similarity between the two secondary collimator pairs.
  - Measured distribution compared to calculated distribution from dose planning software

3.8   Summary of experimental methods

1. Absolute dosimetry in reference phantom

   - An ionization chamber is placed in the Bjerke phantom at the isocenter at $10\text{g}/\text{cm}^2$ depth and a 10x10 cm^2 field
   - The ionization chamber is exposed to a number of MU corresponding to 2 Gy at $10\text{g}/\text{cm}^2$ depth in water (200 MU for most linacs, 260 MU for some).
   - Collected charge is measured at the following energies and chamber voltages:
     - 15 MV and 300V
     - 15 MV and 100V
     - 6 MV and 300V where applicable
     - 6 MV and 100V where applicable
   - Doses are calculated using a standardized TRS-398 worksheet

2. Irradiating the films

   - Radiochromic film is placed under an equivalent 10 cm water phantom and on top of 5 cm solid water
   - Four film pieces are exposed for 15 MV photons:
     (a) Two 5x10 cm^2fields at 200 MU each, as outlined in section 3.4.3
     (b) Two 3x5 cm^2fields at 200 MU each, as outlined in section 3.4.4
     (c) Two 12x4 cm ^{2}fields at 200 MU each, as outlined in section 3.4.5
     (d) Two 12x4 cm ^{2}fields at 200 MU each, as outlined in section 3.4.6
   - The films are stored in room temperature and protected from direct exposure to light for at least 12 hrs prior to scan.

3. Scanning the films

   - Exposed films are scanned five times each, averages of last three scans are saved as 72 dpi 48-bit .Tiff-files.
   - Unexposed calibration film from same batch as exposed films is scanned five times. Average of last three scans is saved as 72 dpi 48-bit .Tiff-file.

4. Processing the films

   - The three image files from step 3 are imported into Matlab/IDL.
   - Image correction factors are applied to the images.
   - Optical density values are obtained from equation:

$$netOD^i(D_j) = \log_{10}\left(\frac{I^i_{unexp}(D_j)}{I^i_{exp}(D_j)}\right) \tag{36}$$

5. Calibration for absolute dosimetry

- One GafChromic® EBT film is cut into pieces of approx. 2.8 cm x 12.5 cm for a total of 10 pieces.
- Calibration films are exposed in a $10x10cm^2$ SAD 100 cm beam at different dose levels:
  - approx. 0.1, 0.2, 0.5, 0.8, 1.2, 1.6, 2, 2.3, 2.8 and 3.5 Gy
- Exposed films, unexposed films and background are scanned as in step 3.
- Image files are processed in Matlab and pixel values are converted into netOD values using equation 36.
- A 10x10 pixel ROI is defined in the center of each calibration film. The median netOD value of this ROI is defined as the netOD value of the corresponding dose.
- The dose of each film is plotted against its netOD. The data points are fitted using a curve of best fit, creating a sensiometric calibration curve on the form $D(OD) = a(OD)^n + b(OD)$.

6. Film dosimetry

- The netOD values are calibrated against the calibration curve as described in step 5as well as section 3.3.2.
- Processed images are imported into Matlab or IDL routines and analyzed, see section 3.7 for details.

4 Method testing and film calibration

In total more than 50 sheets of film cut into several pieces each were exposed, scanned, processed and analyzed during the course of the experiments. The film was first used to measure field size and penumbra of the new Co-60 setup at the SSDL. A report from these measurements can be found in appendix A.5.

4.1 Testing experimental procedures at UUS

Prior to conducting measurements on linacs at different hospitals in Norway, experimental methods were put to the test at Ullevål University Hospital (UUS). The following sections outlines the findings from these tests. Some ad hoc discussion is included.

4.1.1 23.06.08

The experimental procedures were carried out as detailed in section 3.4, at linear accelerator "SB4" at Ullevål university hospital at a 15 MV photon energy. Fields were planned in Eclipse dose planning software. Line profiles through the field isocenters were taken out and stored as raw data files. Due to human error and time constraints the film was placed at a SSD of 94.7 cm, 4.7 cm more than intended. Therefore the dose profiles retrieved from the film could not be readily compared to the dose profiles from Eclipse.

In order to get some sort of comparison between the measured dose using an ionization chamber and the films, a inverse square fall-off calculation was used to provide a crude correction for the SSD error [3]:

$$D\left(d_{max}, f', S, E\right) = D\left(d_{max}, f, \frac{S}{F}, E\right) \times \left(\frac{f + d_{max}}{f' + d_{max}}\right)^2 \tag{37}$$

where $D\left(d_{max}, f', S, E\right)$ is the dose at SSD f' and $D\left(d_{max}, f, \frac{S}{F}, E\right)$ is the dose at SSD f . Thus, the doses at 94.7 cm SSD are expected to be (using a value of 2.5 cm for d_{max}):

$$D\left(d_{max}, 94.7cm, S, E\right) = D\left(d_{max}, 90cm, \frac{S}{F}, E\right) \times \left(\frac{90cm + 2.5cm}{94.7cm + 2.5cm}\right)^2 \tag{38}$$

$$= 0.95 \times D\left(d_{max}, 90cm, \frac{S}{F}, E\right) \tag{39}$$

so

$$D\left(d_{max}, 90cm, \frac{S}{F}, E\right) = 1.05 \times D\left(d_{max}, 94.7cm, S, E\right) \tag{40}$$

All doses d are then approximated using a derived formula:

$$D\left(d, 90cm, \frac{S}{F}, E\right) = 1.05 \times D\left(d, 94.7cm, S, E\right) \tag{41}$$

In reality, more info will be needed about the beam to be able to calculate this dose distribution accurately.This gives a correction for the dose profiles

obtained from the films; the doses should be multiplied with 1.05 to reflect more accurately the doses at 90 cm SSD. Note that this method is just an approximation, and will not produce accurate data!

Dose profiles through the center of the fields as calculated by eclipse compared to measured dose profiles from the film can be seen in figures 37 to 40. From these figures it is evident that the field size is also larger for the profiles extracted from the film. This is consistent with the increased SAD, as the field gets larger for larger SADs.
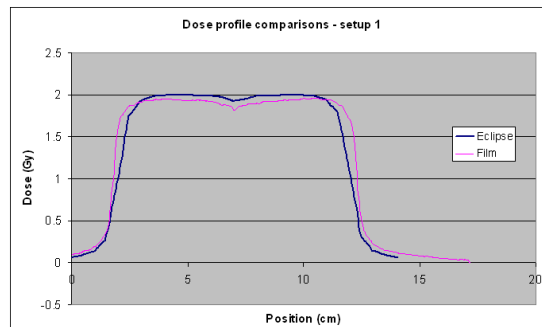
Figure 37: Dose profile comparison for setup 1
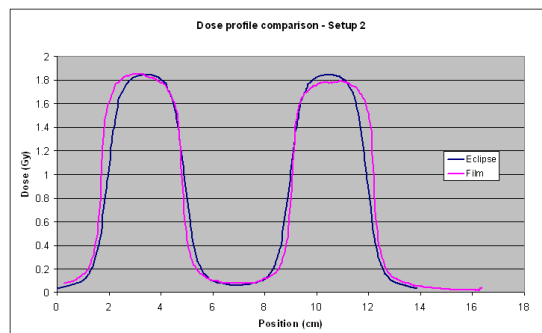
Figure 38: Dose profile comparison for setup 2

Figure 39: Dose profile comparison for setup 3
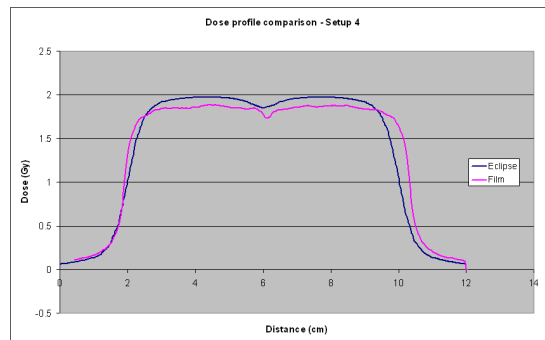
Figure 40: Dose profile comparison for setup 4

4.1.2   21.08.08

The experimental procedures were tested again with some modifications. Changes include:

- A modification was made to the film setup to make a slit under the water phantom to put in films without having to move the phantom to place a new film under it.

- A decision was made to extract a dose matrix of the entire plane at 10 g/cm^2 depth from the dose planning software in order to compare the measured and calculated distributions using the gamma method.

It was discovered during these experiments that the water phantom placed above the films was leaking very slightly from one corner. This was not believed to cause any significant uncertainty. The leak was fixed the following day using Acrifix 116 adhesive. No similar problems were encountered in later experiments. Results are included in chapter 5.

4.2   Film calibration measurements

Film batches were calibrated on the Co-60 gammatron at the NRPA. Two batches were used for the experiments, with lot numbers 47261-03I and 37122-04I. Calibration films were made for each film batch as explained in section 3.3 on 23/09/08. The dose rate of the Co-60 source was measured to be 1.7831 Gy/min at 5 g/cm^2 depth on this date. Doses were measured for all exposure times using a Capintec secondary standard ionization chamber, as it had been observed that the measured doses differed slightly from the expected doses, especially for low exposure times. The results of these measurements are compiled in table 2.

Table 2: Expected and measured doses using an ionization chamber in a water phantom for calibration of film batches. The uncertainty of these dose measurements is taken to be within 0.72 %.

Desired dose (Gy)	Exposure time (min)	Measured dose (Gy)
0.100	0.06	0.134
0.200	0.11	0.223
0.500	0.28	0.527
0.800	0.45	0.830
1.200	0.67	1.222
1.600	0.90	1.632
2.000	1.12	2.024
2.300	1.29	2.327
2.800	1.57	2.826
3.500	1.96	3.522

A modification was made to the scanning procedure of the calibration films to correct for the scattering of light from the scanner lamp: a 8.8 cm x 12.5 cm film piece was placed on each side of the calibration film during scanning, making the film equivalent in size to the clinical films in the direction perpendicular to the scanner lamp. A comparison between the calibration curves with and without correction is shown in section 4.2.3.

4.2.1 Batch #47261-03I calibration curve
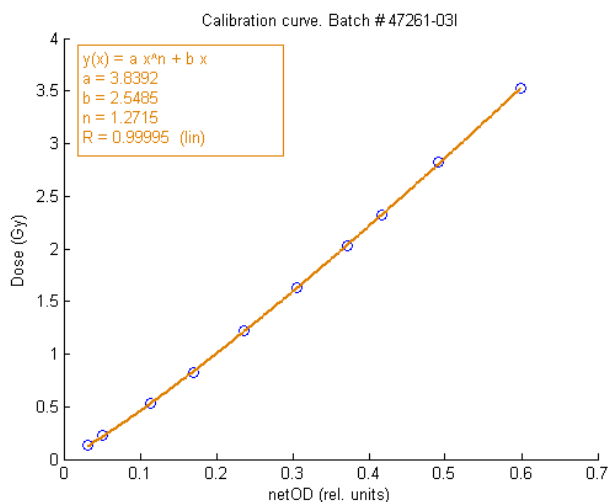
Figure 41: Batch #47261-03I calibration curve. Points are fitted with the curve $D(netOD) = 3.839 \times (netOD)^{1.2715} + 2.549 \times netOD$.

The calibration curve for the batch of films with lot number 47261-03I can be seen in figure 41. The measurement points are fitted with the curve $D(netOD) = 3.839 \times (netOD)^{1.2715} + 2.549 \times netOD$. Where D is the dose and $netOD$ is the

net optical density value. This curve has a coefficient of determination (R^2) of 0.99990 to the measured points.

4.2.2 Batch #37122-04I calibration curve
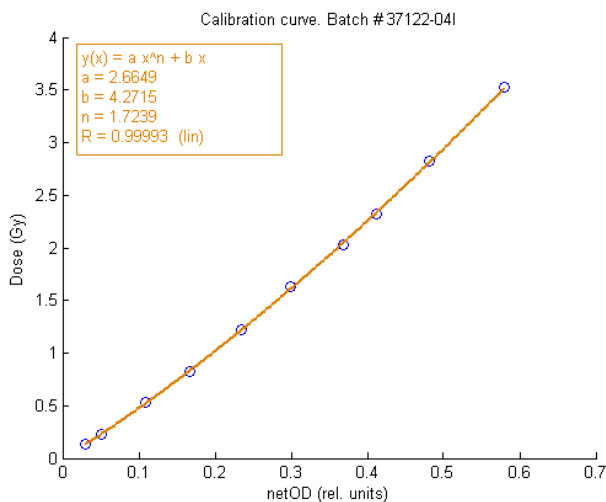
Figure 42: Batch #37122-04I calibration curve. Points are fitted with the curve $D(netOD) = 2.665 \times (netOD)^{1.7239} + 4.272 \times netOD$.

The calibration curve for the batch of films with lot number #37122-04I can be seen in figure 42. The measurement points are fitted with the curve $D(netOD) = 2.665 \times (netOD)^{1.7239} + 4.272 \times netOD$. Where D is the dose and $netOD$ is the net optical density value. This curve has a coefficient of determination (R^2) 0.99986 to the measured points.

4.2.3 Calibration curve comparisons

Figure 43 shows a comparison of the calibration curves before and after the scanning correction. Blue and black data points show the calibration data before light scattering was taken into account. Green and red data points show the calibration data after the correction described above. The old calibration curves would overestimate the dose values by more than 20 % for doses around 2 Gy. Possible reasons for this large variation is discussed further in section 6.1.4.

63
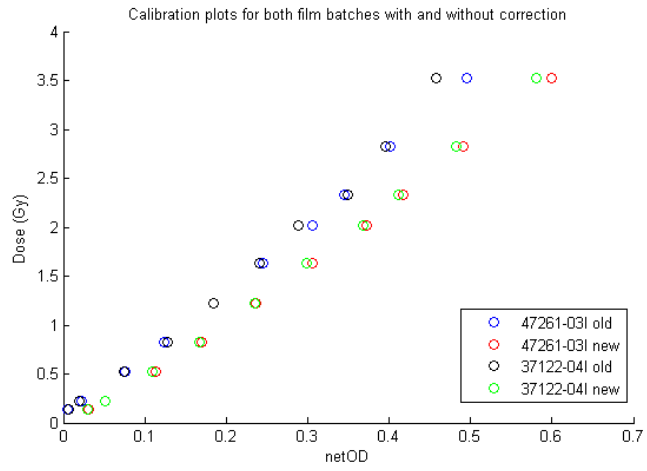
Figure 43: Calibration curve comparisons for both batches with and without correction for light scattering due to film size. For film batch #47261-03I, the old and new curves are plotted with blue and red points, respectively. For film batch #37122-04I, the old and new curves are plotted with black and green points, respectively.

5 Results

A total of 7 hospitals were visited for this thesis. These were:

- Ullevål University Hospital (UUS)

- The Norwegian Radium Hospital (DNR)

- Stavanger University Hospital (SUS)

- Haukeland University Hospital (HUS)

- Tromsø University Hospital (UNN)

- Gjøvik Innlandet Hospital (SIG)

- Ålesund Hospital (AAS)

The names of the hospitals have been omitted from the experimental results. Instead, a "linear accelerator #" identifier from 1 to 14 is used. This number is consistent for all experimental results, including all figures and tables.

In each hospital, measurements were performed on two linear accelerators of the same manufacturer. Measurements were performed first with ionization chamber as described in section 5.1, and then with film as described in section 5.2.

Ionization chamber measurements were not done on linear accelerator 10 due to time constraints. Ionization chamber measurements were only performed for 15 MV photons on treatment units 13 and 14, where the calibration depth for 6 MV photons was different from 10 g/cm^2. Film exposures were done at 15 MV on all 14 linear accelerators. Table 3 shows a summary of linear accelerator and dose planning software manufacturers for the experiments.

Table 3: Manufacturer of linear accelerators and dose planning software on linear accelerators used for measurements.

Hospital	Linac manufacturer	Dose planning software
UUS	Varian	Varian Eclipse
DNR	Elekta	Oncentra MasterPlan
SUS	Varian	Varian Eclipse
HUS	Varian	Varian Eclipse
UNN	Varian	Varian Eclipse
SIG	Siemens	Oncentra MasterPlan
AAS	Elekta	Oncentra MasterPlan

5.1 Ionization chamber dosimetry

The absolute dose was measured with a FC65-G type ionization chamber (Scanditronix Wellhöfer, Schwarzenbruck, Germany) using the water phantom setup outlined in section 3.1.4. The measurement data, including all recorded electrometer readings, can be found in their entirety in appendix A.6.

Table 4 shows the calculated values for coefficients and values described in section 2.2.5, as well as the calculated value for the absolute dose $D_{w,Q}$. This

Table 4: Summary of measurements and calculations for the ionization chamber setup. Measurements were performed for both 6 MV and 15 MV photons where applicable. The table uses symbols introduced in section 2.2.5. $TPR_{20,10}$ is the tissue–phantom ratio, $M_{Q,300V}$ and $M_{Q,100V}$ are electrometer readouts at chamber voltages of 300 V and 100 V, respectively, k_{TP} is the atmospheric correction factor, k_s is the ion recombination factor, k_{Q,Q_0} is the beam quality factor, $N_{D,w,Q}$ is the chamber calibration coefficient, and $D_{w,Q}$ is the measured dose.

Linac #	Energy	$TPR_{20,10}$	$M_{Q,300V}$	$M_{Q,100V}$	k_{TP}	k_s	k_{elec}	k_{Q,Q_0}	$N_{D,w,Q}$ ($\mu Gy/nC$)	$D_{w,Q}$ (Gy)
1	6 MV	0.675	-40.76	-40.47	1.016	1.003	0.9986	0.9935	48.01	1.978
1	15 MV	0.758	-41.24	-40.63	1.016	1.007	0.9986	0.9814	48.01	1.987
2	6 MV	0.675	-41.12	-40.81	1.014	1.003	0.9986	0.9935	48.01	1.994
2	15 MV	0.758	-41.51	-40.92	1.014	1.007	0.9986	0.9814	48.01	1.995
3	6 MV	0.680	-41.12	-40.81	1.016	1.003	0.9986	0.9930	48.01	1.996
3	15 MV	0.768	-42.22	-41.63	1.016	1.007	0.9986	0.9782	48.01	2.025
4	6 MV	0.681	-41.58	-41.43	1.022	1.002	0.9986	0.9929	48.01	2.026
4	15 MV	0.762	-41.95	-41.54	1.022	1.005	0.9986	0.9803	48.01	2.025
5	6 MV	0.665	-40.55	-40.29	1.030	1.003	0.9986	0.9945	48.01	1.998
5	15 MV	0.764	-41.55	-41.03	1.030	1.006	0.9986	0.9796	48.01	2.023
6	6 MV	0.665	-40.15	-39.94	1.032	1.003	0.9986	0.9945	48.01	1.981
6	15 MV	0.764	-40.69	-40.22	1.033	1.006	0.9986	0.9796	48.01	1.984
7	6 MV	0.670	-42.15	-41.81	0.9951	1.004	0.9986	0.9940	48.01	2.007
7	15 MV	0.760	-42.56	-41.89	0.9951	1.008	0.9986	0.9810	48.01	2.008
8	6 MV	0.670	-42.70	-42.36	0.9941	1.004	0.9986	0.9940	48.01	2.031
8	15 MV	0.760	-42.52	-41.83	0.9941	1.008	0.9986	0.9810	48.01	2.004
10	6 MV	0.670	-40.67	-40.51	1.025	1.002	0.9986	0.9940	48.01	1.990
10	15 MV	0.760	-40.97	-40.61	1.025	1.004	0.9986	0.9810	48.01	1.984
11	6 MV	0.574	-42.06	-41.88	0.990	1.002	0.9986	1.0005	48.01	2.002
11	15 MV	0.636	-42.45	-41.89	0.990	1.007	0.9986	0.9969	48.01	2.022
12	6 MV	0.572	-42.19	-41.98	0.990	1.002	0.9986	1.0006	48.01	2.0083
12	15 MV	0.637	-42.68	-41.97	0.990	1.008	0.9986	0.9969	48.01	2.0367
13	15 MV	0.760	-41.77	-41.13	1.013	1.008	0.9986	0.9810	48.01	2.0046
14	15 MV	0.759	-41.55	-40.91	1.007	1.008	0.9986	0.9811	48.01	1.9833

value should be close to the expected value of 2 Gy. A graph of the absolute dose measurements measured with an ionization chamber for 6 MV and 15 MV photons can be seen in figure 44. The measured doses range from 1.980 Gy to 2.037 Gy, corresponding to percentage differences of -1.00 % and +1.85 %. The doses have a mean of 2.004 Gy, and all values are within the general boundary of 2 %, equivalent to the uncertainty in the procedure.
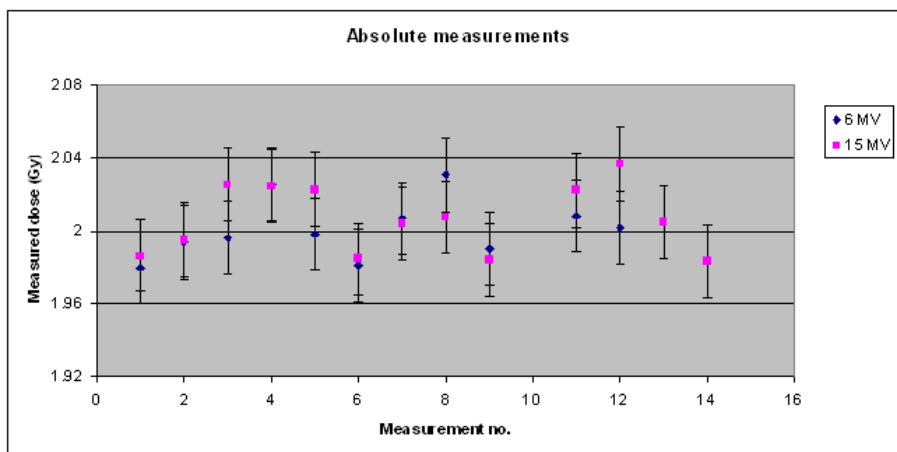
Figure 44: Graph of absolute dose measurements using an ionization chamber in a water phantom, for 6 and 15 MV photon beams. All beams were given a number of MUs equivalent to 2 Gy at the isocenter. For 6 MV, the measured values have a mean of 2.001 Gy with a standard deviation of 0.016 Gy. For 15 MV, the measured values have a mean of 2.006 Gy with a standard deviation of 0.0186.

5.2   Film dosimetry

All film measurement data described in this chapter were collected from measurements made at the 7 radiotherapy centers. 15 MV photons were used for all setups.

As travel by air was required to some of the hospitals, a test was done to see whether air travel had any effect on the films. This test can be found in appendix A.4. The results show that there is no discernible effect on the films from traveling by plane.

5.2.1   10x10 field at reference conditions

The first film setup is a simple 10x10 cm^2 at local reference conditions. This is essentially the same field as the one measured with an ionization chamber. That means that d_{ref} measured at the isocenter using film should be equal to the dose measured with ionization chamber in section 5.1. In addition, parameters that define the field such as field size, penumbra, flatness and symmetry were measured.

67
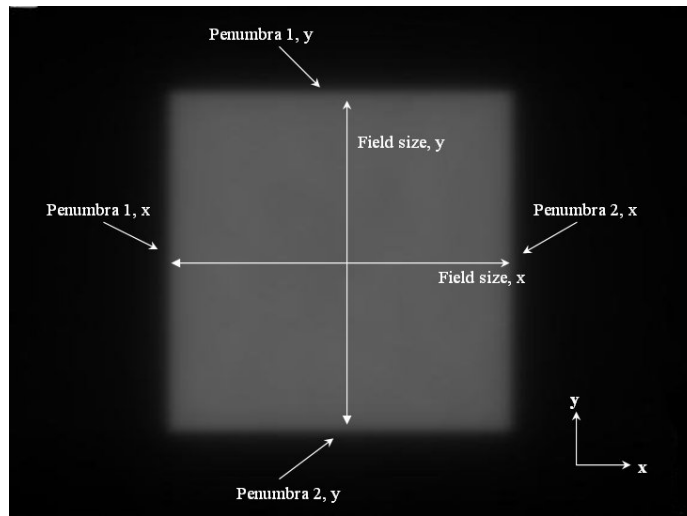
Figure 45: 10x10-field orientation during scanning and analyzing. x points toward the gantry.

Figure 45 shows the orientation of the 10x10-field film piece during scanning, processing and analyzing procedures. The field was rotated to align with the film and the field center was found using a self-written algorithm in Matlab. Two line profiles were extracted from the processed version of the film: one vertically and one horizontally through the field center. From these profiles values for reference dose, max dose, field size, penumbra width, field flatness and symmetry were calculated. Table 20 in appendix A.7 contains these calculated values.

A dose of 2 Gy was given to the isocenter of each field, equivalent to the setup measured with ionization chamber in a water phantom. Results from figure 46 show that many of the reference dose measurements with film are lower than expected. This discrepancy is most likely attributed to the film predicting lower doses than the actual doses. Possible reasons for this are discussed in section 6.

Relatively, the measurements seem to be more accurate. Figure 47 shows that all linear accelerators are able to produce a 10x10 cm^2 field size with accuracy, as all measurements are within 1.1 % of 10 cm. Penumbra measurements in figure 48 range from 0.39 cm to 0.67 cm, with a mean of 0.52 cm. Field flatness and symmetry in figures 49 and 50, respectively, are also within reason and the results will be discussed further in section 6.3.2.
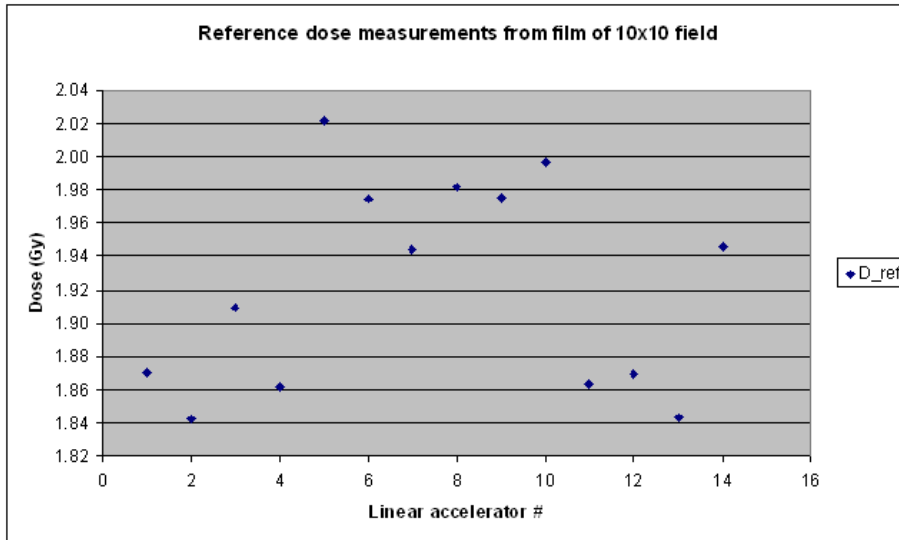
Figure 46: D_{ref} measurements from film measured at the isocenter. The measurements have a mean of 1.92 Gy with a standard deviation of 0.06 Gy. All films were given a number of MUs equivalent to 2 Gy at the isocenter.
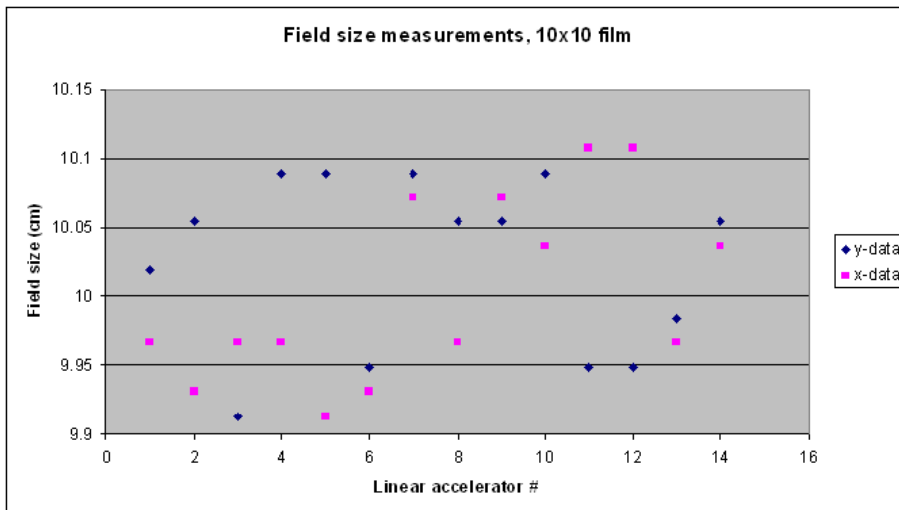
Figure 47: Field size measurements. The field size measurements have a mean value of 10.00 cm with a standard deviation of 0.07 in the y-direction, and a mean of 10.02 cm with a standard deviation 0.06 in the x-direction.

Figure 48: Measured penumbra values for the 10x10 cm^2 field at reference conditions. The penumbra measurements have a mean value of 0.51 cm with a standard deviation of 0.07 cm in the y-direction, and a mean of 0.53 cm with a standard deviation 0.08 cm in the x-direction.

Figure 49: Measured field flatness (homogeneity) values measured in the x- and y-direction. The measurements have a mean value of 1.041 with a standard deviation of 0.012 in the y-direction, and a mean of 1.036 with a standard deviation 0.010 in the x-direction.
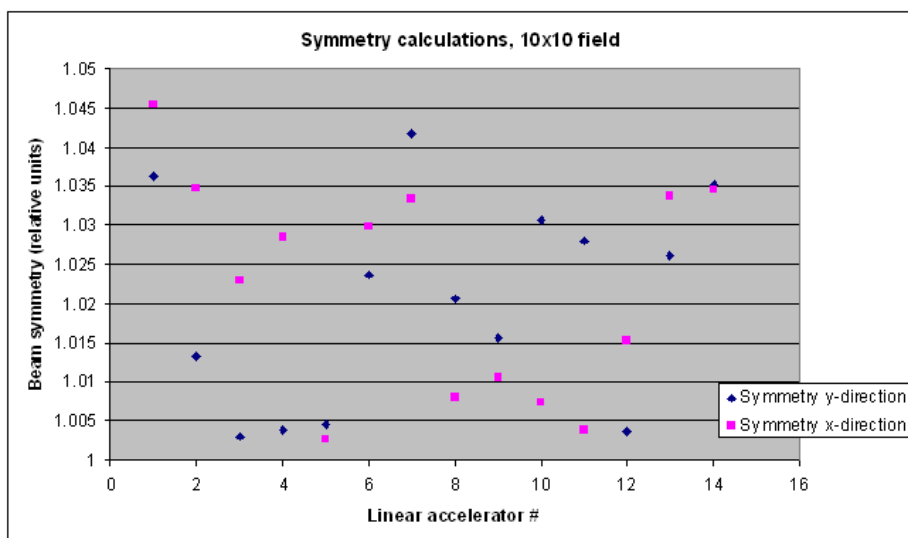
Figure 50: Symmetry measurements in the x- and y-direction. The measurements have a mean value of 1.022 with a standard deviation of 0.014 in the y-direction, and a mean of 1.0205 with a standard deviation 0.013 in the x-direction.

5.2.2   Film setup #1

Film setup #1 is composed of two half-collimated fields that border each other at the isocenter. This border area is of interest as it shows how precise the secondary collimators are at producing this type of field. The orientation is the same as the 10x10-setup in figure 45. For film setup 1, the main point of interest is to check the border between the two fields for under- or overdosage and determine a possible collimator movement error. Table 21 is included in appendix A.7, and shows collected parameters from film setup 1 calculated in Matlab, similar to the parameters calculated for the 10x10 setup. Field flatness and symmetry have been omitted from the analysis as they are not applicable for spliced fields.

Figure 51 shows a comparison of the isocenter dose for setup 1 and the 10x10 cm^2 field at reference conditions, as under- or overdosages are common in the border area between the two fields. Preferably, the values should equivalent, or at least within 3 % (corresponding to the dose difference boundary used for the gamma evaluation), but evidently this is not the case. Figure 52 shows the relative difference in isocenter dose, which ranges from -21.8 % to 22.0 % with a standard deviation of nearly 12.3 %. These deviations could have clinical implications, this is discussed in section 6.3.3.

The cumulative field size and geometry should be equivalent to the geometry of the 10x10 field. Measured penumbra and field size values for setup 1 can be seen in figures 53 and 54, respectively. Penumbra measurements have a mean of 0.52, which is identical to the value found for the 10x10 setup. The mean value for the field size is 10.02 cm, which is essentially equivalent to the value calculated for the 10x10 setup (less than 1 pixel difference). Finally, calculated full width at half maximum values are included in figure 55, with a

71

mean gap/overlap of 0.38 cm. These results will be discussed in greater detail in section 6.3.
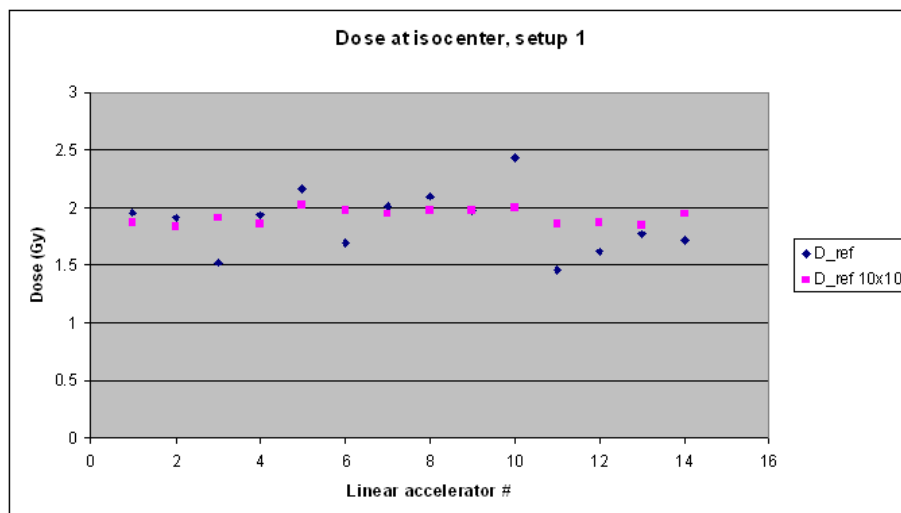
Figure 51: Isocenter dose compared from film setup 1 to the 10x10 cm^2 setup. Some under- and overdosages are apparent. The dose values for setup 1 have a mean of 1.88 Gy with a standard deviation of 0.27 Gy.
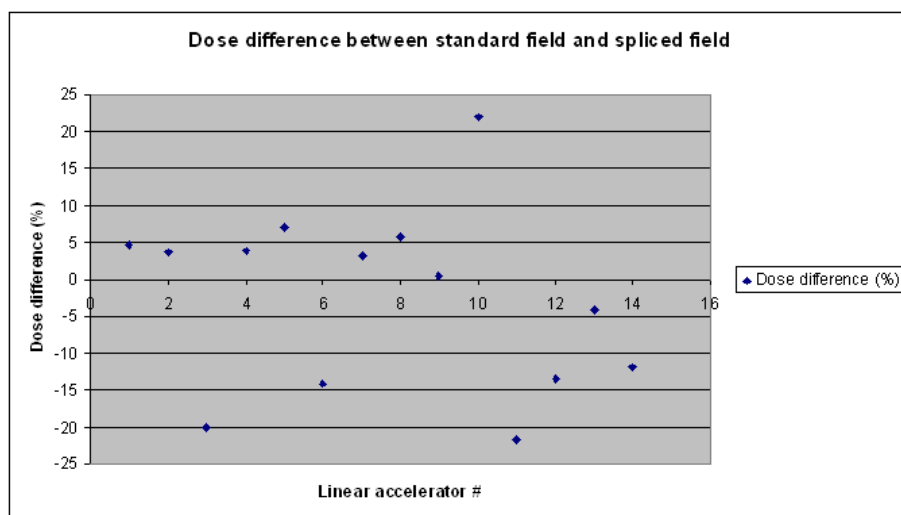
Figure 52: Percentage dose difference between the isocenter dose of setup 1 and the 10x10 cm^2 setup. These values have a mean of -2.51 % with a standard deviation of 12.27 %.
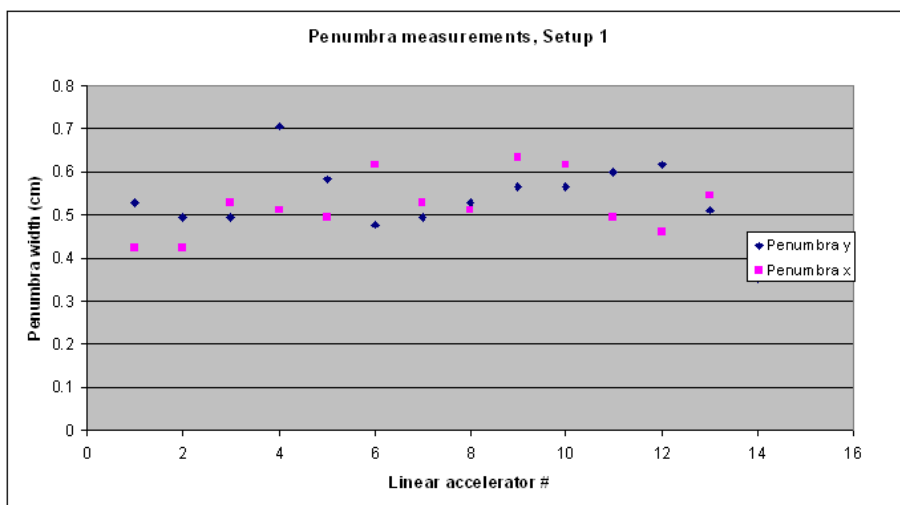
Figure 53: Calculated penumbra values for film setup 1. The penumbra measurements have a mean of 0.52 cm with a standard deviation of 0.07 cm in the x-direction, and a a mean of 0.53 cm with a standard deviation of 0.08 cm in the y-direction.
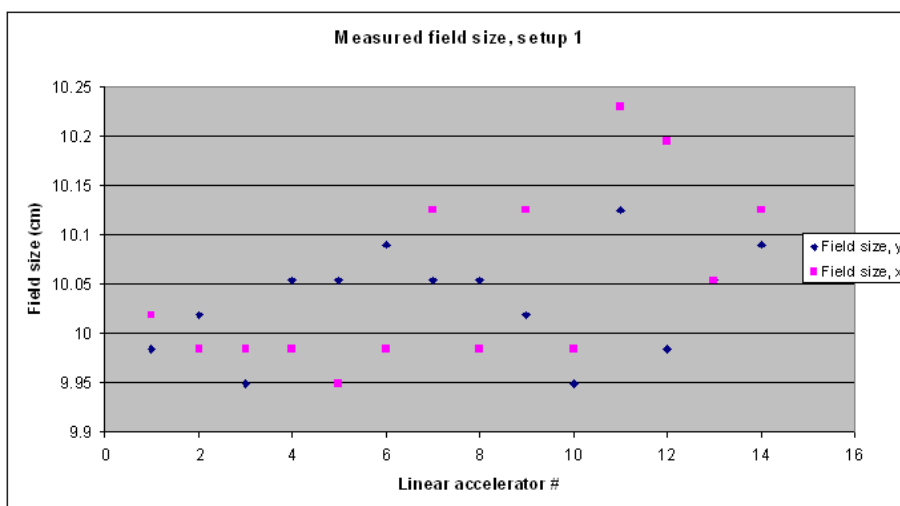
Figure 54: Calculated field size values for film setup 1. These measurements have a mean of 10.00 cm with a standard deviation of 0.07 in the x-direction, and a mean of 10.03 with a standard deviation of 0.05 in the y-direction.
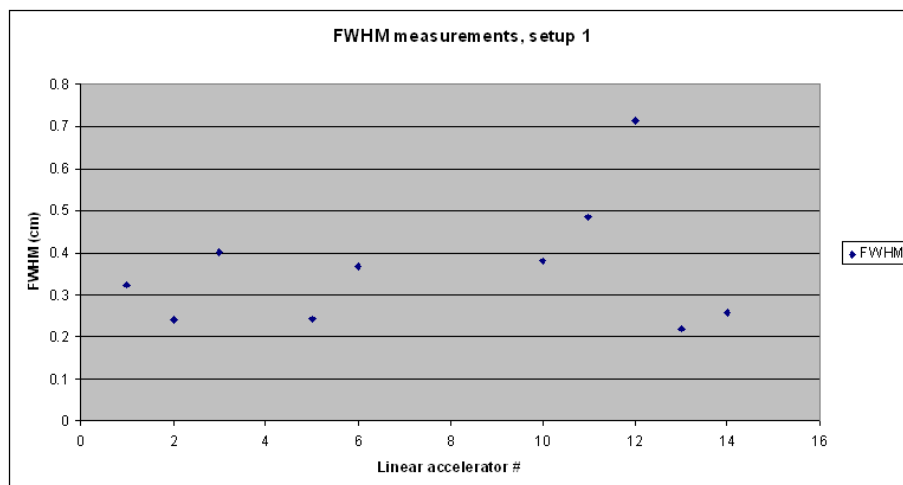
Figure 55: Full Width at Half Maximum values from setup 1, calculated as described in section 3.5.4. Results were omitted for cases where the maximum dose difference was below 5 %, as it was difficult to isolate a peak for the calculations. FWHM values in the plot have a mean of 0.38 cm with a standard deviation of 0.15 cm.

5.2.3   Film setup #2
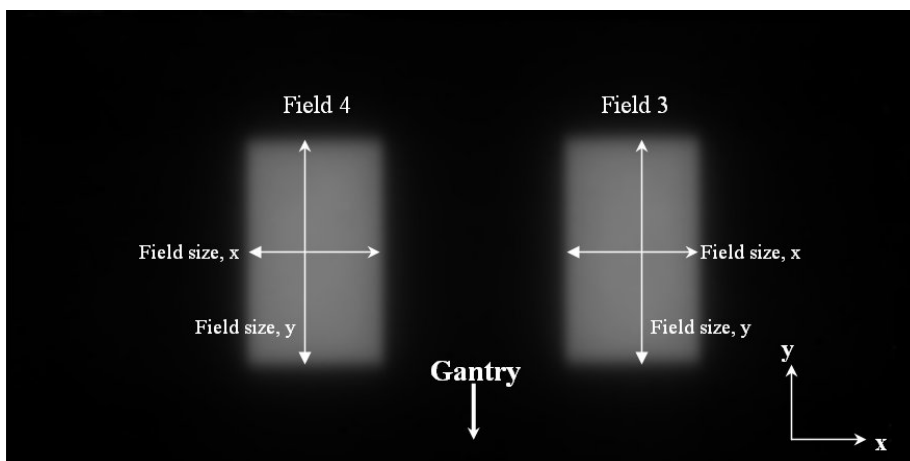
Figure 56: Orientation of setup 2 for scanning, processing and analysis. The gantry is located toward the negative y-direction.

In film setup 2, the main point of interest is to see how precisely the linear accelerator can create small overtravel fields. Overtravel fields, where one or more of the secondary collimators travel past the central axis, are becoming increasingly common, especially in IMRT. The scanning and analysis orientation can be seen in figure 56. Table 22 in appendix A.7 includes dose, field size and penumbra data extracted from fields 3 and 4.

74

Plots of reference dose and field size can be seen in figure 57 and 58, respectively. Dose values vary between 1.72 Gy and 1.90 Gy, which is more than 10 %. Field sizes have a mean of 3.00 cm and 5.01 cm in the x- any y-direction, respectively, which is equivalent to the expected values. Standard deviation is 0.07 cm for field 4 and 0.06 cm for field 3, similar to the standard deviation for the field sizes in the 10x10 setup and setup 1. However, although the absolute standard deviation is similar to what was found for setup 1 and the 10x10 setup, the standard deviation is relatively higher as the field size is smaller. This will be discussed further in section 6.3.3.
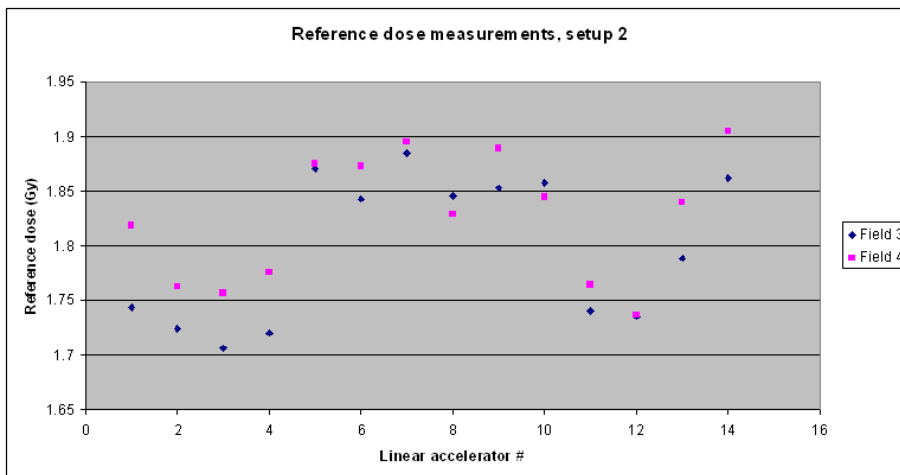
Figure 57: Measured reference dose values for film setup 2. Doses were measured in the center of both fields 3 and 4. The measures doses for field 4 have a mean of 1.80 Gy and a standard deviation of 0.07 Gy. For field 3, the measured doses have a mean of 1.83 Gy and a standard deviation of 0.06 Gy.

In figure 59, the reference dose from setup 2 has been compared to the reference dose from the 10x10 field, to find a percentage difference between the two and see if this value is consistent for all treatment units. Ideally, the value should be similar for all linear accelerators, indicating that overtravel field dosimetry is the same for different treatment units. The mean value of these measurements is 6.40 % with a standard deviation of 1.94 % for field 4 and 4.94 % with a standard deviation of 2.42 % for field 3. The values for the standard deviation indicate that there are notable variations in the dose to the center of the overtravel fields compared to the dose to the isocenter of the reference field.
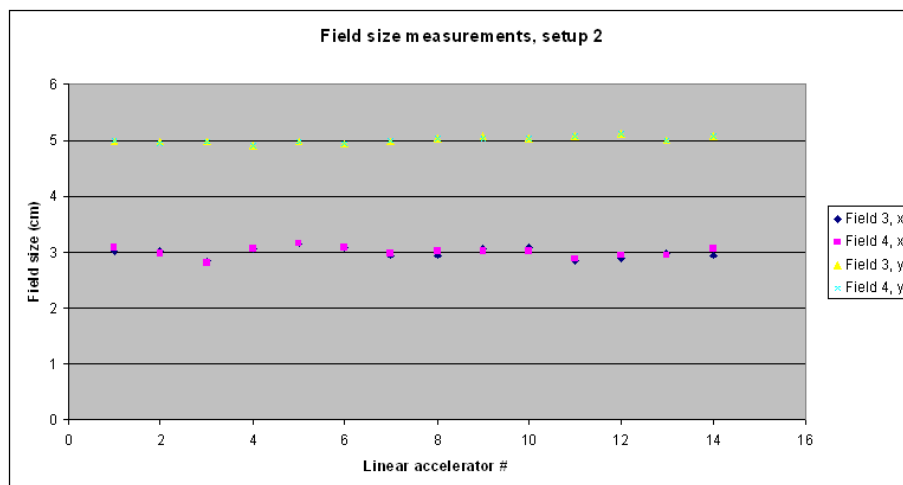
Figure 58: Measured field sizes for film setup 2. The measured values for field 4 have a mean of 2.99 cm with a standard deviation of 0.10 cm in the x-direction, and a mean of 5.01 cm with a standard deviation of 0.06 cm in the y-direction.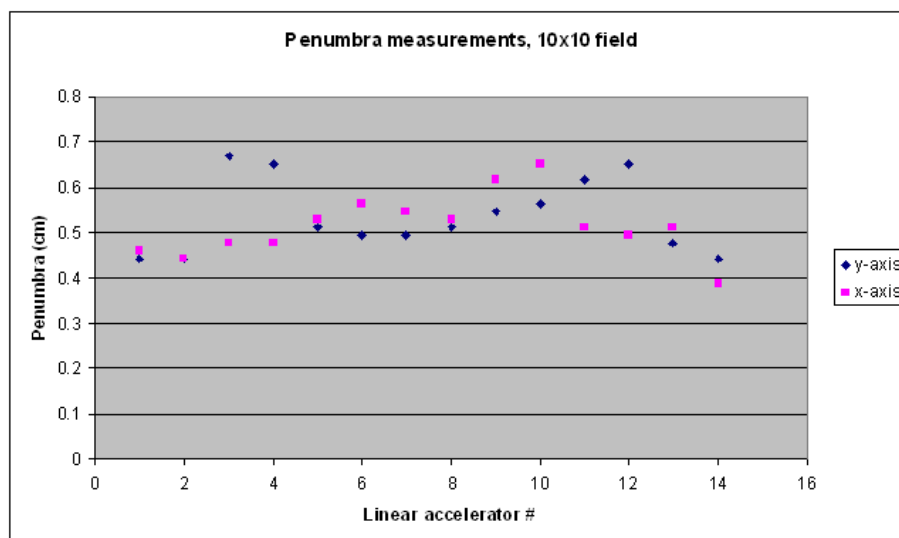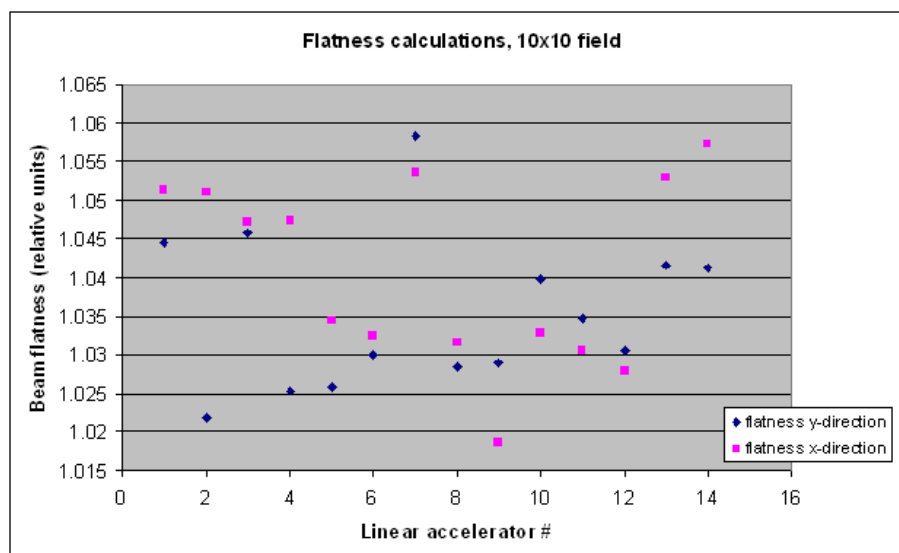 For field 3, the measured values have a mean of 3.00 cm with a standard deviation of 0.09 cm in the x-direction and a mean of 5.01 cm with a standard deviation of 0.06 cm in the y-direction.
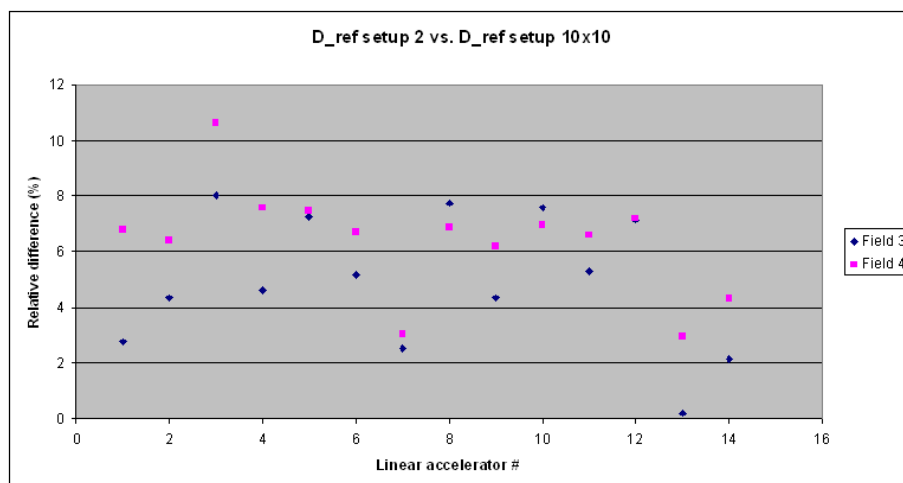
Figure 59: Relative difference between dose values from the field centers of field 3 and field 4 compared to D_{ref} values from the 10x10 reference film setup. For field 4, the mean is 6.40 % with a standard deviation of 1.94 %. For field 3, the mean is 4.94 % with a standard deviation of 2.42 %.

5.2.4 Film setup #3 and #4

For setup 3 and 4, the main point of interest was the border between the two fields. Both setups consist of one field that is rotated 180°. If there is an error on the precision of the movement of a secondary collimator or MLC leaf, this error will be doubled upon rotation. In the cases where there is an error in the collimator rotation, one will typically see a dose gradient in the border between the two fields. Figure 60 shows the orientation of the films during processing and analysis.
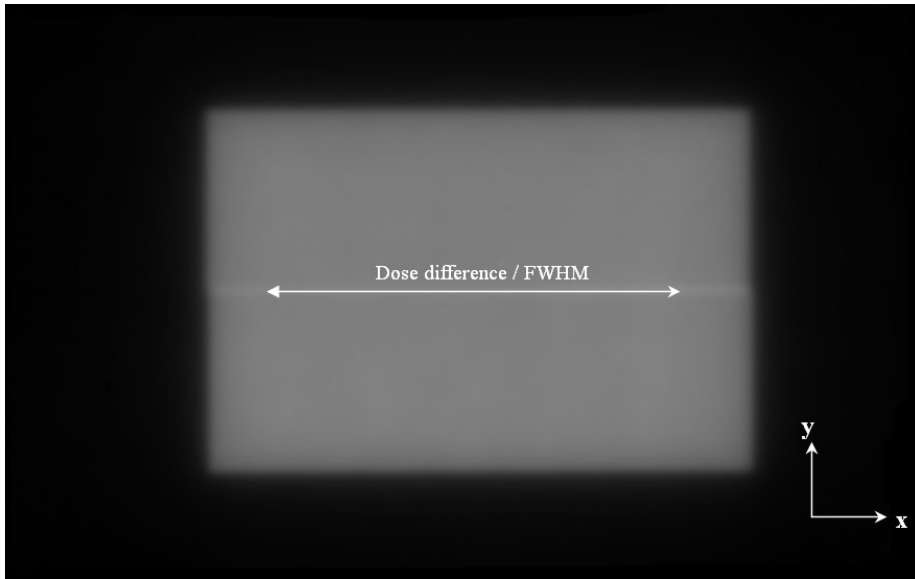
Figure 60: Orientation of the film for scanning, processing and analysis of film setups 3 and 4. The figure also shows the area from which dose difference and FWHM values were extracted. The gantry is located towards the negative y-direction for setup 3, and towards the positive x-direction for setup 4. On Varian treatment units, the gantry is located towards the positive x-direction for setup 3, and towards the negative y-direction for setup 4.

For each film, the percentage dose difference is calculated for each pixel on a line passing through the border area, on the part of the line that is within the flattened width W. From this line the minimum, maximum and mean value of the percentage dose difference and FWHM is calculated. This will give some insight into the precision of the border area. When calculating the FWHM value, the f_{max} value was defined as the absolute amplitude of the peak or valley with respect to the fields.

Median values for dose difference and FWHM are plotted against the linear accelerator number in figures 61 and 62, respectively. Large differences in border area dose are detected, from underdosages of -39.0 % to overdosages of 22.7 %. The trend from these measurements seem to be underdosages, which is reflected in the mean values for setups 3 and 4 of -7.11 % and -7.38 %, respectively. The calculated values of FWHM and dose difference for setups 3 and 4 for all linear accelerators can be found in table 23 in appendix A.7. Comparisons between

FWHM values and dose difference are performed in section 5.3.2 to see if there is a correlation between these parameters.
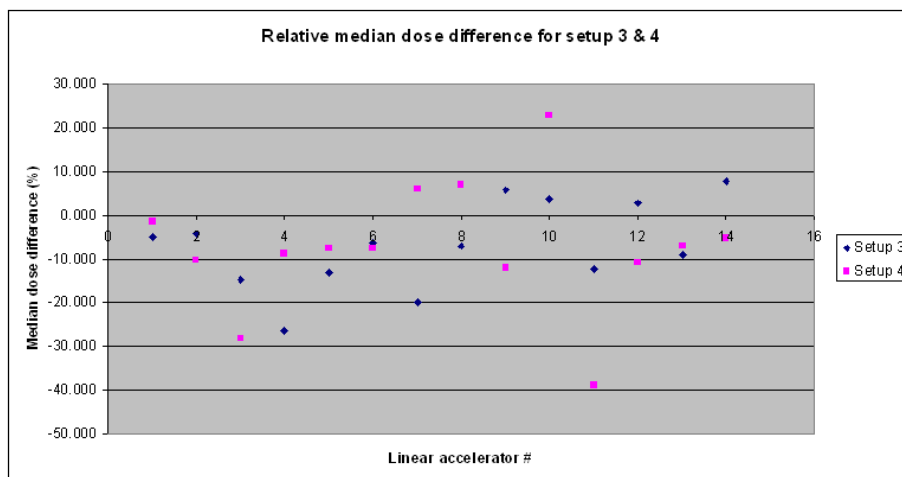
Figure 61: Relative median dose difference from the border between the two fields of each film setup. For setup 3, the mean of these values is -7.11 % with a standard deviation of 9.89 %. For setup 4, the mean of these values is -7.38 % with a standard deviation of 14.70 %.
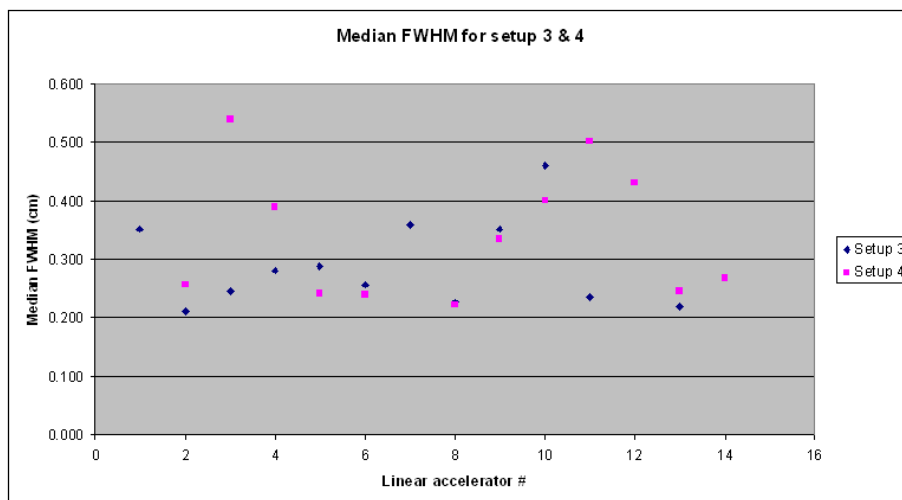
Figure 62: Median full width at half maximum (FWHM) values over the border between the two fields for setup 3 and 4. The mean value for setup 3 is 0.29 cm with a standard deviation of 0.08 cm. For setup 4, the mean value is 0.34 cm with a standard deviation of 0.11 cm.

5.3 Analysis and comparisons

Part of the analysis has been done with gamma evaluation (see section 3.5.5). Four linear accelerators were compared to exported dose profiles from dose planning software. VerA was not able to read any of the profiles extracted from MasterPlan. For the remaining ten linear accelerators, setup 3 and setup 4 were compared gamma evaluation to get a qualitative idea of the similarity between the two setups.

5.3.1 Chamber vs film
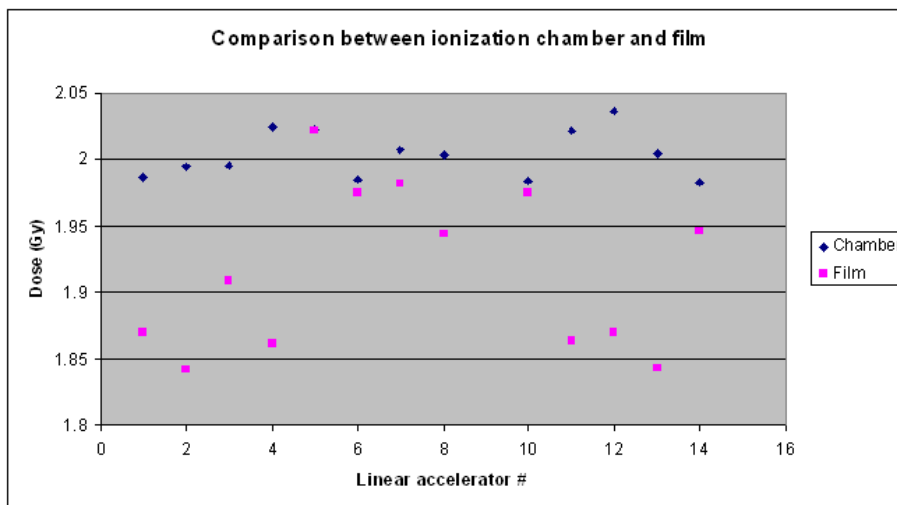
Figure 63: Measured doses using chamber and film. No chamber measurements were performed for linear accelerator #9, it is therefore omitted from these results.

Comparisons between the measured doses using ionization chamber (for 15 MV photons) and film is shown figure 63. As can be seen from the figure, the comparison produced large differences in the measured absolute doses for film and ionization chamber. Figure 5 shows the absolute difference between film and ionization chamber measurements. Large variations above 8 % are detected in certain cases, and some possible reasons for this discrepancy will be discussed in section 6.3.

5.3.2 FWHM vs dose difference

Full width at half maximum (FWHM) has been plotted against dose difference values in figure 64, to see if there is a correlation between mm overlap/gap and percentage over/underdosage. The points are fitted with separate linear trend lines for setup 1 and setup 3+4. The correlation coefficients of these lines are 0.37 and 0.45, respectively, suggesting a trend between gap/overlap width and under/overdosage.

Table 5: Percentage difference between chamber dose and film dose at the isocenter. The table also shows which film batch was used for the film measurements. The dose difference values have a mean of 4.40 % and a standard deviation of 3.34 %.

Linac #	Film batch	Chamber dose (Gy)	Film dose (Gy)	Dose difference (%)
1	03I	1.986	1.87	5.86
2	03I	1.995	1.84	7.67
3	03I	1.996	1.91	4.36
4	03I	2.025	1.86	8.06
5	04I	2.023	2.02	0.04
6	04I	1.984	1.98	0.47
7	04I	2.008	1.98	1.29
8	04I	2.004	1.94	2.97
10	04I	1.984	1.98	0.45
11	04I	2.022	1.86	7.86
12	04I	2.037	1.87	8.20
13	04I	2.005	1.84	8.06
14	03I	1.983	1.95	1.89
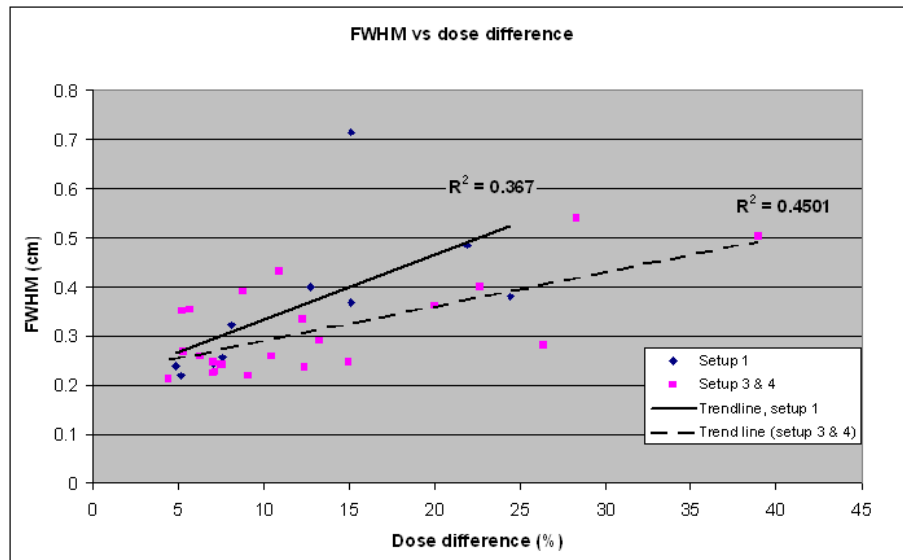
Figure 64: Full width at half maximum (FWHM) values plotted against the relative dose difference for data from film setups 1, 3 and 4. Points have been plotted separately for setup 1 and setup 3+4, and both data sets have been fitted with linear trend lines. These have correlation coefficients of 0.37 and 0.45 for setup 1 and setups 3+4, respectively.
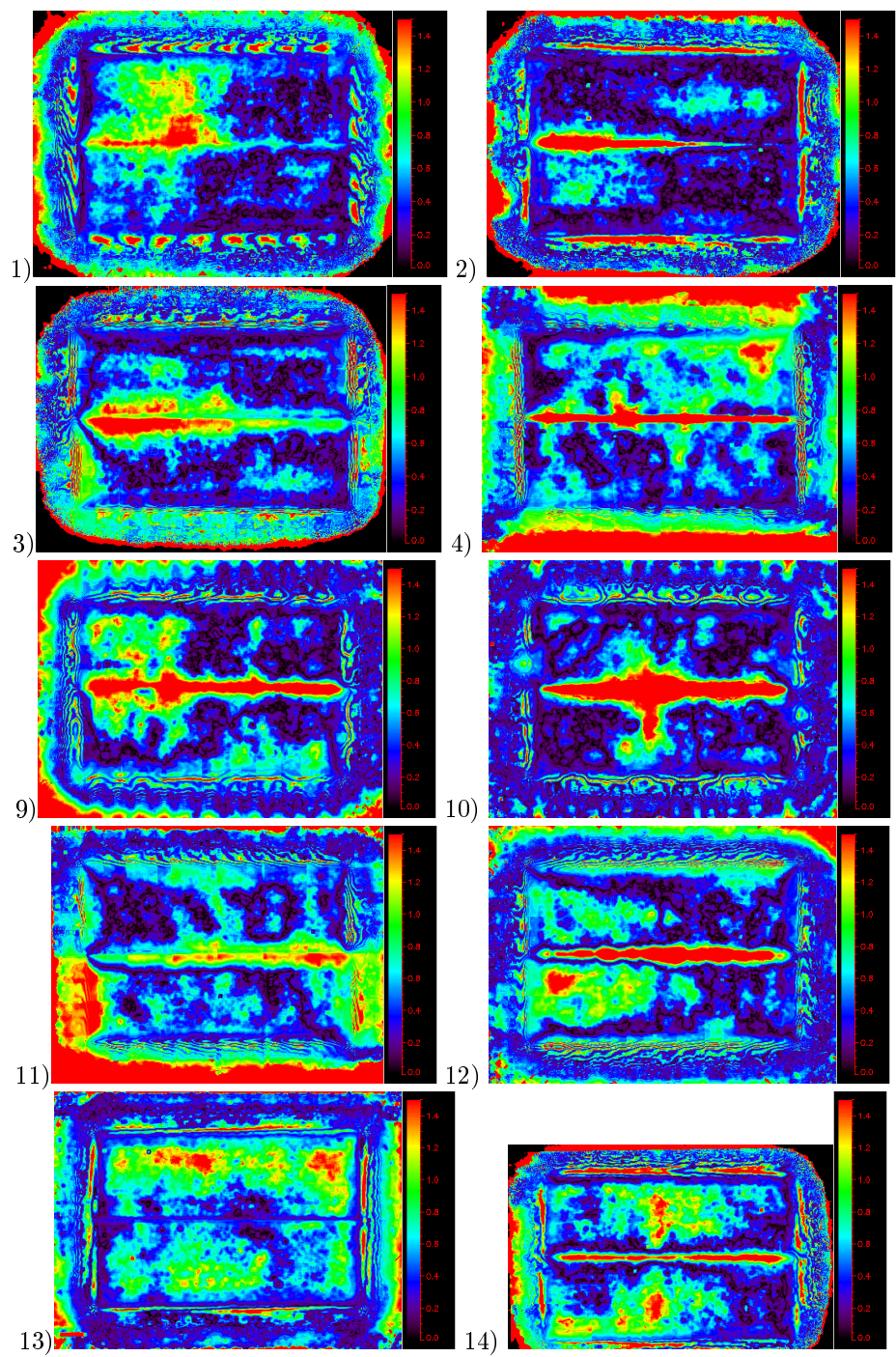
Figure 65: Continuous gamma comparisons of setup 3 and 4.Tolerance levels of 3 % and 3 mm were used for dose difference and distance-to-agreement, respectively. Points with a gamma value of more than 1 fails the criterion. Numbers correspond with the linear accelerator numbers used throughout the thesis.

5.3.3 Setup 3 vs setup 4

As a part of analyzing procedures, dose distributions for setup 3 and 4 were compared to see the similarity between the two. Only continuous gamma was extracted from these comparisons to see general trends as the method cannot be used accurately for the quantitative pass/fail criterion. The results can be seen in figure 65. They show that the border area is where the measured dose values differ most from the predicted values, as most of the pixels that fail are located close to the border between the two fields. This indicates that doses to the border area are not accurately predicted by the dose planning software.

5.3.4 Comparison to dose plan software

All gamma analysis was done in the VerA application developed by Ellen Wasbø. The analysis was performed only for linear accelerators where the dose difference between the measured dose from the film and the chamber was within the set tolerance level for dose difference, 3 %. This corresponded to linear accelerators 5-10. For linear accelerators 9 and 10, dose planning data was not compatible with VerA software meaning they had to be omitted from this part of the analysis.

The tolerance levels for dose difference and distance-to-agreement were set to 3 % and 3 mm, respectively. Results can be seen in figures 66 to 70. For each setup, the percentage of pixels failing all three levels of acceptance as described in section 3.5.5 were recorded. These percentages can be seen in table 6. Failing pixels indicate discrepancies between measured dose using radiochromic film and calculated dose from dose planning software. From the table, it is clear that linac 5 did not perform well for any of the evaluations, which means that they are not comparable to each other. However, the three remaining linear accelerators all had less than 5 % of the pixels failing the comparison of the 10x10 setup. This indicates that there is agreement between the two dose distributions for these linacs.

For the gamma evaluation comparisons, only points that lie within the field or within 1 cm of the field edges are included in the analysis of the percent of pixels that pass or fail. In other words, points that fail all three criteria that border the edge of the film are omitted. This is because of the high chance that these points fail due to scanner factors such as light scattering around the film edges and scanner flatness. Results will be discussed in detail in section 6.3.5.

Table 6: Percentage of pixels that fail all three levels of acceptance for the gamma evaluation of the comparison of the calculated dose distribution from dose planning software to the measured dose distribution from radiochromic film, for linacs 5-8.

Linac #	Setup	% failed pixels	Linac #	Setup	% failed pixels
5	10x10	25.30	7	10x10	4.58
	1	43.09		1	1.60
	2	43.27		2	25.60
	3	41.79		3	12.11
	4	48.76		4	4.84
6	10x10	0.75	8	10x10	0.00
	1	4.04		1	2.48
	2	22.61		2	0.88
	3	61.20		3	6.82
	4	45.25		4	3.96
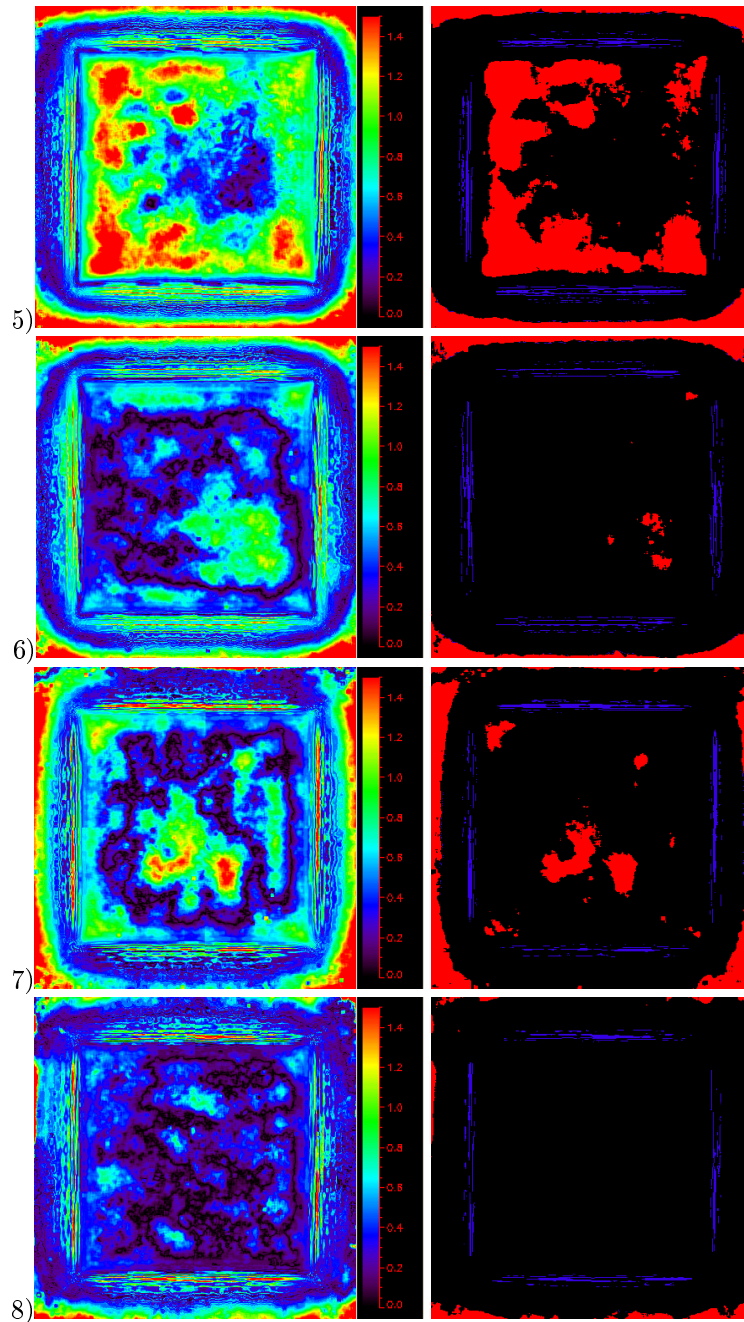
Figure 66: Gamma evaluation of the 10x10 cm^2 reference field setup for linear accelerators 5-8. The images to the left depict continuous gamma values. Images to the right show the discrete gamma distribution as suggested by Depuydt et al (2002), where red pixels have failed all three levels of acceptance.
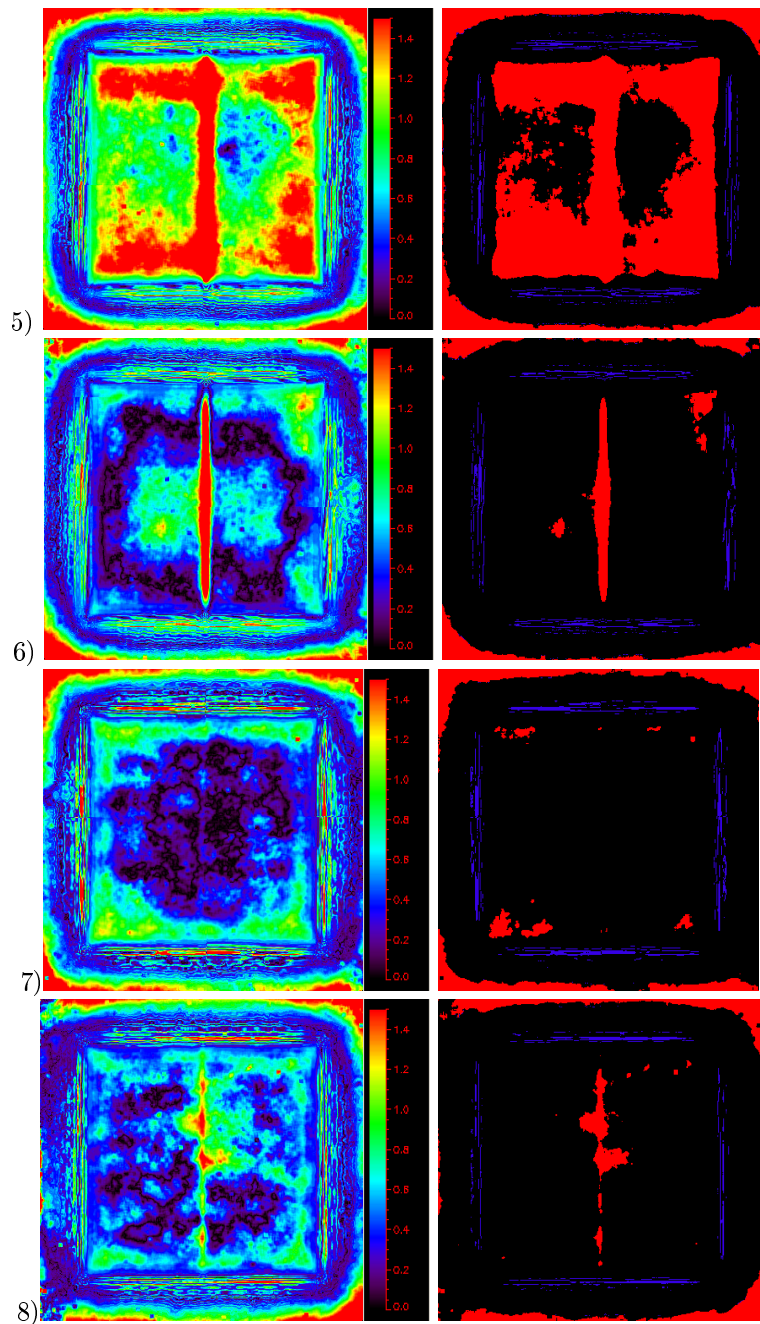
Figure 67: Gamma index for film setup #1 for linear accelerators 5-8. Images to the left show the continuous gamma distribution. Images to the right shows discretely which points pass/fail the criteria - red pixels have failed all three levels of acceptance.
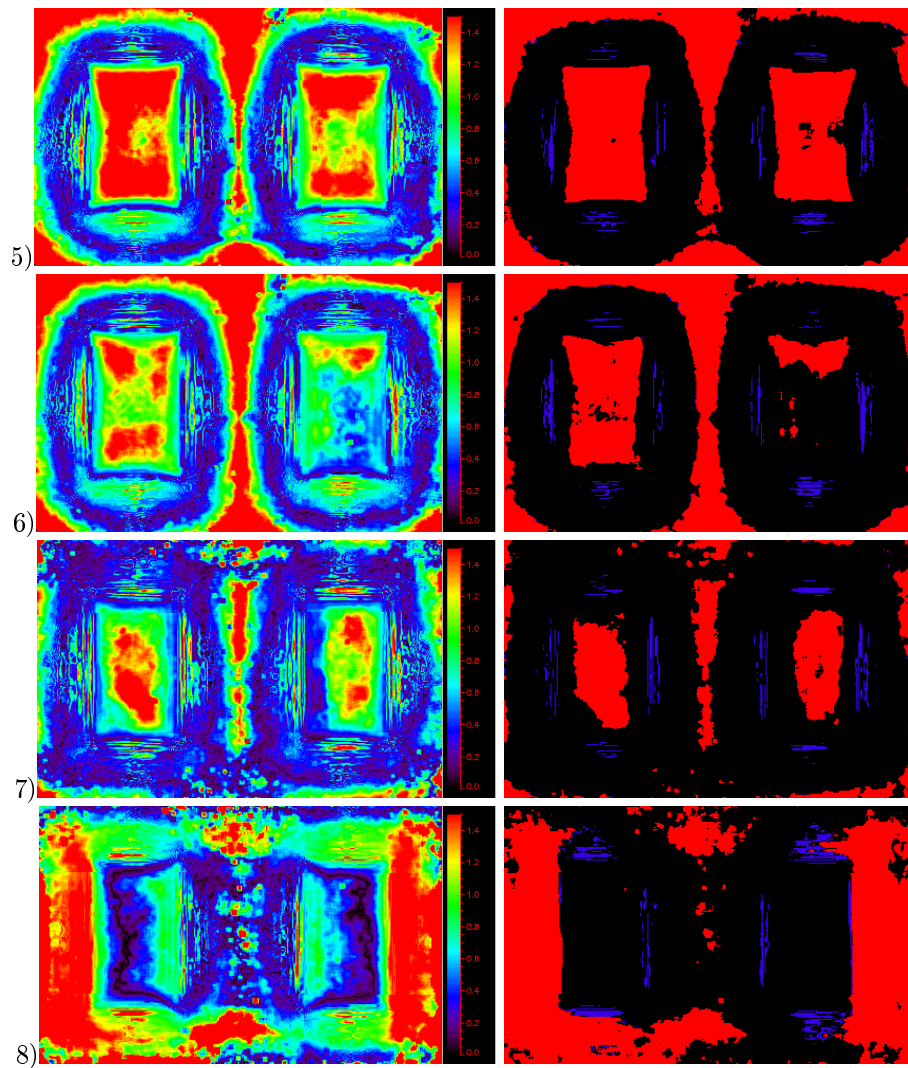
Figure 68: Gamma evaluation for film setup 2. Images to the left show the continuous gamma distribution. Images to the right shows discretely which points pass/fail the criteria - red pixels have failed all three levels of acceptance.
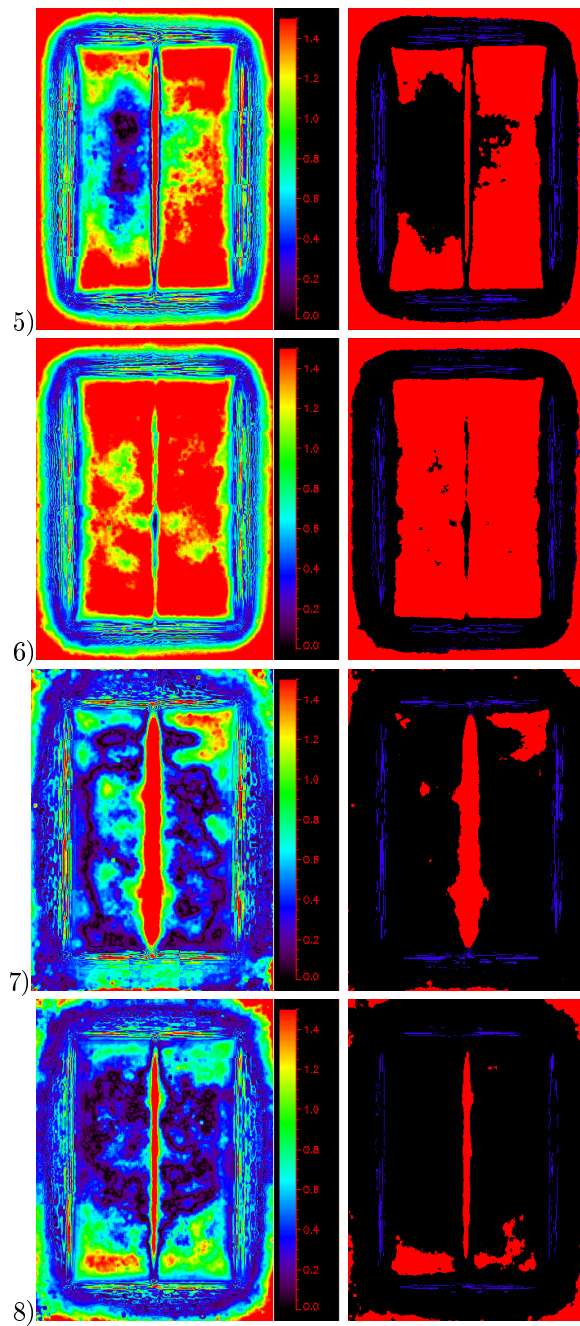
Figure 69: Gamma evaluation for film setup 3. Images to the left show the continuous gamma distribution. Images to the right shows discretely which points pass/fail the criteria - red pixels have failed all three levels of acceptance.
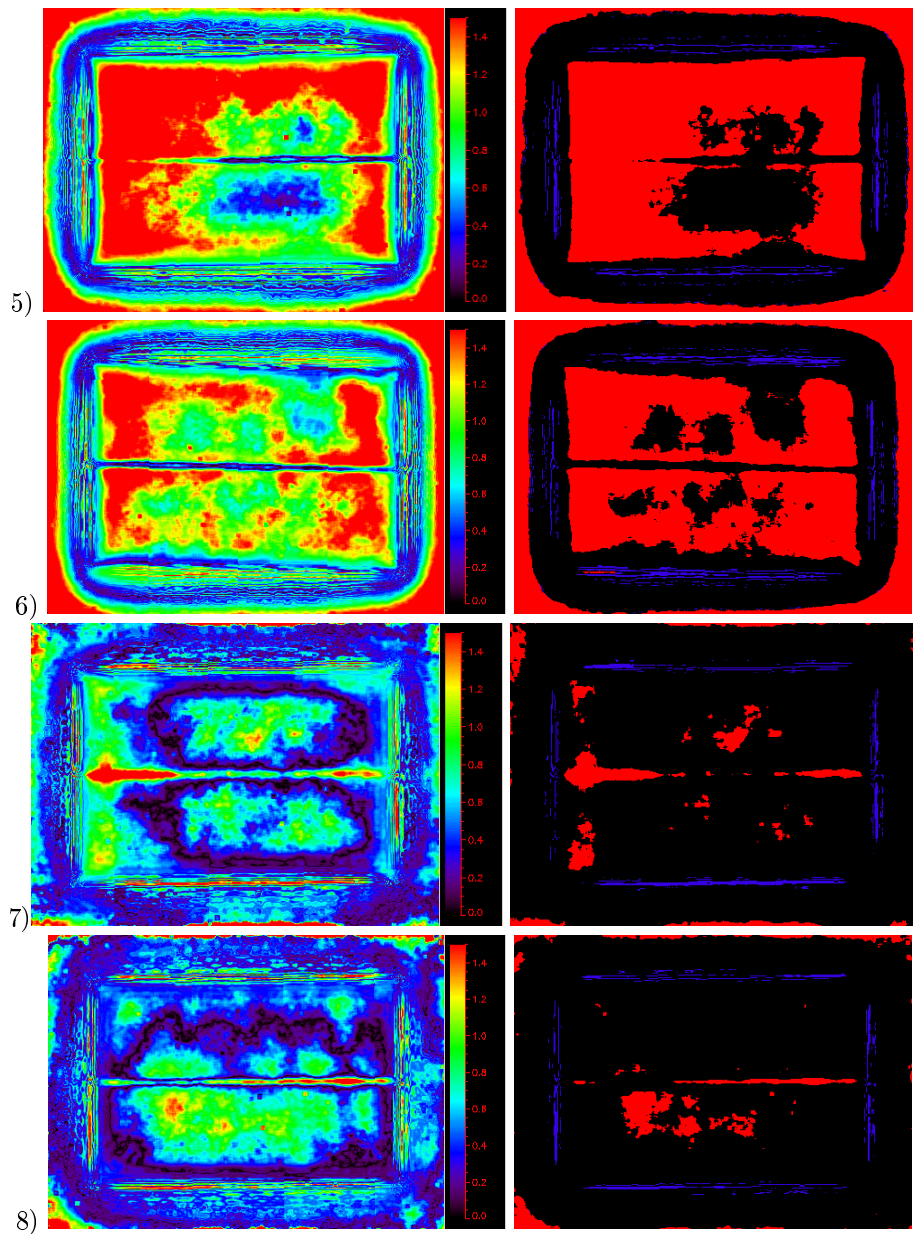
Figure 70: Gamma evaluation for film setup 4. Images to the left show the continuous gamma distribution. Images to the right shows discretely which points pass/fail the criteria - red pixels have failed all three levels of acceptance.

6 Discussion

6.1 Experimental methods

The experimental method took some time to develop due to the lack of previous experience in using film by the NRPA. In other words, everything had to be done from scratch. The initial "article hunt" was tedious at times as there are a myriad of articles on the subject of film dosimetry. Once relevant articles had been selected and studied, a general method started to fall into place. There are lots of different procedures outlined in different literature, but the work done in this thesis was based on the procedure first outlined by Devic et al (2004) [44], with some modifications, as this seemed to be the basis for most procedures.

6.1.1 Visited hospitals

All the hospitals visited were positive to the visit and the measurements performed. Some hospitals had previous experience in using radiochromic film. Many remarked that it had been a long time since clinical equipment had been compared to NRPA's standard equipment, especially with regard to ionization chamber calibration. With the opening of the new SSDL facilities, it seems like there will be more interaction between the NRPA and hospitals.

In total measurements were performed at 7 hospitals, on 14 linear accelerators. 8 Varian, 4 Elekta and 2 Siemens treatment units were investigated. Varian's own Eclipse was used to plan the fields on all Varian units, while Oncentra MasterPlan was used to plan the fields on Elekta and Siemens units. In retrospect, more Siemens and Elekta units should have been investigated to be able to compare different manufacturers to each other.

Some linear accelerators were "twin units", meaning that two machines share the same dose planning data. These included the following linacs: 1 & 2, 3 & 4, 5 & 6, and 7 & 8. These units should exhibit very similar results in all experiments, in order to justify their equality.

6.1.2 Method development and execution

As the method was carried out at hospitals in several different cities, the equipment experienced a lot of stress while in transit. Particularly the barometer, used for air pressure measurements in the ionization chamber setup, suffered from all the traveling. In addition, one piece of perspex used for the film setup broke and had to be replaced during the course of the experiments.

Some concern was expressed prior to traveling of whether the trip by air to several of the hospitals would have any effect on the film due to increased cosmic radiation, x-ray scanning or temperature. Therefore two films were taken to see the effects of plane travel. In fact, even film that was sent through the airport x-ray scanner did not experience any polymerization. This is probably due to the threshold levels of the film - according to the manufacturer, the film is only sensitive to doses above 0.01 Gy [38], which is higher than the dose that can potentially be received from air travel.

The results in figures 71 and 72 show that these effects were negligible. The signal retrieved from the film is most probably attributed to noise and inhomogeneities in the film. However, care should be taken to not travel with the

same films to multiple locations, as there might be an unidentified cumulative effect that is not tested for in this thesis.

Films from two different batches were used for the experiments, hereafter referred to as batch 03I and 04I. Batch 03I was used for linear accelerators 1, 2, 3, 4, and 14, while batch 04I was used for the remaining linacs.

6.1.3 Calibration procedure

There was a wish to use the new SSDL Co-60 for the calibration procedures. Existing apparatus had to be modified to hold the film in place during this procedure. The setup does allow for some uncertainty due to bending of the film from water currents. As much care was taken as possible to make sure that the center of each calibration film (the region from which the calibration dose was extracted) was at exactly 5.0 g/cm^2 depth. The correlation of the calibration curves are very good at 0.99990 and 0.99986 so this uncertainty is seemingly negligible. Using a curve approximation on the form $D(OD) = a(OD)^n + b(OD)$ can thus be said to give a good correlation between dose and optical density. A polynomial of at least third degree will generally also give satisfactory results.

The set desired dose levels ensured evenly spaced data points for the calibration curve. From the desired doses and measured dose rate of the Co-60 source, approximate exposure times were determined. Looking at table 2, the measured doses at the calculated exposure time differed slightly from the desired doses. This is likely due to the movement of the Co-60 source in the gammatron head. A short time is spent as the source is pushed to the opening in the source head, and this transition period will contribute to the measured dose. For doses around 2 Gy or higher doses, this effect is negligible.

The manufacturer claims that GafChromic® EBT type film is energy independent for high-energy photons. A recent work by Rink et al (2006) reports that "delivering the dose with a 6 MV or an 18 MV beam, instead of a Co-60 beam, does not appear to introduce a significant decrease in response (within 5 %)" [59]. In other words, the doses measured at 15 MV might be underestimated by up to 5 % when using Co-60 for the calibration. No comparison between a 15 MV calibration setup and a Co-60 calibration setup have been performed for this thesis, but this would be of interest to investigate before creating a new calibration curve.

There were some difficulties when calibrating the film to reflect absolute dose levels. The method of placing film strips in a water tank allows for the film to bend in the water. The method also requires that a new piece of film be placed in the clamp for each dose level. This makes the film prone to displacement due to human error. To minimize this error the distance from the front of the film to the window of the water phantom was measured prior to every exposure, but uncertainties may have occurred. It would be favorable to fix the film's position more rigidly for future experiments.

6.1.4 Scanning

The scanner flatness correction was in this thesis provided for by subtracting an unexposed scan. In a new work by Menegotti et al (2008), the scanner flatness correction is shown to be dependent on the pixel value (ie dose) as well as the

horizontal position [60]. Dose dependent scanner flatness was not corrected for in this thesis, and is thus a source of possible improvement for future work.

Light scattering from the scanner lamp has also been an issue of frustration. Complications were encountered when scanning the calibration films; the netOD values were lower than expected for the given doses. It was discovered that this discrepancy was due to the light from the scanner lamp scattering differently in the calibration films due to their small size compared to the films used for clinical experiments.

In order for the dose from two films to be comparable, the films need to be very similar in size, particularly in the direction perpendicular to the scanner lamp movement. As can be seen from figure 43, difference in light scattering can lead to a 25 % or higher error in the calculated dose for doses around 2 Gy. This is solely due to different light scattering for the two curves.

Light scattering is such an important parameter due to the transmissive nature of the scan. A cold cathode fluorescent tube above the film emits light that passes through through the film. The transmitted light is then recorded by a linear CCD array on the opposite side of the film. The darker the film is, the less light is transmitted. In other words, higher doses give lower recorded pixel intensities.

A scan of the empty scanner bed generally gave the max pixel value 65535 for all pixels in the scanning area, which means that all transmitted light is detected. Unexposed film gave a pixel value somewhere between 61500-63500, while doses of approximately 2 Gy gave pixel values in the order of 42500-43500.

The scattering of the light from the scanner lamp in the film leads to variations in the detected intensity. Thus, light will be scattered differently for films of different sizes, even when the films are from the same batch and exposed to the same dose. This seems to be most prominent for the size in the direction perpendicular to the scanning direction. These inaccuracies could be minimized if all the films were of the same dimensions, ensuring identical light scattering conditions.

6.1.5   Software tools

As has been mentioned in section 3.6, both Matlab and IDL-based algorithms were used in the data processing and analysis. Matlab was chosen for creating the initial algorithms when testing out the film during the early spring of 2008. Matlab was used as the main platform for analysis and processing even after VerA was discovered in may. It was decided that VerA was to be used for all gamma evaluation. However, VerA was not compatible with the exported dose images from Oncentra MasterPlan software in DICOM format. Both Matlab and IDL are versatile and effective in the processing of film, and there is really no deciding factor on why one should select one or the other when processing and analyzing radiochromic film. Several commercial software packages that support processing and analysis of radiochromic film are also available.

6.2   Absolute dosimetry with ionization chamber

The results from the absolute dosimetry at reference conditions are good; all linear accelerators are within the 2 % limit. This was consistent with the hospitals own measurements. Thus it could be said that all visited hospitals have

good control on their absolute dosimetry according to TRS-398 protocol. As has been mentioned, this result only shows correspondence in a single point for a 10x10 cm^2 field. However, it does shows that the hospitals have their dosimetry within the set boundaries.

During the previous clinical audit conducted in 2002, the mean dose of 43 photon beams was calculated to be 2.020±0.050 Gy, with measured doses ranging from 1.972 Gy to 2.720 Gy [10]. For the measurements conducted for this thesis, the mean dose was calculated to be 2.004±0.040 Gy, with measured doses from 1.980 Gy to 2.037 Gy. Thus the accuracy of the absolute dosimetry measured with an ionization chamber in a water phantom at reference conditions has seemingly improved.

Most hospitals use calibration depth of 10 g/cm^2 for both 6 MV and 15 MV photons. The monitor units for these energies should be normalized so that a certain number of MUs gives the same dose for both energies. The experimental results show that the maximum variation in absorbed dose between 6 MV and 15 MV photons for a single linac is 1.42 %, which is within the 2 % limit. However, the different energies have different TPR$_{20,10}$ values as well as different data in dose planning software, so this difference does not have any impact for clinical treatment.

As has been mentioned, some linear accelerators use the same data for dose planning for two machines. These linacs should give the same value for absorbed dose in a 10x10 cm^2 field at reference conditions. In general the results are fairly similar for both twin units, but in certain cases there are notable deviations. For example, linac 5 and 6 are twin units but the absorbed dose varies with 1.90 % for 15 MV photons when measured with an ionization chamber, which is barely within the 2 % limit.

6.3 Film dosimetry

In the previous section, absolute dose was with an ionization chamber in a water phantom according to the recommendations from IAEA TRS-398 protocol [2]. TRS-398 concerns measuring the absolute dose in a single point, the isocenter. Using film, one can take the absolute dosimetry one step further, and calculate a plane profile of the dose at a certain depth. Both absolute and relative aspects of film dosimetry will be discussed in this section.

Using film, the absolute dosimetry is more unstable than when using a standard ionization chamber in a water phantom setup. This is attributed to the calibration of the film, and not to the hospitals as the relative dosimetry proved to be reasonable (see section 6.3.2).

6.3.1 Absolute dosimetry

Results from the analysis of radiochromic film has to be divided into two categories in terms of results; relative- and absolute dosimetry. The film has given good results for relative dosimetry, but the absolute measurements suggest that more work has to be done to modify and improve calibration and processing procedures.

Between measurements on linear accelerators 10 and 11, a piece of perspex used for the film setup broke and had to be replaced. Table 5 shows the relative difference in isocenter dose measured with film and ionization chamber.

All linear accelerators measured with 03I film have a difference in dose of over 4 percent as compared to ionization chamber measurements, with a mean difference of 8.5 %. However, doses measured with film from batch 04I before the equipment replacement are all within 3 % of the ionization chamber measurements. After the replacement, the measured doses with 04I film at reference conditions have a mean that is 8.1 % lower than the doses measured with an ionization chamber.

After the replacing the perspex plate, the measured doses using film decrease by approximately 8 % for batch 04I. This could perhaps be accounted to that the properties of the slit where the films were inserted during exposure, changed. The most likely explanation for this is that the new setup (after replacement) could have caused there to be an air cavity between the film and the water phantom during exposure. In order to minimize this uncertainty, a CT scan should be conducted of the film setup and and stored in DICOM format for easy access from medical software. The actual phantom can then be imported into dose planning software for better accuracy.

If the energy dependence reported by Rink et al (2006) mentioned in section 6.1.3 is accurate, this could be a reason why the doses measured with film are lower than those measured with an ionization chamber. This does not, however, explain how the doses measured using film for linear accelerators 5-10 were so close to the expected value. Cumulatively, these sources of uncertainty could contribute to the differences in dose between chamber and film.

6.3.2 Relative dosimetry

Relative dosimetry refers to the measurements that do not depend on absolute dose values. These include field size, penumbra, symmetry and flatness. Looking at these quantities, it is clear that the film is useful in measuring such parameters. These parameters are also important for the hospitals, as they influence how the dose is deposited in a body.

Looking at the field sizes for the 10x10 cm^2 field, it is clear that no major discrepancies are present. The mean value is 10.002 cm, and the furthest outliers are within 1.07 % of 10 cm. This is within the reported uncertainty of the film. Being able to precisely create fields of different sizes is important for the patient dose delivery. Cumulative field sizes were also calculated for setup 1, as the sum of the two 5x10 cm^2 should equal a 10x10 cm^2 field similar to the 10x10 cm^2 field at reference conditions. A slightly different algorithm was used as the field edges could no longer be defined according to 50 % d$_{ref}$. All measured field size values from setup 1 were within 0.71 % of the values measured for the reference field, which is well within the uncertainty of the procedure.

Penumbra values range from 0.39 cm to 0.62 cm. Penumbra is a measure of the "sharpness" of the field, as it is desirable to have the dose delivered to an area as clearly defined as possible. The measured values are consistent with clinical values, and no anomalies occur. Film dosimetry seems to be useful for measuring penumbra values with the help of algorithms in Matlab or IDL. Similar penumbra values calculated for linacs in setup 1 are equivalent to the values calculated the reference field within 0.9 mm (less than 3 pixels). All in all the comparison between the 10x10 setup and setup 1 for field size and penumbra shows good agreement.

Beam symmetry and flatness depend on the flattening filter mentioned in

section 2.3.1. It is favorable for these values to be as low as possible. A low value for beam flatness means that the beam profile is flat and homogeneous. A low symmetry value means that the beam is symmetrical on both sides of the central axis.

The measured values for beam flatness range from 1.02 to 1.06, with a mean of 1.04 in both the x- and y-directions. What this means clinically is that the isocenter dose d_{ref} is on average about 4 % lower than d_{max}. This is slightly higher than values calculated from dose planning software, which is about 2 %.

For symmetry, the mean value for all fields is 1.02. This means there is an average of maximum 2 % difference between two sides of a line profile through the isocenter. If this value is accurate, care needs to be taken when considering the orientation of the patient with respect to the gantry and collimator, as there may be more or less dose delivered in some areas than others.

6.3.3 Spliced fields

This section concerns the attributes that are specific to spliced fields, where two fields border each other. This will also be discussed somewhat in section 6.3.5 with relation to gamma evaluation.

The area of interest when looking at spliced fields is the border area. If a secondary collimator or MLC leaf has an error in its position, it could give a large over- or underdosage in the border area between two fields. Two cases were investigated in this thesis; spliced asymmetric fields without collimator rotation and spliced asymmetric fields with collimator rotation.

The fields in setup 1 are the case where two fields are spliced but no collimator rotation occurs. Figure 52 shows the relative difference in measured dose at the isocenter between the 10x10 cm^2 reference field and the fields in setup 1. It is clear from this figure that some clearly noticeable over- and underdosages occur. At the extremes, there is an overdosage of +22.0 % for linac 10 and an underdosage of -21.6 % for linac 11. These values are high, and might have a clinical impact even if the affected area is small.

The deviations are not corrected for in dose planning software, which makes them potentially harmful to a patient undergoing treatment. An overdosage means that more dose is deposited deeper in the tissue than expected, in the worst case leading to organs located behind the tumor being damaged as their absorbed dose will be higher than anticipated. Similarly, an underdosage means that the cancer tumor may not not absorbing as much dose as planned.

Setup 3 and 4 are both cases where fields are spliced with 180 degree collimator rotation. The resulting over- and underdosages in the border between the two fields will be doubled in size due to the rotation. More underdosages occur than overdosages, indicating that there is a trend where the secondary collimator travels past the central axis slightly. If the rotation itself is inaccurate, it could lead to a dose gradient over the border between the two fields, with a higher dose at one end than at the other. Due to this, the median dose difference was calculated over the border area within 2 cm of the field edges. This is shown in figure 61. A parameter that measures the dose gradient over the border was not created for this thesis due to programming difficulties. However, this could possibly be done in the future, thus getting a measure on the precision of the collimator rotation.

The highest measured overdosage for setup 3 and 4 is +22.7 % for linac 10

and the highest underdosage is -39.9 % for linac 11, both for setup 4. These are the same linacs that exhibited the highest variation in the border dose for setup 1, meaning there is agreement between the two setups. The values from setup 3 and 4 are even higher than the ones measured from setup 1. However, hospitals rarely use a spliced field technique together with 180 degree collimator rotation, so the clinical implication of these deviations might not be as big.

The percentage of the target area that receives high over- or underdosages have not been calculated with accuracy for this thesis, partly because the correlation between FWHM and actual collimator error is not explored. Approximations show that over- and underdosages of at least *half the magnitude* of the maximum values mentioned above affect areas equivalent to about of 0.6 % - 0.8 % of the target volume. While this value does not sound high, the margins between successful and unsuccessful treatment can unfortunately be small in some cases, as was mentioned in the introduction.

Full width at half maximum (FWHM) values were calculated for the peaks or valleys in dose in the border area between two the two fields in film setups 1, 3 and 4. This FWHM value should give an indication of by how large the mm error in the secondary collimator movement is. If more experiments are conducted, the FWHM can most likely be related directly to the error in the collimator movement.

The measured FWHM values typically range between 0.3 and 0.6 cm. Several radiotherapy institutions in Norway use ionization chamber arrays such as the I'mRT MatriXX (Scanditronix Wellhöfer, Schwarzenbruck, Germany) for IMRT verification. The I'mRT MatriXX has a spatial resolution of 0.72 cm, the distance between two adjacent ionization chambers [61]. Using the I'mRT MatriXX, gaps between spliced fields and MLC leaf positions error may be underestimated or not detected at all. Therefore, the use of film should be implemented due to its superior resolution compared to ionization chamber arrays.

A larger gap or overlap between the secondary collimators should give a higher over- or underdosage, respectively. Hence FWHM should be related to the dose difference. Figure 64 shows the correlation between the two. The distribution is skewed as the main portion of the data have a dose difference is between 5 % and 15 %. However, the linear fits shows a weak linear relationship between the two. While the existing measurements cannot be said to give a good correlation, there is an apparent trend of higher dose discrepancies with larger FWHM values.

6.3.4   Overtravel fields

Overtravel fields are fields where one or more of the secondary collimators travel past the central axis. Setup 2 is and example of two overtravel fields, where overtravel occurs for both collimator pairs. The dosimetry for such fields is different from symmetric fields such as the 10x10 setup. Both geometric measurements and dose measurements were collected from the scans of setup 2.

Looking at the doses out of context might not be very useful, but looking at the doses to the center of fields 3 and 4 with respect to d_{ref} in the center of the 10x10 cm^2 field is more interesting. The relative difference between these doses can be seen in figure 59. With the exception of linear accelerators 3, 7, 13 and 14, the measured dose in the center of field 4 stays fairly constant (within 0.5 % variation). The dose in the center of field 3 varies slightly more than in

the center of field 4. However, it seems that the doses to the two fields is in the same general range for most linear accelerators. However, the mean dose to field 3 is somewhat lower on average than the mean dose to field 4. A logical explanation to this is that it is because of the inhomogeneous response of the scanner. All films from setup 2 were scanned with exactly the same orientation.

Figure 58 shows the measured field sizes for the fields of setup 2. All measured values are within 2 mm of the expected values of 3 and 5 cm in the x- and y-directions, respectively. The largest deviations are in the x-direction, with measured field sizes up to 3.16 cm, 5.3 % higher than predicted, and down to 2.80 cm, 6.7 % lower than predicted. In the y-direction the field sizes range from 4.90 cm to 5.11 cm, corresponding to a difference of 2.0 % and 2.2 %, respectively. All in all, the measured field size values for setup 2 are found to be more fleeting than for the two previous setups.

In summary, the linear accelerators used were not as precise at creating overtravel fields as they are at creating standard symmetrical fields. Treatments that utilize overtravel fields are becoming more common in radiotherapy today, which means that more rigid quality controls for these cases need to be introduced. In figure 68, gamma evaluation is used to compare calculated dose distributions from dose planning software to dose distributions extracted from the film. Those results will be discussed in detail in section 6.3.5.

6.3.5 Gamma evaluation - film vs dose planning software

One of the most important and useful analyses in this thesis, and for dose profile comparisons in general, is the gamma evaluation. It is a relatively new technique, but is becoming more and more common in clinical environments. The reason this technique is so important is because it can say something about the correlation between what is calculated in dose planning software and what is measured using radiochromic film, ionization chamber arrays, or other similar methods. When planning a treatment, a lot of trust is put upon the dose planning software to maximize the dose to the tumor while minimizing the dose to the surrounding tissue and vital organs.

If the dose planning software cannot accurately predict these doses, it can lead to complications and in the worst case, bad treatment. Thus the gamma evaluation is in principle a test of the dose planning system. For this thesis, four linear accelerators with measured film doses close to the measured chamber doses were selected for gamma evaluation, both continuous and discrete. Continuous gamma is used to see trends and patterns in the gamma distribution, while discrete gamma gives a quantitative measure of the points that fail all three levels of acceptance as defined by Depuydt et al (2002) [57]. This analysis are found in figures 66 to 70.

Of the four linear accelerators considered for the gamma evaluation, linac 5 did not yield good results for any of the comparisons. This could be due to general inaccuracies in the measured dose to the film. This leads to believe that the error lies in the measurement, and not in the dose planning software. Similarly, linac 6 did not give feasible results for film setups 3 and 4. For all gamma evaluation, only points that lie within the field or close to the field are included in the analysis, as explained in section 5.3.4.

The gamma evaluation of the 10x10-setup gives very good results for 3 out of 4 linacs, where the percentage of pixels that fail is less than 5 %. Especially

linac 8 shows remarkably good correlation, as 0.00 % of the pixels fail all three levels. The fact that this setup gives good correlation is an indicator that the gamma evaluation gives reasonable results. The 10x10 cm^2 field at reference conditions is the reference field at all hospitals in Norway, which means that the hospitals should be able to reproduce this "standard" field accurately.

Setup 1 generally has a slightly higher percentage of pixels that fail the criteria compared to the 10x10 setup (except for linear accelerator 7). From figure 67, it is clear that these failing pixels are centered around the border area between the the two fields. The border between two spliced fields seems to be a problem area for many hospitals across the country.

The overtravel fields in setup 2 generally have more points failing all three levels of acceptance that the two previous setups. Something to notice here is that it is the fields themselves that fail the criterion and not the areas around the fields. A possible conclusion to be drawn from this fact is that dose planning systems succeed in predicting the geometric aspect of the fields, but do not accurately calculate the doses. Overtravel fields have a different dosimetry from symmetric fields, and perhaps more accurate measurements and algorithms need to be implemented for dose planning software to handle the differences between the two. A notable exception to this is linac 8, where only 0.88 % of the pixels fail the criteria.

For setups 3 and 4, the border between the two fields is again an area where a lot of pixels fail. In general, it seems that the border area requires more attention, as large over- and underdosages occur (see also section 6.3.3). In the situations where the fields themselves fail the gamma evaluation and the border passes, the conclusion is still that the greatest error lies in the border between the two fields. In clinical radiotherapy, half-collimated spliced fields with rotation are very seldom used, so these results do not have a huge impact on clinical situations. However, the results do back up the corresponding results from setup 1.

6.4 Evaluation of radiochromic film for clinical use

In previous sections, the different field setups using radiochromic film have been discussed. A main goal of this thesis is to evaluate the use of radiochromic film, and this will be discussed here. GafChromic® EBT type film has been evaluated both for absolute and relative dosimetry.

In general, the difficulties in using the film lies in the absolute calibration, as seen in figure 63. More research needs to be conducted to isolate the sources of potential uncertainties. There are certainly more parameters to take into account than at one would think at first eyesight, particularly with respect to scanning and calibration. This makes the successful implementation of radiochromic film dosimetry more time-consuming than what many clinical institutions can afford to spend.

Several hospitals that were visited reported that they had tried to implement the use of radiochromic film in their routines, but had given up due to the previously mentioned difficulties. This urges the development of a simple, universal procedure suitable for clinical audits. The procedure used for the experiments in this thesis has proved to have some shortcomings. In section 6.5.2, a modified procedure is suggested to improve stability and accuracy in the measurements.

For relative dosimetry, the film gives good results. The scanning resolution of the film at 72 dpi corresponds to about 3 pixels/mm. Hence radiochromic film can detect collimator or MLC leaf errors, as well as small artifacts that might not be detected using ionization chamber arrays, making film superior in this respect. It was shown in section 6.3.3 that even small errors can give large relative over- or underdosages. Radiochromic film is also useful in measuring gaps between MLC leaves.

Despite the lower resolution, ionization chamber arrays are among the most commonly used IMRT QA tools. The main reason for this is that they are easier to set up and use in weekly QA. The main reason for this is the ease of use; there is no need to calculate calibration curves or worry about scanner flatness. In addition, radiochromic film requires at least 6 hrs for the polymerization to stabilize, and preferably more than 8 hrs. This means that the results will generally not be available before the next work day. In a work by Reinstein et al (1998), a method is suggested in which the film is heated to 45°C for 2 hrs in order to rapidly stabilize the polymerization in order to shorten the processing time [62]. However, this method has not yet been verified with GafChromic® EBT type film.

The uncertainty associated with the use of radiochromic film has not been assessed in this thesis due to the difficulties in calibration and scanning procedures. A recently published article by Saur and Frengen (2008) outlines a new and accurate way of calculating film uncertainty. In this work, the relative 2σ dose uncertainty at a 95 % confidence level is given by the formula

$$\Delta D_{rel.}^{95\%} = \frac{1}{d} \cdot \frac{2 \cdot \sigma(d)}{\alpha(d)} \cdot 100\% \tag{42}$$

where d is the dose level, α is the pixel value per Gy for this dose level and σ is the standard deviation. The latter is defined as

$$\sigma(d) = \sqrt{\sigma_{fit}^2(d) + \sigma_{film-film}^2(d) + \sigma_{uniformity}^2(d) + \sigma_{noise}^2(d)} \tag{43}$$

Note that the pixel values have not been converted into optical density in this work. Another interesting observation from equation 42 is that the relative uncertainty increases for low doses. The four sources of uncertainty are the fit of the calibration curve, film to film variation, uniformity over the scan field and image noise, respectively. In their work, Saur and Frengen find the relative uncertainty to be within 4 % for doses between 1 and 3 Gy, reaching a minimum at about 2 Gy. For doses below 1 Gy, uncertainty increases rapidly. [63] If this uncertainty is real, the gamma evaluation criteria of 3 mm for DTA and 3 % for dose difference may be too strict, and should be more lenient especially for doses < 1 Gy.

In a work by Ritt et al (2005), the repeatability of GafChromic® EBT film is shown to be "considerably worse" for consumer grade flat bed scanners than for medical grade scanners, showing variations of more than 10 % in the scanner value when scanning the same film [64]. Nevertheless, most articles show good results with the use of radiochromic film. Thus, the use of EBT type film is not entirely without a future in clinical situations, even if the processing of the film may take too much time for daily or even weekly routines. Once the calibration, background correction and experimental procedures have been established, the

film might be used with advantage in monthly or more infrequent linac control routines. Cheaper film alternatives that do not involve scanning, such as GafChromic® RTQA, could be used for qualitative field analysis on a more frequent basis, as MLC leaf errors and blatant over- and underdosages will be easily visible on this type of film as well.

6.5 Future work and development

6.5.1 Further investigation

Experimental results have indicated that light scattering from the scanner lamp has great impact on the final result of the film. Hence a modification to the experimental procedure should be implemented and compared to the existing procedures to see if this could improve the precision of the film measurements. A frame should be created to fit in the scanner bed and used to obtain the same scanning area for each scan. This is of particular interest in relation to the calibration films, due to their small size compared to the clinically used films. Hence a single-film calibration technique could be considered to eliminate this problem. Also, the calibration data from the Co-60 source should be compared to calibration data obtained from 15 MV photons.

A new scanner flatness correction should be made for this modified procedure that takes into account both the optical density and the horizontal position in the scan field. The procedure outlined by Menegotti et al (2008) [60] seems to be a quick and easy way to do this. With this implemented, much fewer background scans need to be taken, thus significantly reducing scanning time.

For processing and analysis, Matlab has proved a useful and flexible solution. In addition to Matlab, IDL is commonly used for image processing tasks. At least one of these are available at most hospitals in Norway that employ physicists. Both Matlab and IDL have the option to export code to a stand-alone executable that does not need the host application to run. However, it might be desirable maximize accessibility for all radiotherapy hospitals in Norway. A migration to free software platforms such as ImageJ [65] or SciLab [66] could be considered. This way, all hospitals would be able to see and edit source code locally without having to purchase a license for neither Matlab nor IDL.

The procedure could be limited to one or two films in addition to the 10x10 cm^2 field at reference conditions. For example, overtravel fields could be combined with collimator rotation. This would cut down on both costs and time spent conducting the procedures. In general, the process should be optimized so that a maximum amount of information can be acquired in a minimum amount of time. The method of keeping the films at 45°C after exposure in order to rapidly stabilize the polymerization process [62] should also be investigated to minimize time use.

Once the procedure has been optimized, there is a world of future development to be done using films. The first step should include determining uncertainty in the procedure. The film could be exposed using dynamic wedges, or films could be exposed to multiple fields to see the cumulative dose. Perhaps most importantly, it could (and should) be implemented for use in verification of advanced IMRT plans, which is probably the area it will prove most useful. While work has been done on this field abroad, there is still a ways to go in Norway.

6.5.2 Suggestions for a new improved method

Due to the short time between testing, calibration and experimental measurements, many possible improvements and anomalies were not discovered until it was too late. In this section, some simple improvements are suggested to the method, primarily scanning and analysis.

1. Films should be of the same size and scanned using a custom-made opaque frame that fits the film and scanner bed perfectly. This frame should be placed on the scanner bed during all scans to ensure that the light scattering and scanner flatness correction is the same for every scan and does not need to be recalculated each day.

2. To save on film costs, the use of larger sheets of film should be considered. GafChromic® EBT is also available in sheets with large form factor 14" x 17" (35.5 cm x 43.2 cm), three times the area of the "standard" sized film. This size can for example easily be cut into 4 pieces of 17x20 cm, which would be more than sufficient for all the film setups used in this thesis.

3. The method of correcting for scanner flatness by subtracting an unexposed scan should be omitted from the procedure. This will both save time and avoid the added uncertainty of film-to-film variation in the film used for the unexposed scan. The $netOD$ value will become obsolete with the omission of the unexposed scan, instead the dose will be related directly to the pixel value. This curve can be fitted with a polynomial or exponential fit.

4. A new scanner flatness method based on the work by Menegotti et al [60] should be performed to establish correction for both position and dose. This setup consists of exposing a single film to several rectangular fields in a stripe pattern. A Co-60 source should be used to create these fields if possible, to ensure good field homogeneity (flatness). As the scanner flatness depends on pixel value only, this setup may not be necessary to perform for all linear accelerators. For this film, the dose should be calibrated to the center of each field using separate calibration data.

5. Calibration curves from Co-60 and 15 MV photons should be compared and checked for similarity - calibration should be performed using 15 MV photons if they are different. Single-film calibration techniques should be tried out. The doses should also be verified using an ionization chamber prior to radiochromic film exposures for maximum precision.

6. All uncertainties should be established and calculated using equation 42 according to the procedure by Saur and Frengen (2008) [63].

7 Conclusion

This thesis has investigated the use of radiochromic film of type GafChromic® EBT as a tool in radiotherapy QA. In addition, absolute measurements using an ionization chamber according to the current standard introduced by the IAEA were performed at all hospitals. Film and ionization chamber measurements were then compared to each other. A procedure was developed and Matlab algorithms were written in-house for handling, processing and analysis of the films.

The results using ionization chamber in a water phantom show good precision. All dose measurements were within 2 % of 2 Gy. When using radiochromic film, there were difficulties in the absolute calibration of the film. However, the film still proved useful in providing information about relative dosimetry. All hospitals have good control on the standard 10x10 cm^2 field at reference conditions. Parameters such as field size, sharpness (penumbra), beam flatness and symmetry are all within reason and uncertainty.

Different spliced field techniques show relatively big variations in the border area between two fields. In the case where two fields are spliced with no collimator rotation, variations from -21.6 % to 22.0 % were detected in the dose along the border between the two fields. For spliced fields with 180°collimator rotation, these variations are from -39.9 % to 22.7 %. These over- and underdosages generally affect small areas and narrow borders with FWHM values of approximately 0.55 cm or less. The variations in dose may not be easily detectable using existing QA due to limitations in spatial resolution. Gamma evaluations of these fields also show discrepancies in the border area.

Measurements done with radiochromic film on overtravel fields show that all linear accelerators can create these types of fields, albeit with a lower precision than the 10x10 cm^2 standard field. Additionally, gamma evaluation of the overtravel fields show that dose planning systems have difficulties in calculating the absolute dose to these fields. As a result, the linear accelerators perform much worse for these fields.

In general, results from the visited hospitals show that all radiotherapy institutions have good dosimetry for standard fields. However, nearly all hospitals perform significantly worse for the special cases of asymmetric, spliced and overtravel fields. Advanced IMRT plans have not been tested for this thesis, but is a relevant topic to investigate further.

The use of radiochromic film in clinical environments is definitely something to consider for the future. The low cost, ease of use and high spatial resolution makes it suitable for periodic controls. The long time between exposure and data collection means that the use will be limited to less frequent controls, such as quarterly controls. For more frequent controls, existing methods will have to suffice. The use of cheaper types of radiochromic film such as GafChromic® RTQA could be considered for performing simple qualitative field analyses.

The method used in the experiments with radiochromic film has some shortcomings that give large unexpected variations in absolute measurements. This method can therefore not be recommended for the use of radiochromic film in a clinical setting. To improve the precision of the experiments, a new method has been introduced as an alternative to the existing method. This method will hopefully give good results both for absolute and relative dosimetry.

A   Appendices

A.1   Image correction filters

For the image processing and analysis, two common noise reduction filters were relevant: median filter and wiener filter. These will be briefly explained in this section. "Input pixel" refers to the pixel before noise filtering, and "output pixel" refers to the pixel after noise filtering.

A.1.1   Median filtering (medfilt2 function in Matlab)

Each input pixel is subjected to an N×M matrix which replaces it's pixel value with the median value of its N×M pixel neighborhood. This type of filtering removes pixel errors and small details like dust, producing a smoother image. [50]

A.1.2   Wiener filtering (wiener2 function in Matlab)

The wiener2 Matlab filters a gray scale image based on statistics around each pixel, using an N×M matrix to define each pixel's local neighborhood. The mean μ and variance σ^2 is calculated around each pixel:

$$\mu = \frac{1}{NM} \sum_{n_1, n_2 \in \eta} a(n_1, n_2) \tag{44}$$

$$\sigma^2 = \frac{1}{NM} \sum_{n_1, n_2 \in \eta} a^2(n_1, n_2) - \mu^2 \tag{45}$$

where n_1 and n_2 are pixel coordinates in the input pixel's local neighborhood η defined by the N×M matrix. The output pixel value is then

$$b(n_1, n_2) = \mu + \frac{\sigma^2 - v^2}{\sigma^2}(a(n_1, n_2) - \mu) \tag{46}$$

where v^2 is the average of all estimated variances. [50, 51]

A.2   Letter sent out to hospitals

Letters were set out to in early July to the 10 hospitals that have linear accelerators. 8 hospitals replied with interest, and 7 hospitals were visited.
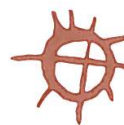
Sjefsfysiker ved sykehuset

Dosimetrikontroll ved bruk av radiokromisk film

Statens Strålevern ønsker å bidra til utvikling av nye metoder innen dosimetri i stråleterapi. I første omgang vil det utføres målinger med radiokromisk film på lineærakseleratorer ved et utvalg av sykehus i Norge som en del av en masteroppgave ved seksjon for Kvalitetsutvikling innen medisinsk strålebruk. Oppgaven utføres av Alexander Mauring, og går ut på å gjøre målinger med film av typen Gafchromic EBT med et standardisert oppsett på de ulike sykehusene. Dette vil bidra til å kvalitetssikre dosimetrien, samtidig som filmen i seg selv blir vurdert i forhold til videre bruksområde. Veiledere for oppgaven er Hans Bjerke (Statens Strålevern), Hilde Olerud (Statens Strålevern), Ståle Ølberg (Ullevål Universitetssykehus) og Eli Olaug Hole (Universitetet i Oslo).

Noen av testene som gjøres i oppgaven vil være:
- Bruk av film for absolutt dosimetri
- Måling av usikkerhet i bruk av film til relativ og absolutt dosimetri
- Dosimetri til skjøtede felt med og uten rotasjon av blendere
- Test av overtravel beam geometri og halvblending
- Sammenlikning av målte verdier med doseplan
- Sammenlikne lineærakseleratorer ved ulike sykehus og regioner, fra forskjellige produsenter og for ulike fotonenergier

Absolutt dosimetri vil verifiseres mot Strålevernets normal (Bjerkefantomet) ved lokale målebetingelser. Målingene vil utføres med medbrakt utstyr fra Statens Strålevern.

Det vil bli aktuelt å reise rundt til sykehusene i august og september. Mauring vil selvfølgelig være fleksibel og vil tilpasse sin reiserute etter når det passer for de enkelte sykehusene. Det er ønskelig å måle på minst to lineærakseleratorer per sykehus der det er mulig. Velger dere å takke ja til besøk vil det være nødvendig med tre timer til planlegging av felt i doseplan per sykehus samt klargjøring av utstyr, og to timer per lineærakselerator. Dette kan gjennomføres enten på dagtid eller på kveldstid, og det vil være ønskelig med bistand fra lokal fysiker. I tillegg vil det bli aktuelt å fylle ut et spørreskjema angående lokale kontrollprosedyrer på lineærakselerator.
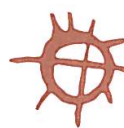
I ettertid vil dere få mulighet for innsyn i rapporten.

For å avtale tidspunkt for besøk eller hvis dere har noen spørsmål kan undertegnede kontaktes på e-post:
Alexander.Mauring@nrpa.no eller alexander.mauring@fys.uio.no
Eller på telefon 975 00 538

Med hilsen

Tor Wøhni   Alexander Mauring
seksjonssjef   student

A.3 Selected Matlab algorithms

This appendix contains selected algorithms from Matlab written especially for
this thesis and its experimental procedures. While commercial solutions for the
analysis of radiochromic film exists, no standard Matlab algorithms are generally
available. This led to the development of algorithms in Matlab for analysis of
films for this thesis. These algorithms grew into two applications: ProcessEBT
and SensiometriCal. Both are briefly described in section 3.6.

ProcessEBT and SensiometriCal have graphical front-ends and contain ap-
proximately 850-950 lines of code each, so the algorithms below are heavily
abbreviated for clarity. Full code is available from the author upon request.
Lines that begin with "%" are comments and not a part of the program code.

Algorithm 1 Algorithm for importing three image files, averaging them and
saving the averaged image in .tiff format

```
% Algorithm for selecting and averaging 3 images
% By Alexander Mauring
% Reads an image from file
[FileExp,PathExp] = uigetfile('*.tif','Select scan #1');
cd(PathExp);
scan1 = imread(FileExp);

[FileExp,PathExp] = uigetfile('*.tif','Select scan #2');
cd(PathExp);
scan2 = imread(FileExp);

[FileExp,PathExp] = uigetfile('*.tif','Select scan #3');
cd(PathExp);
scan3 = imread(FileExp);

%Averages th
img = scan1./3+scan2./3+scan3./3;
[FileWrite,PathWrite]=uiputfile('*.tif','Save averaged image as');
cd(PathWrite);

%Saves output image
imwrite(img, FileWrite, 'tif');
```

Algorithm 2 Algorithm for processing a GafChromic® EBT film and saving
the processed image

```
% Algorithm to process GafChromic® EBT images
% by Alexander Mauring

% Reads .tif images from file for exposed and unexposed scans
[FileExp,PathExp] = uigetfile('*.tif','Select averaged exposed image');
cd(PathExp);
I = imread(FileExp);

[FileUnexp,PathUnexp] = uigetfile('*.tif','Select averaged unexposed image');
cd(PathUnexp);
J = imread(FileUnexp);

% Red channel data is extracted from both images
I=I(:,:,1);
J=J(:,:,1);

% Images are filtered with a 5x5 wiener filter
I=wiener2(I, [5 5]);
J=wiener2(J, [5 5]);

% Pixel values are converted to "double" format to perform
% remaining calculations
I=im2double(I);
J=im2double(J);

% netOD is calculated
K=log10(J./I);

% Image is converted back to image format and saved
K = uint16(round(doseout*65535));
[FileWrite,PathWrite]=uiputfile('*.tif','Save processed image as');
cd(PathWrite);
imwrite(K, FileWrite, 'tif');
```

Algorithm 3 Algorithm for creating a calibration curve with n points. The code assumes that all calibration images have already been processed like described in algorithm 2.

```
% Algorithm for creating a calibration curve for
% GafChromic® EBT film
% by Alexander Mauring

i=1
% This loop is repeated n times
while i <= n

    % Load image file from which to extract calibration data
    [FileCal,PathCal] = uigetfile('*.tif','Select calibration ...
        image to extract ROI');
    cd(PathCal);
    I = imread(FileCal);

    % Select ROI using imSelectROI and extract ROI from image
    ROI=imSelectROI(I);
    cropmatrix=[ROI.Xmin ROI.Ymin (ROI.DX-1) (ROI.DY-1)];
    roi=imcrop(I,cropmatrix);

    % Retrieve median value from ROI
    caldata(i)=median(median(roi));

    % Input corresponding dose value
    dosedata(i)=input('Corresponding dose value: ');

    i=i+1;

end

% Uses ezyfit to approximate a curve to the values
f = ezfit(x,y,'a*x.^n+b*x');
cal = f.m;

% Plots the points and the curve
hold on
scatter(handles.caldata,handles.dosedata);
x = (min(caldata):(max(caldata)-min(caldata))/100:max(caldata));
y = cal(1)*x.^cal(3) + cal(2)*x;
plot(x,y,'r');
hold off
```

A.4 Effects on radiochromic film from air travel

Several of the hospitals that were visited are located quite far from Oslo, and the equipment had to be sent by plane. Tests were made to see if there were any measurable effects on the radiochromic film from the air travel. Two pieces 10x20 cm^2 of radiochromic film from the same batch were brought on the plane; one was sent with the checked-in luggage, the other was sent in the hand luggage and scanned in the security x-ray machine. Flight time for both films was approximately 45 minutes both ways, or 1.5 hrs in total.

Upon return, both film pieces were scanned and processed according to the procedure described in sections 3.5.1 and 3.5.2, subtracting the signal from a piece of film that had stayed at the NRPA. Line profiles were taken through the center in the direction perpendicular to the scanner lamp movement. Results can be found in figures 71 and 72.

Mean values from the line profiles are 0.005 Gy and 0.008 Gy. However, EBT type film is only sensitive for doses above 0.010 Gy according to the manufacturer [38]. This means that the measured dose values are outside the sensitivity range of the radiochromic film, and are thus not accurate. The measured doses are attributed to noise and uncertainty in the film homogeneity.
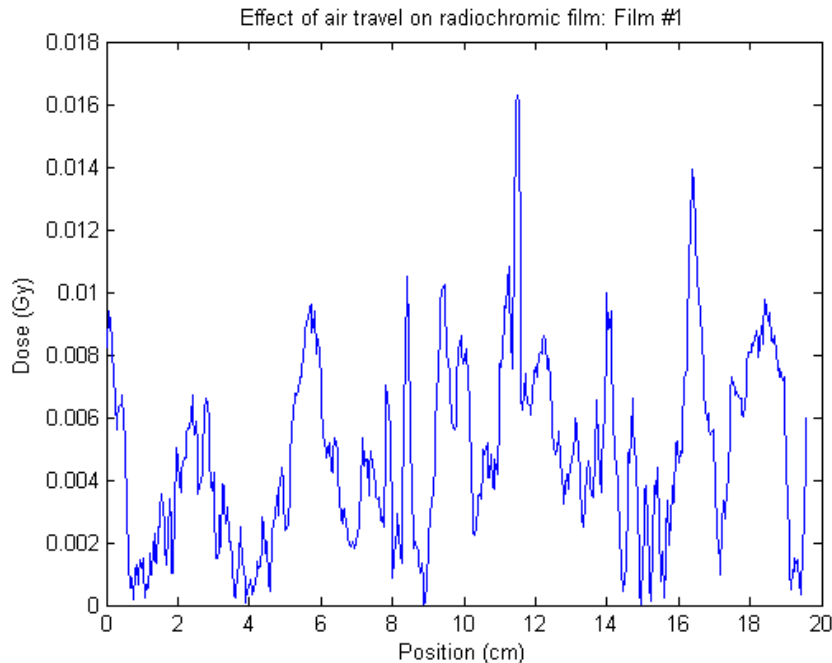
Figure 71: Signal from film 1 of the air travel effect test, total flight time was about 1.5 hrs. The film was carried in the hand luggage during travel. Measurements have a mean of 0.0048 Gy with a standard deviation of 0.0030 Gy.
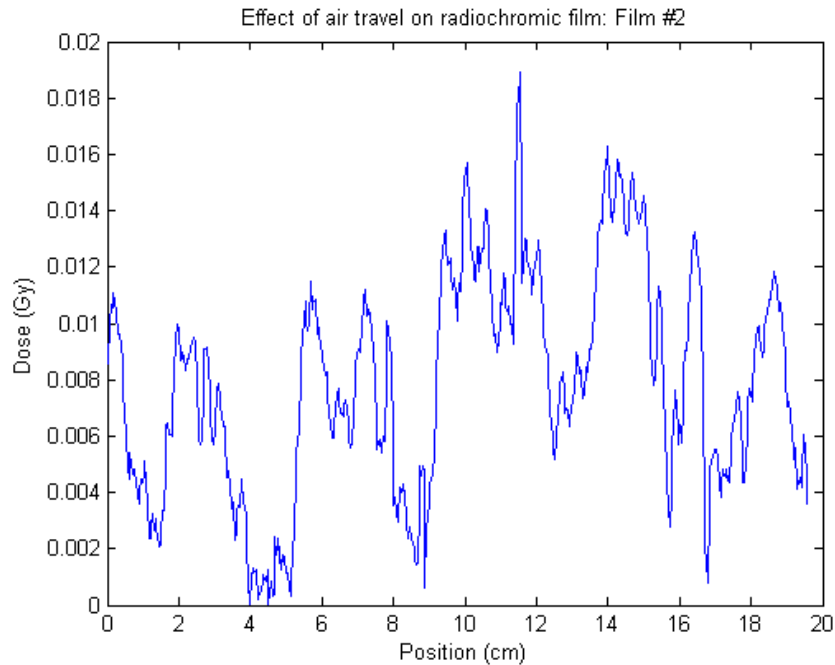
Figure 72: Signal from film 2 of the air travel effect test, total flight time was about 1.5 hrs. The film was transported in the checked-in baggage during travel. Measurements have a mean of 0.0079 Gy with a standard deviation of 0.0039 Gy.

A.5 Calibration of Co-60 beam at the SSDL

GafChromic® EBT film was used to measure the dose profile and determine field size and penumbra as a part of calibrating the geometry of the Co-60 beam at the secondary standard dosimetry laboratory (SSDL) at the NRPA. The measurement data obtained from the film was compared to measurements done with an ionization chamber setup.

A.5.1 Setup

Dose profile measurements were carried out on June 17th 2008 on the Co-60 beam. A 12.5x20cm^2 film piece was placed at a SAD of 100 cm under a 5.5 mm perspex slab to create build-up. A 10x10 cm^2 field was set up against a field size template and the film was exposed for 2.0 minutes. The activity of the source was 475 TBq at the time of installation. The setup can be seen in figure 73.
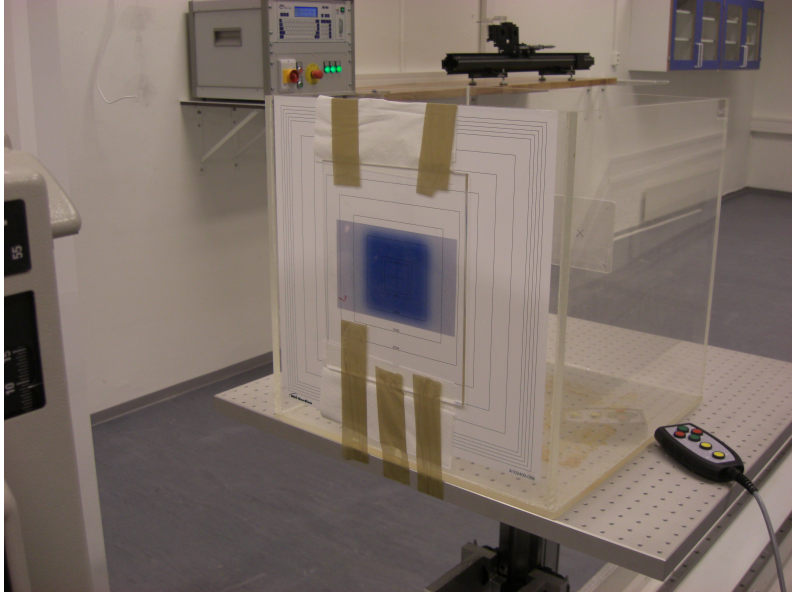
Figure 73: The setup after exposure. The Co-60 source is located to the left.

After exposure the film was stored overnight in dark and dry conditions. The following day the film was scanned according to the procedure outlined in section 3.5.1. Averages of the last three scans of the exposed film and the unexposed film were used in the analysis.

A.5.2 Image processing and analysis

The averaged images were imported into self-written algorithms in Matlab. The red color channel was isolated to get the best signal, and noise was reduced with a 5x5 pixel median filter. Then the optical density value of each pixel was calculated using the formula

$$OD_i = log_{10} \frac{I^i_{unexp}}{I^i_{exp}} \tag{47}$$

where I^i_{unexp} and I^i_{exp} are the pixel intensities of pixel i for the unexposed and exposed scans, respectively.

Then the dose equivalents of the OD values were calculated using the formula

$$D(OD) = 25.582(OD)^{1.031} - 19.837(OD) \tag{48}$$

which had been calculated from previous calibration data.

An enhanced processed version of the Co-60 field can be seen in figure 74.
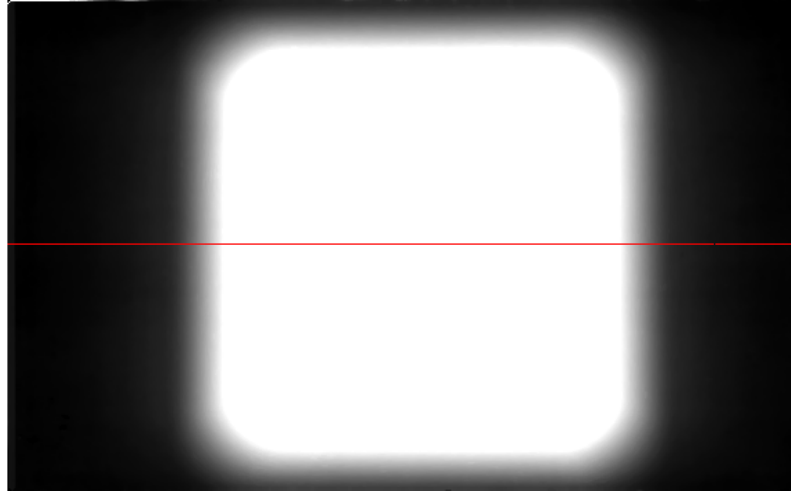
Figure 74: Enhanced version of the 10x10cm^2 Co-60 field. The image has been normalized so the max dose is completely white and zero dose is completely black. The red line shows the location of the line profile used for later analysis.

A.5.3   Analysis

A line profile taken in the x direction can be seen in figure 75. The profile taken is represented by the red line in figure 74.
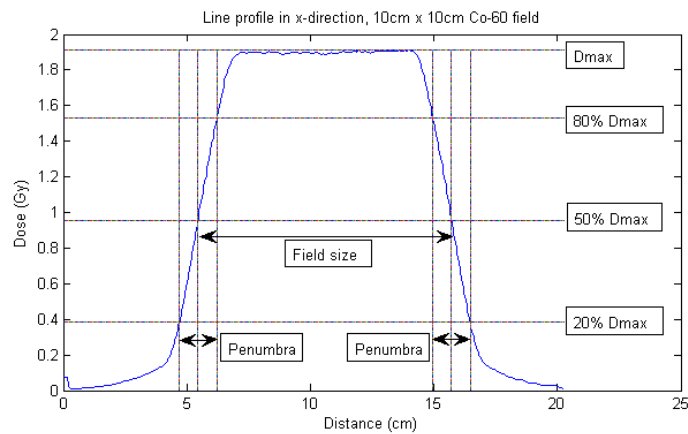
Figure 75: Line profile of the Co-60 beam in the x-direction, created in Matlab. Field size and penumbra are shown in the figure.

Matlab produces the following statistics:

Type	Dose statistics (Gy)
min	0.0043
max	1.9102
mean	0.9869
median	1.0166
mode	1.8935

The fact that the minimum dose is more than zero can be explained by x-ray scattering and the use of a median filter. From figure 75 the field size and penumbra can be calculated.

- *Field size*: The beam edge is defined as the difference in distance between the points where the dose equals 50 % of Dmax. From figure 75 the field size was calculated to be **10.26 cm.**

- *Penumbra*: The penumbra is defined as the distance between 80% of Dmax and 20% of Dmax. The penumbra was calculated on both sides of the field, see figure 75. The penumbra on the left was calculated to be **1.52 cm.** The penumbra on the right was calculated to be **1.51 cm.**

A.6 Ionization chamber measurement tables

This section of the appendix presents data from the measurements of absolute dose using an ionization chamber: electrometer readings, temperature and pressure.

Table 7: Measurement data from the ionization chamber setup for linear accelerator #1.

15 MV	#	nC	°C	kPa	**6 MV**	#	nC	°C	kPa
300 V	1	-41.24	23.6	100.93	**300 V**	1	-40.76	23.6	100.92
	2	-41.24	23.6	100.93		2	-40.77	23.6	100.92
	3	-41.24	23.6	100.93		3	-40.75	23.6	100.92
	avg.	**-41.24**	**23.6**	**100.93**		**avg.**	**-40.76**	**23.6**	**100.92**
100 V	1	-40.62	23.6	100.93	**100 V**	1	-40.47	23.6	100.92
	2	-40.63	23.6	100.93		2	-40.48	23.6	100.92
	3	-40.63	23.6	100.93		3	-40.48	23.6	100.92
	avg.	**-40.63**	**23.6**	**100.93**		**avg.**	**-40.48**	**23.6**	**100.92**

Table 8: Measurement data from the ionization chamber setup for
linear accelerator #2.

15 MV	#	nC	°C	kPa	**6 MV**	#	nC	°C	kPa
300 V	1	-41.49	23.0	100.93	**300 V**	1	-41.11	23.0	100.93
	2	-41.52	23.0	100.93		2	-41.13	23.0	100.93
	3	-41.53	23.0	100.93		3	-41.12	23.0	100.93
	avg.	**-41.51**	**23.0**	**100.93**		avg.	**-41.12**	**23.0**	**100.93**
100 V	1	-40.92	23.0	100.94	**100 V**	1	-40.81	23.0	100.94
	2	-40.91	23.0	100.94		2	-40.81	23.0	100.94
	3	-40.93	23.0	100.94		3	-40.82	23.0	100.94
	avg.	**-40.92**	**23.0**	**100.94**		avg.	**-40.81**	**23.0**	**100.94**

Table 9: Measurement data from the ionization chamber setup for
linear accelerator #3.

15 MV	#	nC	°C	kPa	**6 MV**	#	nC	°C	kPa
300 V	1	-42.21	20.5	99.91	**300 V**	1	-41.11	20.5	99.90
	2	-42.23	20.5	99.91		2	-41.13	20.5	99.90
	3	-42.22	20.5	99.91		3	-41.12	20.5	99.90
	avg.	**-42.22**	**20.5**	**99.91**		avg.	**-41.12**	**20.5**	**99.90**
100 V	1	-41.63	20.5	99.90	**100 V**	1	-40.81	20.5	99.90
	2	-41.62	20.5	99.90		2	-40.81	20.5	99.90
	3	-41.64	20.5	99.90		3	-40.82	20.5	99.90
	avg.	**-41.63**	**20.5**	**99.90**		avg.	**-40.81**	**20.5**	**99.90**

Table 10: Measurement data from the ionization chamber setup for
linear accelerator #4.

15 MV	#	nC	°C	kPa	**6 MV**	#	nC	°C	kPa
300 V	1	-41.98	21.9	99.79	**300 V**	1	-41.61	21.8	99.78
	2	-41.93	21.9	99.79		2	-41.56	21.8	99.78
	3	-41.95	21.9	99.79		3	-41.56	21.8	99.78
	avg.	**-41.95**	**21.9**	**99.79**		avg.	**-41.58**	**21.8**	**99.78**
100 V	1	-41.55	21.9	99.79	**100 V**	1	-41.42	21.8	99.78
	2	-41.54	21.9	99.79		2	-41.43	21.8	99.78
	3	-41.54	21.9	99.79		3	-41.43	21.8	99.78
	avg.	**-41.54**	**21.9**	**99.79**		avg.	**-41.43**	**21.8**	**99.78**

Table 11: Measurement data from the ionization chamber setup for
linear accelerator #5.

15 MV	#	nC	°C	kPa	6 MV	#	nC	°C	kPa
300 V	1	-41.56	20.4	98.50	**300 V**	1	-40.54	20.4	98.50
	2	-41.54	20.4	98.50		2	-40.57	20.4	98.50
	3	-41.55	20.4	98.50		3	-40.55	20.4	98.50
	avg.	**-41.55**	**20.4**	**98.50**		**avg.**	**-40.55**	**20.4**	**98.50**
100 V	1	-41.03	20.4	98.50	**100 V**	1	-40.27	20.4	98.48
	2	-41.03	20.4	98.50		2	-40.30	20.4	98.48
	3	-41.03	20.4	98.50		3	-40.29	20.4	98.48
	avg.	**-41.03**	**20.4**	**98.50**		**avg.**	**-41.29**	**20.4**	**98.48**

Table 12: Measurement data from the ionization chamber setup for
linear accelerator #6.

15 MV	#	nC	°C	kPa	6 MV	#	nC	°C	kPa
300 V	1	-40.69	21.1	98.50	**300 V**	1	-40.16	21.0	98.48
	2	-40.70	21.1	98.50		2	-40.15	21.0	98.48
	3	-40.68	21.1	98.50		3	-40.15	21.0	98.48
	avg.	**-40.69**	**21.1**	**98.50**		**avg.**	**-40.15**	**21.0**	**98.48**
100 V	1	-40.22	21.1	98.50	**100 V**	1	-39.92	21.0	98.50
	2	-40.23	21.1	98.50		2	-39.95	21.0	98.50
	3	-40.21	21.1	98.50		3	-39.95	21.0	98.50
	avg.	**-40.22**	**21.1**	**98.50**		**avg.**	**-39.94**	**21.0**	**98.50**

Table 13: Measurement data from the ionization chamber setup for
linear accelerator #7.

15 MV	#	nC	°C	kPa	6 MV	#	nC	°C	kPa
300 V	1	-42.51	20.2	102.0	**300 V**	1	-42.70	20.2	102.0
	2	-42.52	20.2	102.0		2	-42.71	20.2	102.0
	3	-42.52	20.2	102.0		3	-42.69	20.2	102.0
	avg.	**-42.52**	**20.2**	**102.0**		**avg.**	**-42.70**	**20.2**	**102.0**
100 V	1	-41.85	20.2	102.0	**100 V**	1	-42.35	20.2	102.0
	2	-41.82	20.2	102.0		2	-42.37	20.2	102.0
	3	-41.83	20.2	102.0		3	-42.35	20.2	102.0
	avg.	**-41.83**	**20.2**	**102.0**		**avg.**	**-42.36**	**20.2**	**102.0**

Table 14: Measurement data from the ionization chamber setup for
linear accelerator #8.

15 MV	#	nC	°C	kPa	**6 MV**	#	nC	°C	kPa
300 V	1	-42.54	20.5	102.0	**300 V**	1	-42.15	20.5	102.0
	2	-42.54	20.5	102.0		2	-42.16	20.5	102.0
	3	-42.57	20.5	102.0		3	-42.14	20.5	102.0
	avg.	**-42.56**	**20.5**	**102.0**		**avg.**	**-42.15**	**20.5**	**102.0**
100 V	1	-41.88	20.5	102.0	**100 V**	1	-41.81	20.5	102.0
	2	-41.89	20.5	102.0		2	-41.81	20.5	102.0
	3	-41.89	20.5	102.0		3	-41.81	20.5	102.0
	avg.	**-41.89**	**20.5**	**102.0**		**avg.**	**-41.81**	**20.5**	**102.0**

Table 15: Measurement data from the ionization chamber setup for
linear accelerator #10.

15 MV	#	nC	°C	kPa	**6 MV**	#	nC	°C	kPa
300 V	1	-40.97	22.9	99.80	**300 V**	1	-40.64	22.9	99.80
	2	-40.98	22.9	99.80		2	-40.66	22.9	99.80
	3	-40.97	22.9	99.80		3	-40.70	22.9	99.80
	avg.	**-40.97**	**22.9**	**99.80**		**avg.**	**-40.67**	**22.9**	**99.80**
100 V	1	-40.63	22.9	99.80	**100 V**	1	-40.50	22.9	99.80
	2	-40.61	22.9	99.80		2	-40.51	22.9	99.80
	3	-40.58	22.9	99.80		3	-40.51	22.9	99.80
	avg.	**-40.58**	**22.9**	**99.80**		**avg.**	**-40.51**	**22.9**	**99.80**

Table 16: Measurement data from the ionization chamber setup for
linear accelerator #11.

15 MV	#	nC	°C	kPa	**6 MV**	#	nC	°C	kPa
300 V	1	-42.45	21.8	103.0	**300 V**	1	-42.05	21.8	103.0
	2	-42.47	21.8	103.0		2	-42.07	21.8	103.0
	3	-42.44	21.8	103.0		3	-42.06	21.8	103.0
	avg.	**-42.45**	**21.8**	**103.0**		**avg.**	**-42.06**	**21.8**	**103.0**
100 V	1	-41.87	21.8	103.0	**100 V**	1	-41.90	21.8	103.0
	2	-41.91	21.8	103.0		2	-41.87	21.8	103.0
	3	-41.89	21.8	103.0		3	-41.86	21.8	103.0
	avg.	**-41.89**	**21.8**	**103.0**		**avg.**	**-41.88**	**21.8**	**103.0**

Table 17: Measurement data from the ionization chamber setup for linear accelerator #12.

15 MV	#	nC	°C	kPa	6 MV	#	nC	°C	kPa
300 V	1	-42.67	21.9	103.0	**300 V**	1	-42.20	21.8	103.0
	2	-42.68	21.9	103.0		2	-42.17	21.8	103.0
	3	-42.70	21.9	103.0		3	-42.21	21.8	103.0
	avg.	**-42.68**	**21.9**	**103.0**		**avg.**	**-42.19**	**21.8**	**103.0**
100 V	1	-41.95	21.9	103.0	**100 V**	1	-41.98	21.8	103.0
	2	-41.98	21.9	103.0		2	-41.99	21.8	103.0
	3	-41.97	21.9	103.0		3	-41.97	21.8	103.0
	avg.	**-41.97**	**21.9**	**103.0**		**avg.**	**-41.98**	**21.8**	**103.0**

Table 18: Measurement data from the ionization chamber setup for linear accelerator #13. Measurements were performed for 15 MV photons only.

15 MV	#	nC	°C	kPa
300 V	1	-41.77	21.6	100.6
	2	-41.77	21.6	100.6
	3	-41.77	21.6	100.6
	avg.	**-41.77**	**21.6**	**100.6**
100 V	1	-41.13	21.6	100.6
	2	-41.13	21.6	100.6
	3	-41.13	21.6	100.6
	avg.	**-41.13**	**21.6**	**100.6**

Table 19: Measurement data from the ionization chamber setup for linear accelerator #14. Measurements were performed for 15 MV photons only.

15 MV	#	nC	°C	kPa
300 V	1	-41.55	20.3	100.7
	2	-41.55	20.3	100.7
	3	-41.55	20.3	100.7
	avg.	**-41.55**	**20.3**	**100.7**
100 V	1	-40.93	20.3	100.7
	2	-40.90	20.3	100.7
	3	-40.91	20.3	100.7
	avg.	**-40.91**	**20.3**	**100.7**

A.7 Film setup measurement tables

This section of the appendix contains tables of measurements performed on the film. All values have been calculated using Matlab.

Table 20: Table of data extracted from the 10x10 field setup. Table contains measured values of dose, max dose, penumbra, field size, field flatness and symmetry.

Linear accelerator #	Direction	D_{ref} (Gy)	D_{max} (Gy)	Penumbra 1 (cm)	Penumbra 2 (cm)	Average penumbra (cm)	Field size (cm)	Flatness	Symmetry
1	x	0.49	0.42	0.46	9.97	1.05	1.05	1.051	1.045
	y	0.42	0.46	0.44	10.02	1.04	1.04	1.044	1.036
2	x	0.46	0.42	0.44	9.93	1.05	1.03	1.051	1.035
	y	0.42	0.46	0.44	10.05	1.02	1.01	1.022	1.013
3	x	0.46	0.49	0.48	9.97	1.05	1.02	1.047	1.023
	y	0.71	0.64	0.67	9.91	1.05	1.00	1.046	1.003
4	x	0.49	0.46	0.48	9.97	1.05	1.03	1.047	1.029
	y	0.67	0.64	0.65	10.09	1.03	1.00	1.025	1.004
5	x	0.53	0.53	0.53	9.91	1.03	1.00	1.034	1.003
	y	0.53	0.49	0.51	10.09	1.03	1.00	1.026	1.005
6	x	0.56	0.56	0.56	9.93	1.03	1.03	1.033	1.030
	y	0.49	0.49	0.49	9.95	1.03	1.02	1.030	1.024
7	x	0.56	0.53	0.55	10.07	1.05	1.03	1.054	1.033
	y	0.49	0.49	0.49	10.09	1.06	1.04	1.058	1.042
8	x	0.53	0.53	0.53	9.97	1.03	1.01	1.032	1.008
	y	0.49	0.49	0.49	10.05	1.03	1.02	1.029	1.021
9	x	0.60	0.64	0.62	10.07	1.02	1.01	1.019	1.011
	y	0.53	0.56	0.55	10.05	1.03	1.02	1.029	1.016
10	x	0.64	0.67	0.65	10.04	1.03	1.01	1.033	1.007
	y	0.56	0.56	0.56	10.09	1.04	1.03	1.040	1.031
11	x	0.53	0.49	0.51	10.11	1.03	1.00	1.031	1.004
	y	0.64	0.60	0.62	9.95	1.03	1.03	1.035	1.028
12	x	0.49	0.49	0.49	10.11	1.03	1.02	1.028	1.015
	y	0.64	0.67	0.65	9.95	1.05	1.03	1.053	1.034
13	x	0.49	0.53	0.51	9.97	1.05	1.03	1.042	1.004
	y	0.49	0.46	1.00	9.98	1.04	1.03	1.057	1.026
14	x	0.39	0.39	0.39	10.04	1.06	1.03	1.057	1.035
	y	0.46	0.39	0.42	10.05	1.04	1.04	1.041	1.035

Table 21: Table of data extracted from film setup 1. Table contains measured values of dose, max dose, penumbra and field size.

Linear accelerator #	Direction	D_{ref} (Gy)	D_{max} (Gy)	Penumbra 1 (cm)	Penumbra 2 (cm)	Average penumbra (cm)	Field size (cm)
1	x	1.957	2.069	0.39	0.46	0.42	9.97
	y	1.957	1.957	0.49	0.56	0.53	9.98
2	x	1.909	2.000	0.42	0.42	0.42	9.93
	y	1.909	1.909	0.49	0.49	0.49	10.02
3	x	1.527	1.585	0.56	0.49	0.53	9.97
	y	1.527	1.806	0.53	0.46	0.49	9.95
4	x	1.934	2.058	0.46	0.56	0.51	9.93
	y	1.934	1.945	0.74	0.67	0.71	10.05
5	x	2.164	2.225	0.49	0.49	0.49	9.90
	y	2.164	2.164	0.60	0.56	0.58	10.05
6	x	1.694	1.737	0.60	0.64	0.62	9.93
	y	1.694	1.956	0.49	0.46	0.48	10.09
7	x	2.006	2.060	0.53	0.53	0.53	10.07
	y	2.006	2.050	0.49	0.49	0.49	10.05
8	x	2.095	2.116	0.49	0.53	0.51	9.97
	y	2.095	2.101	0.53	0.53	0.53	10.05
9	x	1.983	1.993	0.64	0.64	0.64	10.07
	y	1.983	2.012	0.53	0.60	0.56	10.02
10	x	2.435	2.451	0.60	0.64	0.62	10.04
	y	2.438	2.438	0.56	0.56	0.56	10.09
11	x	1.457	1.599	0.49	0.49	0.49	10.11
	y	1.457	1.904	0.60	0.60	0.60	9.95
12	x	1.619	1.734	0.46	0.46	0.46	10.11
	y	1.619	1.858	0.60	0.64	0.62	9.98
13	x	1.768	1.862	0.56	0.53	0.55	10.00
	y	1.768	1.973	0.53	0.49	0.51	10.05
14	x	1.712	1.787	0.46	0.39	0.42	10.07
	y	1.712	1.888	0.35	0.35	0.35	10.09

Table 22: Table containing data extracted from the film in film setup 2. Table contains measured values of dose, max dose, field size and penumbra.

Linear accelerator #		Field 3				Field 4			
		Dose at center (Gy)	Penumbra, 1 (cm)	Penumbra, 2 (cm)	Field size (cm)	Dose at field center (Gy)	Penumbra, 1 (cm)	Penumbra, 2 (cm)	Field size (cm)
1	x	1.743	0.39	0.42	3.02	1.819	0.42	0.39	3.09
	y	1.770	0.46	0.46	4.97	1.819	0.46	0.42	5.01
2	x	1.725	0.39	0.39	3.02	1.762	0.39	0.39	2.98
	y	1.725	0.42	0.42	4.97	1.762	0.42	0.39	4.94
3	x	1.707	0.53	0.53	2.84	1.756	0.60	0.53	2.80
	y	1.707	0.39	0.39	4.97	1.756	0.42	0.39	4.97
4	x	1.721	0.56	0.56	3.05	1.775	0.64	0.53	3.05
	y	1.721	0.42	0.39	4.90	1.775	0.42	0.39	4.90
5	x	1.871	0.46	0.46	3.16	1.875	0.46	0.46	3.16
	y	1.871	0.46	0.46	4.97	1.875	0.42	0.46	4.97
6	x	1.843	0.42	0.42	3.09	1.873	0.46	0.46	3.09
	y	1.843	0.46	0.46	4.94	1.873	0.46	0.46	4.94
7	x	1.885	0.42	0.46	2.95	1.895	0.42	0.42	2.98
	y	1.885	0.49	0.49	4.97	1.895	0.49	0.49	5.01
8	x	1.845	0.42	0.46	2.95	1.828	0.42	0.42	3.02
	y	1.845	0.46	0.46	5.04	1.828	0.46	0.42	5.04
9	x	1.853	0.53	0.53	3.05	1.889	0.49	0.49	3.02
	y	1.853	0.53	0.53	5.08	1.889	0.49	0.53	5.04
10	x	1.858	0.49	0.53	3.09	1.845	0.49	0.49	3.02
	y	1.858	0.53	0.56	5.04	1.845	0.53	0.56	5.04
11	x	1.740	0.53	0.53	2.84	1.765	0.56	0.46	2.88
	y	1.740	0.42	0.39	5.08	1.765	0.42	0.42	5.08
12	x	1.736	0.53	0.60	2.88	1.736	0.56	0.53	2.95
	y	1.736	0.60	0.42	5.12	1.736	0.42	0.39	5.12
13	x	1.789	0.46	0.46	2.98	1.839	0.46	0.42	2.95
	y	1.789	0.46	0.46	5.01	1.839	0.42	0.46	5.01
14	x	1.862	0.39	0.42	2.95	1.905	0.42	0.39	3.05
	y	1.862	0.46	0.42	5.08	1.905	0.46	0.42	5.08

Table 23: Calculated values of dose difference and full width at half maximum (FWHM) values for setup 3 and 4 for all linear accelerators.

Linear accelerator #		Dose difference (%)					FWHM (cm)				
		max	min	mean	median	SD	max	min	mean	median	SD
1	3	52.18	3.79	5.57	5.23	3.44	0.78	0.00	0.36	0.35	0.11
	4	1.98	1.20	1.60	1.61	0.19					
2	3	6.79	1.55	4.17	4.46	1.34	0.86	0.14	0.26	0.21	0.14
	4	12.66	7.36	10.32	10.48	1.74	0.34	0.18	0.26	0.26	0.03
3	3	21.63	8.93	14.85	14.99	3.53	0.31	0.21	0.24	0.25	0.02
	4	34.39	24.28	28.58	28.31	2.32	0.60	0.48	0.54	0.54	0.03
4	3	31.39	25.37	26.96	26.35	1.37	0.32	0.24	0.28	0.28	0.02
	4	16.93	1.52	8.58	8.82	4.38	0.97	0.13	0.38	0.39	0.12
5	3	15.09	11.96	13.45	13.22	0.93	0.36	0.24	0.29	0.29	0.02
	4	10.80	5.47	7.70	7.63	1.26	0.30	0.19	0.25	0.24	0.03
6	3	8.52	4.80	6.46	6.33	0.72	0.43	0.19	0.26	0.26	0.05
	4	14.75	5.55	7.36	7.52	1.09	0.41	0.14	0.24	0.24	0.04
7	3	21.86	19.01	20.06	20.00	0.56	0.42	0.30	0.36	0.36	0.03
	4	8.35	4.42	6.11	5.87	1.09					
8	3	9.18	5.53	7.23	7.19	0.84	0.41	0.19	0.24	0.23	0.04
	4	11.23	4.38	7.03	7.03	1.34	0.40	0.14	0.23	0.22	0.04
9	3	7.18	2.12	5.32	5.68	1.37	0.87	0.17	0.41	0.35	0.17
	4	20.64	3.23	13.29	12.23	4.39	0.53	0.27	0.34	0.33	0.05
10	3	7.58	2.17	4.10	3.71	1.36	0.99	0.16	0.50	0.46	0.20
	4	43.62	12.93	24.21	22.66	7.60	0.47	0.34	0.40	0.40	0.03
11	3	16.17	9.20	12.37	12.40	1.84	0.31	0.18	0.24	0.24	0.03
	4	42.77	34.39	39.23	38.98	2.03	0.56	0.43	0.50	0.50	0.03
12	3	5.80	1.06	2.75	2.66	1.12					
	4	16.92	6.60	11.52	10.89	2.45	0.55	0.34	0.43	0.43	0.04
13	3	11.31	3.75	9.17	9.07	0.72	0.30	0.18	0.23	0.22	0.03
	4	8.32	5.55	7.03	7.03	0.78	0.42	0.16	0.27	0.25	0.07
14	3	10.21	5.76	7.74	7.64	0.85					
	4	6.97	3.21	5.09	5.34	0.94	0.51	0.15	0.30	0.27	0.10

A.8 Dose planning reports from Varian Eclipse

Eclipse
External Beam Planning 7.5.51   A Ullevål, Oslo

Pasientnavn:	TEST, Alexander NRPA	**Fødselsnr:**	240608
Course Id:	C1	Behandlingsintensjon:	Unknown
Plan Id:	**Oppsett 10 10**	Plan Name:	PS1
Plan Created:	24. juni 2008 14:14:07 by stol	Diagnosegruppe:	-
Plan Last Modified:	24. juni 2008 14:24:16 by stol		
Pasientleie:	Head First-Supine		

Dose og fraksjonering

Target Volume:	-
Plan Normalization Value:	92.3 %
Prescribed Dose Percentage:	100.0 %
Primary Reference Point:	None
Relative Dose in Primary Reference Point:	100.0 %
Rekvirert dose:	2.000 Gy (2.000 Gy / fraksjon)
Antall fraksjoner:	1

Field 9

Behandlingsapparat:	SB4
Energi:	**15X**
Source-Axis-Distance (SAD):	100.0 cm
Source-Skin-Distance (SSD):	90.0 cm
Feltstørrelse (Y x X):	**10.0 cm x 10.0 cm**
Gantryvinkel:	0.0 deg
Kollimatorvinkel:	0.0 deg
Bordvinkel:	0.0 deg
Vektfaktor:	1.000
Reference Dose:	2.666 Gy
Monitorenheter:	**200 MU**

Dose punkt

Fractionation Id	Point Id	3D-coordinates			Fraction Dose	Total Dose	Primary Point	Volume Id
		X	Y	Z				
F1	None	-	-	-	2.000 Gy	2.000 Gy	X	None

Warnings
None

Approvals

Pasient: TEST, Alexander NRPA (240608)   Utskrift: 24.06.2008 14:25 av stol
Course: C1
Plan: Oppsett 10 10   Side: 1/1

Eclipse

External Beam Planning 7.5.51

Pasientnavn:	**TEST, Alexander NRPA**	**Fødselsnr:**	**240608**
Course Id:	C1	Behandlingsintensjon:	Unknown
Plan Id:	**Oppsett 1**	Plan Name:	PS1
Plan Created:	24. juni 2008 13:16:51 by stol	Diagnosegruppe:	-
Plan Last Modified:	24. juni 2008 14:07:31 by stol		
Pasientleie:	Head First-Supine		

Dose og fraksjonering

Target Volume:	-
Plan Normalization Value:	95.6 %
Prescribed Dose Percentage:	100.0 %
Primary Reference Point:	None
Relative Dose in Primary Reference Point:	100.0 %
Rekvirert dose:	2.000 Gy (2.000 Gy / fraksjon)
Antall fraksjoner:	1

Field 1

Behandlingsapparat:	SB4
Energi:	**15X**
Source-Axis-Distance (SAD):	100.0 cm
Source-Skin-Distance (SSD):	90.0 cm
Feltstørrelse (Y x X):	**10.0 cm x 5.0 cm (Y1: +5.0 cm Y2: +5.0 cm X1: +5.0 cm X2: +0.0 cm)**
Gantryvinkel:	0.0 deg
Kollimatorvinkel:	0.0 deg
Bordvinkel:	0.0 deg
Vektfaktor:	1.000
Reference Dose:	2.571 Gy
Monitorenheter:	**200 MU**

Field 2

Behandlingsapparat:	SB4
Energi:	**15X**
Source-Axis-Distance (SAD):	100.0 cm
Source-Skin-Distance (SSD):	90.0 cm
Feltstørrelse (Y x X):	**10.0 cm x 5.0 cm (Y1: +5.0 cm Y2: +5.0 cm X1: +0.0 cm X2: +5.0 cm)**
Gantryvinkel:	0.0 deg
Kollimatorvinkel:	0.0 deg
Bordvinkel:	0.0 deg
Vektfaktor:	1.000
Reference Dose:	2.571 Gy
Monitorenheter:	**200 MU**

Dose punkt

Fractionation Id	Point Id	3D-coordinates X	Y	Z	Fraction Dose	Total Dose	Primary Point	Volume Id
F1	None	-	-	-	2.000 Gy	2.000 Gy	X	None

Warnings

None

Approvals

Pasientnavn:	**TEST, Alexander NRPA**	**Fødselsnr:**	**240608**
Course id:	C1	Behandlingsintensjon:	Unknown
Plan Id:	**Oppsett 2**	Plan Name:	PS1
Plan Created:	24. juni 2008 13:31:12 by stol	Diagnosegruppe:	-
Plan Last Modified:	24. juni 2008 14:07:31 by stol		
Pasientleie:	Head First-Supine		

Dose og fraksjonering

Target Volume:	-
Plan Normalization Value:	101.2 %
Prescribed Dose Percentage:	100.0 %
Primary Reference Point:	None
Relative Dose in Primary Reference Point:	100.0 %
Rekvirert dose:	2.000 Gy (2.000 Gy / fraksjon)
Antall fraksjoner:	1

Field 3

Behandlingsapparat:	SB4
Energi:	**15X**
Source-Axis-Distance (SAD):	100.0 cm
Source-Skin-Distance (SSD):	90.0 cm
Feltstørrelse (Y x X):	**5.0 cm x 3.0 cm (Y1: -2.0 cm Y2: +7.0 cm X1: +5.0 cm X2: -2.0 cm)**
Gantryvinkel:	0.0 deg
Kollimatorvinkel:	0.0 deg
Bordvinkel:	0.0 deg
Vektfaktor:	1.000
Reference Dose:	2.428 Gy
Monitorenheter:	**200 MU**

Field 4

Behandlingsapparat:	SB4
Energi:	**15X**
Source-Axis-Distance (SAD):	100.0 cm
Source-Skin-Distance (SSD):	90.0 cm
Feltstørrelse (Y x X):	**5.0 cm x 3.0 cm (Y1: -2.0 cm Y2: +7.0 cm X1: -2.0 cm X2: +5.0 cm)**
Gantryvinkel:	0.0 deg
Kollimatorvinkel:	0.0 deg
Bordvinkel:	0.0 deg
Vektfaktor:	1.000
Reference Dose:	2.428 Gy
Monitorenheter:	**200 MU**

Dose punkt

Fractionation Id	Point Id	3D-coordinates			Fraction Dose	Total Dose	Primary Point	Volume Id
		X	Y	Z				
F1	None	-	-	-	2.000 Gy	2.000 Gy	X	None

Warnings

None

Approvals

Eclipse

Pasientnavn:	**TEST, Alexander NRPA**	**Fødselsnr:**	**240608**
Course Id:	C1	Behandlingsintensjon:	Unknown
Plan Id:	**Oppsett 3**	Plan Name:	PS1
Plan Created:	24. juni 2008 13:58:59 by stol	Diagnosegruppe:	-
Plan Last Modified:	24. juni 2008 14:07:31 by stol		
Pasientleie:	Head First-Supine		

Dose og fraksjonering

Target Volume:	-
Plan Normalization Value:	97.0 %
Prescribed Dose Percentage:	100.0 %
Primary Reference Point:	None
Relative Dose in Primary Reference Point:	100.0 %
Rekvirert dose:	2.000 Gy (2.000 Gy / fraksjon)
Antall fraksjoner:	1

Field 5

Behandlingsapparat:	SB4
Energi:	**15X**
Source-Axis-Distance (SAD):	100.0 cm
Source-Skin-Distance (SSD):	90.0 cm
Feltstørrelse (Y x X):	**4.0 cm x 12.0 cm (Y1: +0.0 cm Y2: +4.0 cm X1: +6.0 cm X2: +6.0 cm)**
Gantryvinkel:	0.0 deg
Kollimatorvinkel:	90.0 deg
Bordvinkel:	0.0 deg
Vektfaktor:	1.000
Reference Dose:	2.521 Gy
Monitorenheter:	**200 MU**

Field 6

Behandlingsapparat:	SB4
Energi:	**15X**
Source-Axis-Distance (SAD):	100.0 cm
Source-Skin-Distance (SSD):	90.0 cm
Feltstørrelse (Y x X):	**4.0 cm x 12.0 cm (Y1: +0.0 cm Y2: +4.0 cm X1: +6.0 cm X2: +6.0 cm)**
Gantryvinkel:	0.0 deg
Kollimatorvinkel:	270.0 deg
Bordvinkel:	0.0 deg
Vektfaktor:	1.000
Reference Dose:	2.521 Gy
Monitorenheter:	**200 MU**

Dose punkt

Fractionation Id	Point Id	3D-coordinates			Fraction Dose	Total Dose	Primary Point	Volume Id
		X	Y	Z				
F1	None	-	-	-	2.000 Gy	2.000 Gy	X	None

Warnings

None

Approvals

Pasientnavn:	TEST, Alexander NRPA	**Fødselsnr:**	240608
Course Id:	C1	Behandlingsintensjon:	Unknown
Plan Id:	**Oppsett 4**	Plan Name:	PS1

Plan Created:	24. juni 2008 14:08:43 by stol	Diagnosegruppe:	-
Plan Last Modified:	24. juni 2008 14:13:58 by stol		
Pasientleie:	Head First-Supine		

Dose og fraksjonering

Target Volume:	-
Plan Normalization Value:	96.2 %
Prescribed Dose Percentage:	100.0 %
Primary Reference Point:	None
Relative Dose in Primary Reference Point:	100.0 %
Rekvirert dose:	2.000 Gy (2.000 Gy / fraksjon)
Antall fraksjoner:	1

Field 7

Behandlingsapparat:	SB4
Energi:	**15X**
Source-Axis-Distance (SAD):	100.0 cm
Source-Skin-Distance (SSD):	90.0 cm
Feltstørrelse (Y x X):	**12.0 cm x 4.0 cm (Y1: +6.0 cm Y2: +6.0 cm X1: +0.0 cm X2: +4.0 cm)**
Gantryvinkel:	0.0 deg
Kollimatorvinkel:	90.0 deg
Bordvinkel:	0.0 deg
Vektfaktor:	1.000
Reference Dose:	2.542 Gy
Monitorenheter:	**200 MU**

Field 8

Behandlingsapparat:	SB4
Energi:	**15X**
Source-Axis-Distance (SAD):	100.0 cm
Source-Skin-Distance (SSD):	90.0 cm
Feltstørrelse (Y x X):	**12.0 cm x 4.0 cm (Y1: +6.0 cm Y2: +6.0 cm X1: +0.0 cm X2: +4.0 cm)**
Gantryvinkel:	0.0 deg
Kollimatorvinkel:	270.0 deg
Bordvinkel:	0.0 deg
Vektfaktor:	1.000
Reference Dose:	2.542 Gy
Monitorenheter:	**200 MU**

Dose punkt

Fractionation Id	Point Id	3D-coordinates			Fraction Dose	Total Dose	Primary Point	Volume Id
		X	Y	Z				
F1	None	-	-	-	2.000 Gy	2.000 Gy	X	None

Warnings

None

Approvals

References

[1] S. Devic, J. Seuntjens, E. Sham, E. B. Podgorsak, C. R. Schmidtlein, A. S. Kirov, and C. G. Soares, "Precise radiochromic film dosimetry using a flat-bed document scanner." *Med Phys*, vol. 32, pp. 2245–2253, 2005.

[2] IAEA Technical Report Series 398, "Absorbed Dose Determination in External Beam Radiotherapy" Wien: International Atomic Energy Agency, 2001.

[3] P. Metcalfe, T. Kron, and P. Hoban, *The Physics of Radiotherapy X-rays from Linear Accelerators*. Medical Physics Publishing, 2004.

[4] N. Suntharalingam, E. Podgorsak, and J. Hendry, "Basic Radiobiology" in *Radiation Oncology Physics: A Handbook for Teachers and Students* (E. Podgorsak, ed.), ch. 14, pp. 485–504, Wien: International Atomic Energy Agency, 2005.

[5] Statens Strålevern, "Dosimetrilaboratoriet ved Statens strålevern" StrålevernInfo 4:2003, Østerås, 2003.

[6] Statens Strålevern, "Åpning av SSDL ved Statens strålevern" StrålevernInfo 9:2008, Østerås, 2008.

[7] Statens Strålevern, "Kvalitetssikring I Stråleterapi (KVIST)" StrålevernInfo 2:2003, Østerås, 2003.

[8] Statens Strålevern, "Quality assurance in radiotherapy - 8 years outcome" NRPABulletin 8:2008, Østerås, 2008.

[9] Sosial og helsedepartementet, "Omsorg og kunnskap: Norsk kreftplan, NOU 1997:20" Oslo, 1997.

[10] Hans Bjerke, "Dosimetry in Norwegian Radiotherapy: Implementation of the absorbed dose to water standard and code of practice in radiotherapy in Norway" StrålevernRapport 11:2003, Østerås: Statens Strålevern, 2003.

[11] J. Seuntjens, W. Strydom, and K. Shortt, "Dosimetric principles, quantities and units" in *Radiation Oncology Physics: A Handbook for Teachers and Students* (E. Podgorsak, ed.), ch. 2, pp. 45–70, Wien: International Atomic Energy Agency, 2005.

[12] F. M. Khan, *The Physics of Radiation Therapy*. Philadelpia: Lippincott, Williams & Wilkins, 3rd ed., 2003.

[13] F. H. Attix, *Introduction to Radiological Physics and Radiation Dosimetry*. New York: Wiley-VCH, 1986.

[14] F. H. Attix, "Energy imparted, energy transferred and net energy transferred." *Phys Med Biol*, vol. 28, pp. 1385–1390, 1983.

[15] P. Andreo, A. Nahum, and D. Thwaites, "Ionisation Chambers" in *Handbook of Radiotherapy Physics: Theory and Practice* (P. Mayles, A. Nahum, and J.-C. Rosenwald, eds.), ch. 15, pp. 279–302, New York: Taylor & Francis, 2007.

[16] H. E. Johns and J. R. Cunningham, *The Physics of Radiology, 4th Edition.* Springfield, IL: Charles C. Thomas, 1983.

[17] D. Rogers, "Ionizing Radiation Dosimetry and Medical Physics" *Physics in Canada*, vol. 51(4), pp. 178–181, 1995.

[18] J. Izewska and G. Rajan, "Radiation Dosimeters" in *Radiation Oncology Physics: A Handbook for Teachers and Students* (E. Podgorsak, ed.), ch. 3, pp. 71–99, Wien: International Atomic Energy Agency, 2005.

[19] M. S. Weinhous and J. A. Meli, "Determining Pion, the correction factor for recombination losses in an ionization chamber." *Med Phys*, vol. 11, no. 6, pp. 846–849, 1984.

[20] D. Greene and P. C. Williams, *Linear Accelerators for Radiation Therapy, Second Edition.* Bristol: Institute of Physics Publishing, Medical Science Series, 1997.

[21] E. Podgorsak, "Treatment Machines for External Beam Radiotherapy" in *Radiation Oncology Physics: A Handbook for Teachers and Students* (E. Podgorsak, ed.), ch. 5, pp. 123–160, Wien: International Atomic Energy Agency, 2005.

[22] L. Loverock, P. Williams, D. Thwaites, A. McKenzie, and P. Mayles, "Linear Accelerators" in *Handbook of Radiotherapy Physics: Theory and Practice* (P. Mayles, A. Nahum, and J.-C. Rosenwald, eds.), ch. 11, pp. 197–240, New York: Taylor & Francis, 2007.

[23] IEC International standard 61217, "Radiotherapy equipment: coordinates, movements and scales" Geneve: International Electrotechnical Commission, 2002.

[24] H. Bjerke, A. S. Alfredsen, B. E. Johansson, and S. Ølberg, "Kvalitetskontroll av linac: Rapport fra en arbeidsgruppe under KVIST" Statens Strålevern: Østerås.

[25] J. Saunders, "Cobalt Machines" in *Handbook of Radiotherapy Physics: Theory and Practice* (P. Mayles, A. Nahum, and J.-C. Rosenwald, eds.), ch. 12, pp. 241–250, New York: Taylor & Francis, 2007.

[26] International Commission on Radiation Units and Measurements: ICRU Report 64, "Dosimetry of High-Energy Photon Beams based on Standards of Absorbed Dose to Water" Ashford: Nuclear Technology Publishing, 2001.

[27] E. Podgorsak, "External Photon Beams: Physical Aspects" in *Radiation Oncology Physics: A Handbook for Teachers and Students* (E. Podgorsak, ed.), ch. 6, pp. 161–217, Wien: International Atomic Energy Agency, 2005.

[28] P. Mayles and P. Williams, "Megvoltage Photon Beams" in *Handbook of Radiotherapy Physics: Theory and Practice* (P. Mayles, A. Nahum, and J.-C. Rosenwald, eds.), ch. 22, pp. 451–482, New York: Taylor & Francis, 2007.

[29] I. Rosenberg, "Manual Dose Calculations In Photon Beams" in *Handbook of Radiotherapy Physics: Theory and Practice* (P. Mayles, A. Nahum, and J.-C. Rosenwald, eds.), ch. 23, pp. 483–518, New York: Taylor & Francis, 2007.

[30] F. M. Khan, B. J. Gerbi, and F. C. Deibel, "Dosimetry of asymmetric x-ray collimators." *Med Phys*, vol. 13, no. 6, pp. 936–941, 1986.

[31] *Detectors for Relative and Absolute Dosimetry*, Schwarzenbruck: IBA dosimetry, 2007.

[32] H. Bjerke and E. A. Hult, "A Water Phantom for Cross Calibration and Reference Dose Determination in High Energy Photon Beams (IAEA-96-34P)" in *Book of Extended Synopsis. IAEA-CN-96* (IAEA, ed.), pp. 68–69, International Symposium on Standards and Codes of Practice in Medical Radiation Dosimetry, 2002.

[33] E. A. Hult, "Co-60 dose til vann og doserate til vann" , Østerås: Statens Strålevern, 2005.

[34] B. S. Avset and H. Bjerke, "Uncertainty budget - Dose to Water Cobalt-60" , Østerås: Statens Strålevern, 2006.

[35] IAEA tecdoc 1455, "Implementation of the International Code of Practice on Dosimetry in Radiotherapy (TRS 398): Review of testing results" Wien: International Atomic Energy Agency, 2005.

[36] "The most Comprehensive, Reliable, Economical and Easy to use GafChromic ® film based IMRT QA system" Presentation, Wayne, NJ: International Specialty Products, 2006.

[37] M. J. Butson, P. K. N. Yu, T. Cheung, and P. Metcalfe, "Radiochromic film for medical radiation dosimetry" *Materials Science and Engineering*, vol. 41, pp. 61–120, 2003.

[38] Advanced Materials Group, "Gafchromic® EBT: Self-developing film for radiotherapy dosimetry" Wayne, NJ: International Specialty Products, 2006.

[39] M. J. Butson, T. Cheung, and P. K. N. Yu, "Weak energy dependence of EBT gafchromic film dose response in the 50 kVp-10 MVp X-ray range." *Appl Radiat Isot*, vol. 64, pp. 60–62, 2006.

[40] S.-T. Chiu-Tsao, Y. Ho, R. Shankar, L. Wang, and L. B. Harrison, "Energy dependence of response of new high sensitivity radiochromic films for megavoltage and kilovoltage radiation energies." *Med Phys*, vol. 32, pp. 3350–3354, 2005.

[41] T. Cheung, M. J. Butson, and P. K. N. Yu, "Post-irradiation colouration of Gafchromic EBT radiochromic film." *Phys Med Biol*, vol. 50, pp. N281–N285, 2005.

[42] Advanced Materials Group, "GafChromic® RTQA Product Brochure" Wayne, NJ: International Specialty Products, 2006.

[43] L. J. van Battum, D. Hoffmans, H. Piersma, and S. Heukelom, "Accurate dosimetry with GafChromic[trademark sign] EBT film of a 6 MV photon beam in water: What level is achievable?" *Med Phys*, vol. 35, no. 2, pp. 704–716, 2008.

[44] S. Devic, J. Seuntjens, G. Hegyi, E. B. Podgorsak, C. G. Soares, A. S. Kirov, I. Ali, J. F. Williamson, and A. Elizondo, "Dosimetric properties of improved GafChromic films for seven different digitizers." *Med Phys*, vol. 31, pp. 2392–2401, 2004.

[45] L. Paelinck, W. D. Neve, and C. D. Wagter, "Precautions and strategies in using a commercial flatbed scanner for radiochromic film dosimetry." *Phys Med Biol*, vol. 52, pp. 231–242, 2007.

[46] J. P. Sage, J. N. H. Brunt, and P. Mayles, "Data Communication with DICOM" in *Handbook of Radiotherapy Physics: Theory and Practice* (P. Mayles, A. Nahum, and J.-C. Rosenwald, eds.), ch. 42, pp. 909–919, New York: Taylor & Francis, 2007.

[47] Advanced Materials Group David F. Lewis, "New Developments in Scanning Radiochromic Film" Wayne, NJ: International Specialty Products, 2007.

[48] Advanced Materials Group, "Scanner user's protocol for use with the GAFCHROMIC® film based IMRT QA system" Wayne, NJ: International Specialty Products.

[49] "Epson Scan User's Manual" Nagano: Seiko Epson Corp, 2006.

[50] The MathWorks, Inc., *Image Processing Toolbox 6 User's Guide*, 2008.

[51] J. S. Lim, *Two-Dimensional Signal and Image Processing*. Upper Saddle River: Prentice Hall, 1990.

[52] Wikipedia, The Free Encyclopedia, "Full width at half maximum" 2008. [Online; accessed 3-November-2008].

[53] Eric W. Weisstein, "Full Width at Half Maximum From MathWorld–A Wolfram Web Resource" http://mathworld.wolfram.com/FullWidthatHalfMaximum.html [Online: accessed 11-October-2008].

[54] D. A. Low, W. B. Harms, S. Mutic, and J. A. Purdy, "A technique for the quantitative evaluation of dose distributions." *Med Phys*, vol. 25, pp. 656–661, 1998.

[55] J. V. Dyk, R. B. Barnett, J. E. Cygler, and P. C. Shragge, "Commissioning and quality assurance of treatment planning computers." *Int J Radiat Oncol Biol Phys*, vol. 26, pp. 261–273, 1993.

[56] D. A. Low and J. F. Dempsey, "Evaluation of the gamma dose distribution comparison method." *Med Phys*, vol. 30, pp. 2455–2464, 2003.

[57] T. Depuydt, A. V. Esch, and D. P. Huyskens, "A quantitative evaluation of IMRT dose distributions: refinement and clinical assessment of the gamma evaluation." *Radiother Oncol*, vol. 62, pp. 309–319, 2002.

[58] Frederic Moisy, "ezyfit: A free curve fitting toolbox for Matlab" http://www.fast.u-psud.fr/ezyfit/.

[59] A. Rink, I. A. Vitkin, and D. A. Jaffray, "Energy dependence (75 kVp to 18 MV) of radiochromic films assessed using a real-time optical dosimeter." *Med Phys*, vol. 34, pp. 458–463, 2007.

[60] L. Menegotti, A. Delana, and A. Martignano, "Radiochromic film dosimetry with flatbed scanners: a fast and accurate method for dose calibration and uniformity correction with single film exposure." *Med Phys*, vol. 35, pp. 3078–3085, 2008.

[61] *MatriXX Evolution: The Solution for Rotational Treatment QA*. Schwarzenbruck: IBA dosimetry, 2007.

[62] L. E. Reinstein, G. R. Gluckman, and A. G. Meek, "A rapid colour stabilization technique for radiochromic film dosimetry." *Phys Med Biol*, vol. 43, pp. 2703–2708, 1998.

[63] S. Saur and J. Frengen, "GafChromic EBT film dosimetry with flatbed CCD scanner: a novel background correction method and full dose uncertainty analysis." *Med Phys*, vol. 35, pp. 3094–3101, 2008.

[64] DM Ritt, GH Pierce, ML Whitaker, and RS Poling, "Repeatability and calibration results of GAFchromic EBT film with flatbed and medical scanners" Radiological Imaging Technology, Inc., Colorado Springs, 2005.

[65] M. Abramoff, P. Magelhaes, and S. Ram, "Image Processing with ImageJ" *Biophotonics International*, vol. 11, pp. 36–42, 2004.

[66] The Scilab Consortium, "Scilab, the open source platform for numerical computation" http://www.scilab.org/.

Software list

- L$_Y$X: L^{A}T$_E$X environment in which this thesis was written.
  URL: http://www.lyx.org

- JabRef: BibT$_E$X reference manager, used for the references.
  URL: http://jabref.sourceforge.net

- Matlab® Student Edition 7.4 with Image Processing Toolbox™ 5.4: Used for image processing and analysis, as well as the development of Sensio-metriCal and ProcessEBT applications.
  URL: http://www.mathworks.com

  - Ezyfit: Free curve fitting toolbox for Matlab that can fit data to almost any standard curve, used for calibration curve fitting:
    URL: http://www.fast.u-psud.fr/ezyfit/

- The GIMP: Image manipulation program for image editing and creating most of the original figures.
  URL: http://www.gimp.org

- IDL 7.0: The interface language in which the VerA application is written.
  URL: http://www.ittvis.com/idl

Statens strålevern
Norwegian Radiation Protection Authority

Lobo Media 461 88